

**Department of Pharmacy
School of Medicine and Surgery
University of Naples Federico II**



**Ph.D. Thesis in
"PHARMACEUTICAL SCIENCE"**

XXXIV CYCLE

**Rational design and sustainable synthesis of
combinatorial libraries of heterocyclic scaffolds with
potential therapeutic effects**

Ph.D. Course Coordinator and Tutor

Prof. Maria Valeria D'Auria

Candidate

Dr. Martina Sciarretta

*“Life is not easy for any of us. But what of that?
We must have perseverance and above all confidence in ourselves.
We must believe that we are gifted for something, and that
this thing, at whatever cost, must be attained.”*

Marie Curie

Preface

My three years Ph.D. research in Pharmaceutical Science at the Department of Pharmacy of University of Naples Federico II, was started in November 2018 under the supervision of Prof. Maria Valeria D'Auria.

My project was mainly focused on the design and synthesis of small heterocyclic molecules as potential modulators of emerging targets with therapeutical effects. In detail, my research was addressed to the investigation of anti-inflammatory, anticancer and antibiotic activity.

In collaboration with the research team of Prof. Bifulco (University of Salerno), a multistep computational approach was carried out for the generation of an extensive library of compounds to select the best virtual candidates for the development of new potential agents interfering with several pathways.

My attention on the synthetic phase of a multidisciplinary workflow was focused on the identification of novel promising anti-inflammatory and anticancer chemical entities. I took care about the synthetic procedures and their optimization, followed by the purification and characterization of final products.

Biological assays on small molecules that I synthesized, were performed in collaboration with different pharmacological partners to confirm the predicted activity towards the targets.

A secondary and parallel research line focused on isolation of secondary metabolites from bacterial strains isolated from unexplored and unique habitats was carried out in collaboration with research group at Institute of Protein (IBP-CNR). In this framework, I had the chance to deal with the chemical investigation on several bacterial strains taking care of the isolation and characterization of secondary metabolites structure in order to evaluate

their biological potential. This work experience led me to acquire greater and updated competences in the analysis of NMR data.

Furthermore, I had the opportunity to enrich my background in the field of innovative and sustainable organic synthetic approaches. Specifically, I worked on a photocatalysis project at the Autònoma University of Madrid, Faculty of Sciences, to perform the synthesis of heterocyclic scaffold in line with my research topic under the supervision of Prof. José Alemán.

List of publications related to the scientific activity performed during the three years Ph.D. course in Pharmaceutical Science

Buommino E.*, Di Marino S.*, Sciarretta M., Piccolo M., D'Auria M.V., Festa C., Synergism of a Novel 1,2,4-oxadiazole-containing Derivative with Oxacillin against Methicillin-Resistant *Staphylococcus aureus*, *Antibiotics*, **2021**, *10*, 1258.

Potenza M.*, Sciarretta M.*, Chini M. G., Saviano A., Maione F., D'Auria M.V., Di Marino S., Giordano A., Hofstetter R. K., Festa C., Werz O., Bifulco G., Structure-based screening for the discovery of 1,2,4-oxadiazoles as promising hits for the development of new anti-inflammatory agents interfering with eicosanoid biosynthesis pathways, *European Journal of Medicinal Chemistry*, **2021**, *224* 113693.

Vitale G.A., Sciarretta M., Cassiano C., Buonocore C., Festa C., Mazzella V., Núñez Pons L., D'Auria M.V., de Pascale D., Molecular Network and Culture Media Variation Reveal a Complex Metabolic Profile in *Pantoea cf. eucrina D2* Associated with an Acidified Marine Sponge, *International Journal of Molecular Science*, **2020**, *21*, 6307.

Vitale G.A., Sciarretta M., Palma Esposito F., January G.G, Giaccio M., Bunk B., Spröer C., Bajerski F., Power D., Festa C., Monti M.C., D'Auria M.V., de Pascale D., Genomics–Metabolomics Profiling Disclosed *Marine Vibrio spartinae 3.6* as a Producer of a New Branched Side Chain Prodigiosin, *Journal of Natural Products*, **2020**, *83* (5) 1495–1504.

*These authors contributed equally to this work

TABLE OF CONTENTS

INTRODUCTION

CHAPTER 1.....	1
1.1 <i>Drug Discovery strategies</i>	2
1.2 <i>Privileged scaffold in Drug Discovery</i>	7
1.3 <i>Lead discovery: the role of organic chemistry</i>	11

CHAPTER 2.....	14
2.1 <i>Oxadiazoles as privileged scaffold</i>	15
2.2 <i>1,2,4-oxadiazoles: synthesis and reactivity</i>	17
2.3 <i>Biological applications of 1,2,4-oxadiazoles</i>	20

CHAPTER 3

1,2,4-oxadiazoles as useful scaffolds for the development of new anti-inflammatory and antibacterial agents.....	24
3.1 <i>Structure-based screening for the discovery of 1,2,4-oxadiazoles as promising hits for the development of new anti-inflammatory agents interfering with eicosanoid biosynthesis pathways</i>	25
3.1.1 <i>Overview on inflammatory response</i>	25
3.1.2 <i>Inflammatory mediators and eicosanoids pathway: the role of PGE₂</i>	27
3.1.3 <i>Microsomal prostaglandin E₂ synthase-1 (mPGES-1)</i>	31
3.1.4 <i>Combinatorial Approach</i>	36
3.1.5 <i>Synthesis of compounds</i>	44
3.1.6 <i>Biological evaluation</i>	45
3.1.7 <i>A new small-molecules library and future perspectives</i>	56
3.2 <i>Synergism of a novel 1,2,4-oxadiazole-containing derivative with oxacillin against methicillin-resistant <i>Staphylococcus aureus</i></i>	62
3.2.1 <i>Drug-resistance: methicillin-resistant <i>S. aureus</i></i>	62
3.2.2 <i>1,2,4-oxadiazoles as antimicrobial agents</i>	65
3.2.3 <i>Compounds and chemistry</i>	68
3.2.4 <i>Antimicrobial activity</i>	70
3.2.5 <i>Synergistic study</i>	74
3.2.6 <i>Molecular analysis</i>	74
3.2.7 <i>Cytotoxic assays</i>	76

CHAPTER 5

Design and synthesis of compounds from natural source

inspiration as potential anticancer agents.....	78
<i>5.1 The importance of natural compounds in drug discovery.....</i>	<i>79</i>
<i>5.2 Bromodomains as epigenetic targets.....</i>	<i>80</i>
<i>5.2.1 BRD9: a promising target for the treatment of cancer.....</i>	<i>84</i>
<i>5.3 Viridicatin derivatives as potential inhibitors of BRD9.....</i>	<i>92</i>
<i>5.3.1 Viridicatin and viridicatol.....</i>	<i>92</i>
<i>5.3.2 In silico stuies.....</i>	<i>93</i>
<i>5.3.3 Synthesis of viridicatin derivatives.....</i>	<i>96</i>
<i>5.3.4 Biological evaluation and future plans.....</i>	<i>99</i>
CONCLUSIONS.....	100
EXPERIMENTAL SECTION.....	104
<i>Computational studies.....</i>	<i>105</i>
<i>Chemistry.....</i>	<i>106</i>
<i>Pharmacology.....</i>	<i>127</i>
NMR SPECTRA.....	139
REFERENCES.....	159

INTRODUCTION
CHAPTER 1

1.1 Drug Discovery strategies

The challenging process by which new candidate medications are discovered, is named Drug Discovery, and includes a wide variety of disciplines and approaches applied to identify chemical compounds as new potential active compounds.

The origin of drug discovery process takes back to ancient times, when drugs were entirely derived from natural sources such as plants, micro-organisms, marine organisms, and fungi used in the treatment of various diseases with many applications in the fields of medicine, pharmacy, and general biology.¹ However, it has only been in the past half century that searching for new drugs has found itself in the realm of science. Historically, the discovery of a new drug was mainly related to a combination of trials and error experiments as a serendipitous event, while nowadays it includes a rational design in which many steps are involved to obtain a selective and effective compound for a pharmacological treatment.²

Drug discovery process has undergone many changes over the years, maintaining the same goal: to uncover safer medicines for all diseases. Starting from an initial idea, the development of a new drug could take around 12-15 years until its entry into the commercial market and this process requires enormous amount of costs and risks. Expertise of many eminent researchers are required, and the discovery of a single drug takes exhaustive research and a huge amount of financial investment.³

The research starts from an original hypothesis that the inhibition or the activation of a selected target could result in a therapeutic effect in a disease state.⁴ Recently, with the development of new technologies such as computational studies, the process is becoming a less risky business, because of the ability of computers to predict possible outcomes.⁵

The molecular target should be fully validated with appropriate techniques ranging from *in vitro* tools to the use of whole animal's models and its modulation should provide an unambiguous therapeutical effect without any resistance mechanism.⁶

The initial and continued success of a drug on the market depends on the next phase of identification of the lead compound, which is the most crucial point in the research of new chemical entity able to meet the clinical need.⁷

The goal of this preclinical research program is to select one or more clinical candidate molecules. Each of them must go through many tests to ensure their potency and safety, and sufficient evidence of biologic activity towards the receptor as well as drug-like properties let them enter in human testing.

In this phase, scientists need to assess a multitude of chemical and biological parameters on many compounds to choose the best candidate for development. Chemists and pharmacologists, working in close collaboration, will carefully study the structure activity relationship and will synthesize such other derivatives, with the best possible desired activity.

As soon as the lead structure is identified, an intensive and iterative optimization is required for the next step of preclinical trial, in which cells and animals' assays are performed giving lot of useful information.⁸

Once its results completed and the treatment still seems promising, the *US Food and Drug Administration* (FDA) must give the permission and the research must be approved before clinical trials can be started and the treatment can be tested people.⁹

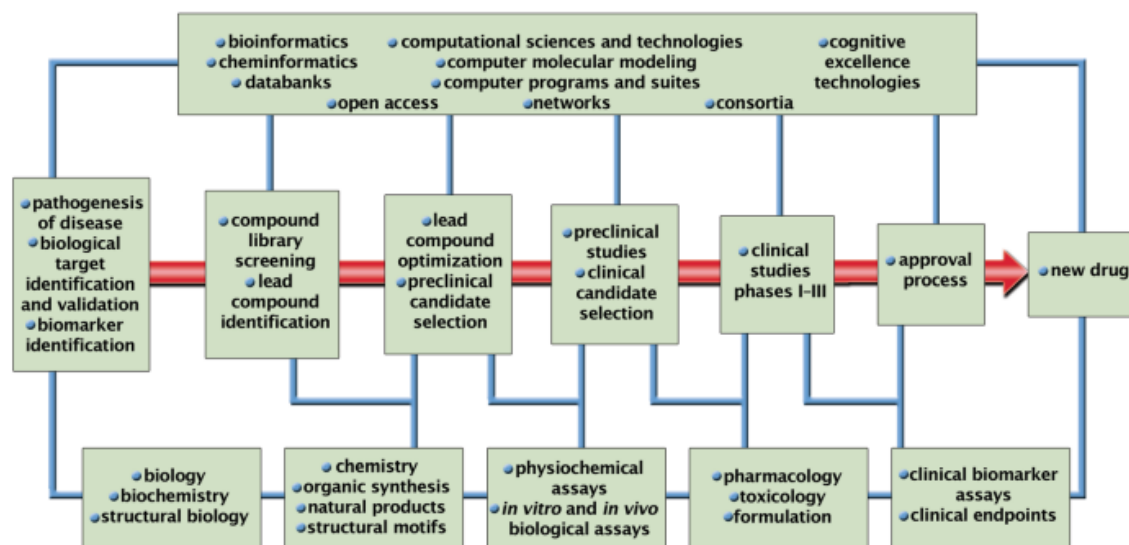


Figure 1. *The drug discovery and development process with its auxiliary arms.*¹⁰

In recent times, a significant drop of new hits has been detected. The lack of efficiency, a poor pharmacokinetic profile and preclinical toxicity are the main reasons for the failure in the drug development, in addition to problems with safety, potency, or other factors, preventing many molecules to move through next phase of clinical studies.¹⁰

This represents a very complex issue and the first point to focus on is the selection of the scaffold, in which modular structure makes it susceptible to structural variations, considering that the chemical diversity of the core affects the selectivity and the binding affinity towards the receptor.

At this stage, organic synthesis plays a key role to generate a large variety of structurally diverse compounds.¹¹ As becoming progressively more sophisticated, synthesis assumed a leading role in drug development, particularly in refining or optimizing the activity of compounds.¹² Many goals are expected to achieve in drug discovery process, such as the

developments of new synthetic strategies and novel structural models with more favourable pharmacokinetic properties, or the applications of biological knowledges on the target in order to synthesize a molecule able to fit the active pocket of the receptor. Nowadays, an active compound referred as “*hit*” could arise in different ways. The identification of ideal cores is based on empirical and retrospective observations of products from natural origin and bioactive molecules already on the market. Most drugs in clinical use are natural products or derivatives and analogues of natural products and many of them were used as lead compounds. Natural compounds, as already mentioned, have a historical importance, and represent an important resource in pharmaceutical field. For a long time, drugs have been discovered by studying their biological activity as a potential source of innovative therapeutic solutions for human health.¹³

Compounds from natural sources have retained their relevance in the drug discovery process, even considering the slight downturn determined by the development of combinatorial chemistry.

In the last decades, computational methods have increasingly acquired strong importance in the detection of new active molecules and their optimization in terms of efficacy and selectivity, effectively supporting the drug discovery process.

The advent of combinatorial chemistry has made possible the synthesis of large libraries of compounds and revolutionized the process involved in the discovery of new bioactive compounds.¹⁴ Those techniques allow to simultaneously synthesize large populations of compounds to screen for novel bioactivities, instead of synthesizing compounds in a conventional one at a time manner. Once the most promising compounds have been identified, more rational design of compounds let them to be tested, and *high*

throughput screening (HTS) led to quick in vitro assays for desired properties all at once, testing thousands of samples.¹⁵

Alternatively, starting from the 3D structure of the protein, the active site is identified through *Structure-based drug design* (SBDD) approach. Lot of information are combined from NMR, X-ray crystallography or homology modelling methods to elucidate crystal structures of proteins then deposited in available databank over the years, helping molecules design.¹⁶

To perform the structure-based drug design, a *de novo* approach can be used. New ligands are tested into the active pocket of the receptor, performing a preliminary essential analysis of the binding site and the key interactions for the determination of the biological activity.

A *Virtual Screening* (VS) study can also be applied to generate promising compounds libraries belonging to an available commercial database or starting from the synthons of a synthetic accessible way.¹⁷ Various types of drug-like or lead-like molecules are screened computationally against the well-known 3D structures of target proteins. The filtering of molecules libraries is provided by docking approach, where compounds are evaluated based on their binding affinity. It can also be useful to look for novel patent space around existing compound structures.

Not always the 3D protein's structure is available, and in this case *ligand-based drug design* (LBDD) approach helps to design drugs starting from the pharmacophore screening of already known binders of the chosen target in order to select new potential ligands with different scaffold but similar arrangement of functional groups.¹⁸

Combinatorial techniques are having a significant impact on all branches of chemistry, but especially on drug discovery by helping pharmaceutical companies to find new drug candidates in short times and at reasonable costs

in preclinical development phase. All such approaches generate a huge amount of data, assisting chemists in the lead optimization to the best possible structure and providing the basis to improve efficacy and safety profile of the chemical series. The output from a screening campaign is typically termed a molecule with demonstrated specific activity towards the target protein.

It is clear that a multidisciplinary approach including organic synthetic chemistry, computational methods and structural studies, represents the rational workflow for the identification of new chemical entities with therapeutic potentiality.¹⁹

1.2 Privileged scaffold in Drug Discovery

Small-molecules drug discovery programs requires a careful choice of the starting chemical scaffold.²⁰ A potential ligand must ensure high affinity for the selected target involved in the insurgence of the pathological condition. Moreover, the presence of several diversification points that could be modified or decorated, ensure a high structural variability and versatility which represent important starting points to develop libraries of biologically validated compounds. The chemical core and its diversification are crucial for the selectivity towards the selected receptor and affect at the same time chemical-physical properties and the pharmacokinetic profile of the molecule.^{21,22}

To identify new potential drugs and making compound libraries more chemically diverse and drug-like, the research has moved on the selection of “*privileged scaffold*”.

This term, firstly coined by Evans in the late 1980s, refers to structures could be a starting point to create active and selective compound collections. This

observation occurs from the development of selective antagonists of peripheral CCK-A receptor (*Cholecystokinin A receptor*) using 1,4-benzodiazepine-2-one as a scaffold. Making rational changes on the nucleus of known benzodiazepine anxiolytics, has favoured a gain in terms of affinity and selectivity for another target involved in gastrointestinal cancer, neuroprotection, and satiety. This scaffold has been demonstrated to be privileged as it is able to structurally mimic the peptide beta-turn, and a modest number of interactions rationally positioned can ensure a high binding affinity.²³

According to Evans, privileged structures can provide useful ligands as starting points for fragment-based design and rational modifications of such molecules could be a viable alternative in the search for new agonists and antagonists of selected receptors. The cores building blocks are characterized by a certain promiscuity that promotes a binding versatility for several biological targets and it is so common in drug molecules.^{22,24}

Most of these structures have been identified by retrospective analysis of bioactive molecules, in which recurrent features serve as interactions for a diverse array of receptors.²⁵

Although these properties are not entirely defined, certain regularly structural motifs occur as templates for derivatization. These chemical features share the presence of two or more condensed cycles or connected by simple bond, ensuring a certain rigidity and a strict orientation of functional groups that allow to decorate the structure through the introduction of specific substituents.²⁶

The most common structures are shown in fig 2. Many of these are commercially available and represents a valid source of lead with excellent drug-like properties for the design of compound screening libraries.

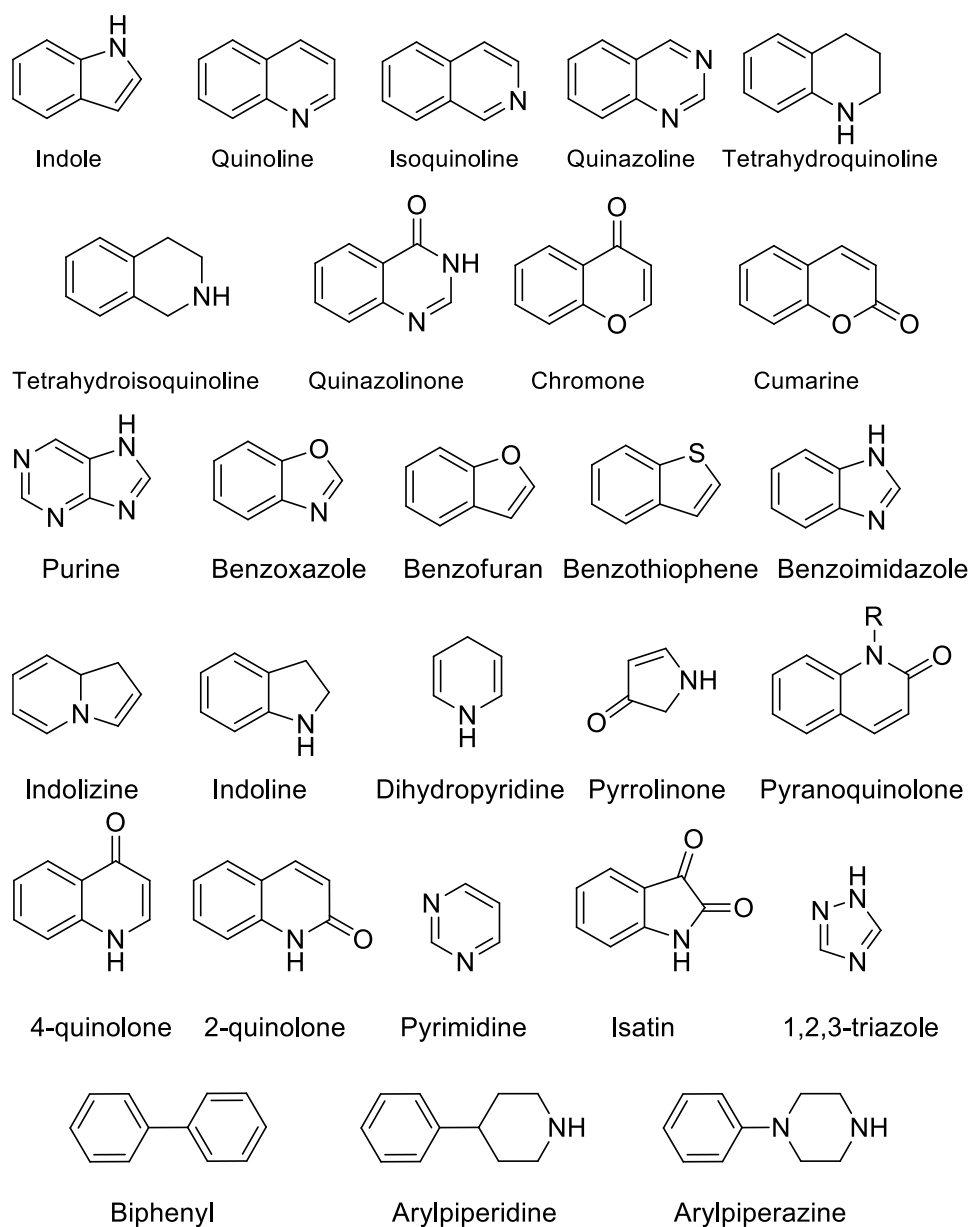


Figure 2. Structures of the most representatives privileged scaffolds.

The concept of privileged scaffolds has been evolved all over the years in parallel with the technologies for the drug discovery process, becoming an integrant part of the modern search of new chemical agents supporting combinatorial chemistry.

Nowadays, many techniques are applied aiming to prove a therapeutic benefit of the selected molecule towards the receptor, then used for the screening of small-molecule libraries.²⁷

Starting from a privileged scaffold, combinatorial approach represents one of the most used methods for the generation of *in silico* library.

The main purpose of combinatorial calculations such as the application of Virtual Screening is to accelerate lead discovery times and reduce the risk of failure in the next phases of experimental trials.¹⁷

Molecular modelling software has also played a key role in studying the binding site of the macromolecule to find a lead able to fit and bind the selected target.²⁸ When structural information of the chosen receptor is available, privileged fragment could be rapidly optimized. Low values kcal/mol of binding free energy are sufficient to ensure a significant selectivity, which can then be achieved with few key interactions towards the protein. In this way, is possible to rationally modify the chemical structure by introducing substituents able to interact selectively with specific target regions, reducing the promiscuity of the scaffold.

However, many candidate molecules are not accessible to the clinical trial stage due to poor pharmacokinetic profile and *in vivo* toxicity.

Obtaining a favourable pharmacokinetic profile in the design of a library is crucial to evaluate if a molecule is a right candidate to become a drug, or if its properties are not suitable to consider it in the development of new hit compounds.

1.3 Lead discovery: the role of organic chemistry

The advent of high throughput screening and the rapid generation of libraries of small molecules, define a new era in which the role played by organic chemistry in both academic and industries fields, continues to be one of the main drivers in the drug discovery process.¹⁴

Chemists need to keep up the demands of current research looking for ways to obtain large numbers of novel chemical entities, with sufficient activity in the initial screen that needs to be optimized into leads.

The recent process of synthetic approaches and subsequent biological assays cannot compete with the faster construction of *in silico* libraries through computational processes, without reagent consumption. The evaluation of the binding poses and the prediction of binding affinity by virtual screening provide at the same time the selection of the most promising compounds in a collection of thousands of molecules. Modern software led to analyse the binding mode for the molecular docking calculations and permits to identify the key points to be modified on the chosen hit or lead.²⁹

The possibility of maximising structural diversity through combinatorial studies increases the probability of finding new hits and leads but is not the only point to be taken in account. Other factors such as the chemical-physical properties of molecules which influence the pharmacokinetics, the cost of reagents and solvents and their availability on the market, the synthetic accessibility, affect the discovery process of lead compounds.

According to the virtual docking studies in the protein target, the chemical structure of the lead compound is used as a starting point for chemical modifications and the choice of a synthetic strategy is driven by computational prediction. Anyway, is not possible to synthesize all the

designed compounds, but, with the use of appropriate filters, the most synthetically accessible molecules can be selected.

During this stage, adequate pharmacokinetic properties for an examination of the efficacy *in vivo*, must be taken into due account.³⁰

Once a molecule is identified, the next step is to check its ADMET (Adsorption, Distribution, Metabolism, Excretion and Toxicity) properties. If the molecule has no toxicity and no mutagenicity either, it has potential for use as lead molecule.

To overcome pharmacokinetic liabilities, close attention needs to be paid to molecular weights, as well as to the physicochemical properties of lead molecules, such as lipophilicity (logP) and aqueous solubility which will affect oral bioavailability.

For the prediction of drug-likeness of new leads, Lipinski *et al.* reported the “rule of five”,³¹ based on a rationalization of experimental and computational approaches. It represents one of the most important tools to estimate the adsorption of valid scaffold.

It's clear that the aim of lead optimization step is maintaining favourable properties in lead compound and improving any deficiencies in its structure. The *in silico* prediction makes possible to exclude not-drug-like molecules before the synthesis, reducing the time and the costs needed.³²

The chemical synthesis of selected compound is performed relying on a wide range of tools as faster synthetic technologies, microwave-assisted,³³ sustainable techniques as flow³⁴ and photo chemistry,³⁵ as well as advances in nuclear magnetic resonance (NMR) methods,³⁶ rapid separations, and automated synthesis.^{37,38}

Synergistic workflow including several knowledges of organic and medicinal chemistry allows the preparation of various compound libraries, taking care of information generated at this stage.^{39,40}

CHAPTER 2

2.1 Oxadiazoles as privileged scaffolds

Oxadiazoles are aromatic penta-atomic heterocycles containing two nitrogen, two carbon, and one oxygen atoms that could be located in different position generating different regioisomers (Figure 3).

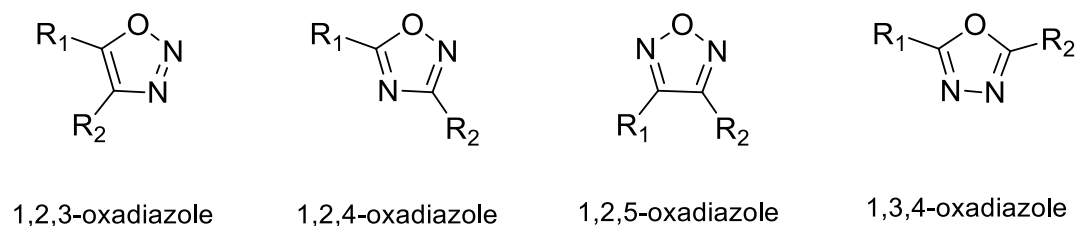


Figure 3. *Regioisomers of oxadiazolic nucleus.*

This nucleus presents several features that makes it an interesting scaffold for the synthesis of new classes of drugs.^{41,42}

In drug discovery process, oxadiazoles can be used as cyclic bioisosters of several groups such as esters, amides, carbamides, generally known to be not stable in biological media, making difficult the design of new potential drugs. Moreover, their stability in aqueous medium justifies the interest in the development of bioactive molecules containing this motif.

The number of publications related to oxadiazoles on medicinal chemistry has strongly increased in last twenty years. Moreover, many examples of bioactive molecules containing oxadiazolic systems in their structure have been described, with reported activity as antitumor, antioxidant, antibacterial, antiviral, antifungal, anti-inflammatory, insecticidal and antiparasitic agents.^{41,43,44,45}

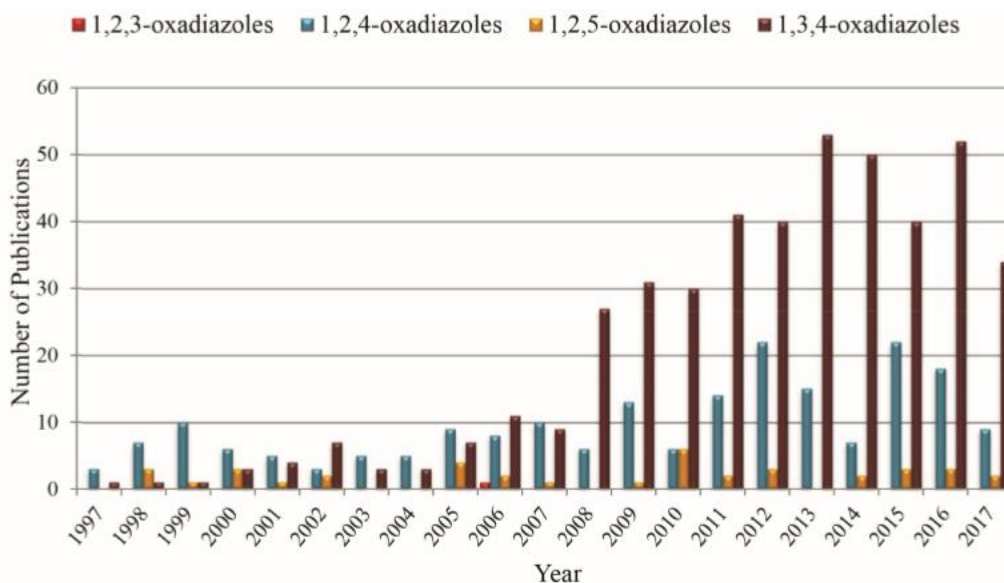


Figure 4. Publications related to oxadiazoles over the period from 1997 to 2017.⁴⁵

1,2,4 and 1,3,4- oxadiazoles are the most common used isomers in medicinal chemistry. The promiscuity of these structures confers them a high binding affinity for different targets, because of their aromaticity that promotes π - π *stacking* interactions with hydrophobic amino acids, and the presence of heteroatoms as hydrogen bonds acceptors that interact with polar amino acids sidechains.⁴⁵

Considerable differences have been shown in terms of aromaticity, although both regioisomer rings satisfy Hückel rule (a cyclic and planar system containing $4n + 2$ electrons).

Several studies, based on UV analysis of the bathochromic effect of 3,5-diphenyloxadiazole derivatives, demonstrated that 1,2,4 isomer does not have a satisfying aromaticity. These rings are characterized by poor aromaticity, better behaving as a conjugated diene. On the other hand, 1,3,4 derivatives show a greater aromaticity; the presence of two phenyl rings

considerably increases the observed λ_{\max} value, probably due to the symmetry of substituents.⁴⁶

These physiochemical properties reflect in the reactivity of each compound. Their stability represents a metabolic advantage to increase the half-life of a drug, while their less reactivity could affect the relative yield in the synthesis of some derivatives.

The two regioisomers are also characterized by a different lipophilic-hydrophilic balance mainly related to the evaluation of the dipole moment. 1,2,4-oxadiazoles shows a low level of dipole moment resulting more lipophilic than 1,3,4 regioisomer.^{44,45}

All these parameters need to be considered in the use of oxadiazolic scaffold as they strongly affect the pharmacokinetic profile, even if the presence of different substituents on the building blocks is crucial for the target modulation.

2.2 1,2,4-oxadiazoles: synthesis and reactivity

1,2,4-oxadiazoles and their versatility as starting synthons and target compounds, have strongly increased the curiosity of chemists particularly in the last decades.

Nowadays, these heterocyclic scaffolds have gained importance considering their ability to behave as bioisoster of esters and amides, with several applications in medicinal chemistry and material science. Many researchers have synthesized different derivatives containing oxadiazoles with the concept of bioisosterism.

The first synthesis of 1,2,4-oxadiazoles was achieved by Tiemann and Krüger in 1884, initially named furo[ab]diazoles.⁴⁷ Only in the early 70's

their employment as main scaffold have been explored following the developments of drug design process.

The majority of 1,2,4-oxadiazoles presents a general structure with two substituents in both positions C-3 and C-5.

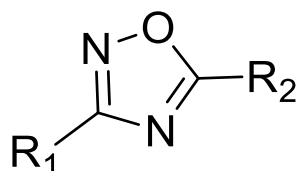


Figure 5. Structure of general 3,5 disubstituted 1,2,4-oxadiazole.

The classical approach for the synthesis of these heterocyclic compounds can be carried out following the two most common strategies: via 1,3-dipolar cycloaddition and the amidoxime route.⁴⁵

Both consider different reagent sources for the C-3 and C-5 substituents and require the use of nitrile as precursor, that can end up being linked either at position 3 in case of 1,3-dipolar cycloaddition, or at 5 in case of the amidoxime one. Moreover, the choice of each synthetic approach could be driven by the commercial availability of precursor in order to obtain a specific functional group on the heterocyclic building block.

The 1,3-dipolar cycloaddition is a chemical reaction between a 1,3-dipole and a dipolarophile to give five-membered ring and it's widely used to perform a regio- and stereoselective synthesis.

The synthesis of 1,2,4-oxadiazoles through this route can be achieved by cycloaddition between nitrile and nitrile N-oxide, as shown in Figure 6. However, nitrile N-oxide is not a commercially available reagent, so it needs to be synthesized from the aldehyde, which is reacted with hydroxylamine

to obtain the correspondent oxime, and then converted to the desired intermediate by chlorination reaction. Such reactions are characterized by the use of less manageable reagents and uncontrolled reaction conditions.

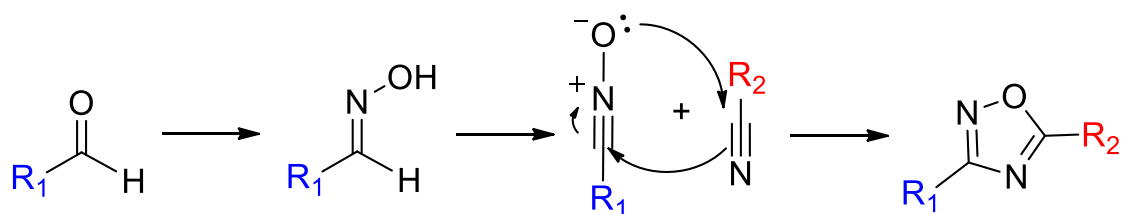


Figure 6. 1,3-dipolar cycloaddition.

Generally, the amidoxime procedure is the most common used strategy for the synthesis of 1,2,4-oxadiazoles (Figure 7).

The amidoxime intermediate is an oxygen nucleophile that can be easily obtained by reaction of the corresponding nitrile with hydroxylamine. It reacts with an activated carboxylic acid derivative such as carboxylic acid groups, esters, anhydrides, acid chlorides, aldehydes, and followed by intramolecular cyclodehydration resulting in the formation of O-acylamidoxime, an intermediate that which further undergo heterocyclization.

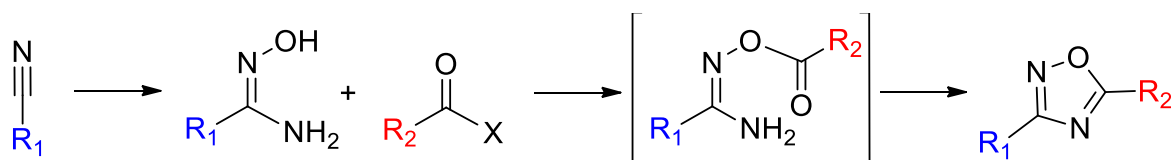


Figure 7. Amidoxime route.

However, these methods have many drawbacks such as the requiring of coupling and oxidizing reagents to activate carboxylic group. These reagents are costly, and reaction is performed using organic solvents at drastic condition.

By considering the importance of this procedure, many progresses have been made in the field of green chemistry to make environmentally friendly and economically beneficial. Important key points are the elimination of solvents in the synthesis or the substitution of hazardous solvents with environmentally benign ones, use of catalysts, solid support materials, microwave-mediated heating, and others.

This class of heterocycles characterized by different and complementary features, can be considered multi-functional rings and results to be the protagonists of several reactions.⁴⁸

2.3 Biological applications of 1,2,4-oxadiazoles

A wide gamut of 1,2,4-oxadiazoles are found to possess several biological activities as anticancer, anti-inflammatory, anticonvulsant, antiviral, antibacterial, anti-Alzheimer as well as specific inhibitor proprieties against enzymes.^{44,45}

1,2,4-oxadiazoles have been started to become an essential part of pharmacophores since their ability to act as bioisosters of esters and amides have been taken into account in the frame of a drug design process.

Moreover, their drug-like desirable properties such as lipophilicity, aqueous solubility, metabolic stability, strongly influence and highlight their relevance as “*druggable*” compounds.⁴⁹

The first marketed drug containing 1,2,4-oxadiazoles moiety dates to 1960's is named *Oxolamine* and have cough suppressant activity.⁵⁰

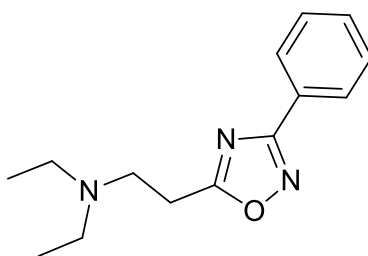


Figure 8. *Oxolamine.*

In recent years, many medicinal chemistry's studies have been focused on the use of 1,2,4-oxadiazoles. This pharmacophore component can be found in the structure of molecules with reported bioactivity to different targets and related to a wide range of diseases. Different applications have been described in many classes drugs as anti-asmatic, antidiabetic, anti-inflammatory, antimicrobial agents, immunosuppressants, anticancer.

Recently, a new 1,2,4-oxadiazole derivative known as *Ataluren* has been successfully tested against cystic fibrosis and Duchenne muscular dystrophy. These genetic disorders are caused by the presence of premature stop codons (PTCs), that ribosomes recognize as early termination signal and translate for abnormal proteins.^{45,51}

Ataluren acts in the translation phase allowing to bypass the PTC sequence to obtain a functional protein. New fluorinated derivatives have been synthesized through the esterification of the carboxylic group and by varying the position and number of fluorine atoms on the aromatic ring. These compounds showed an improved readthrough activity than the lead compound. Moreover, a series of new derivatives, without fluorine and

carboxylic group, have been selected from a database using a ligand based virtual screening.

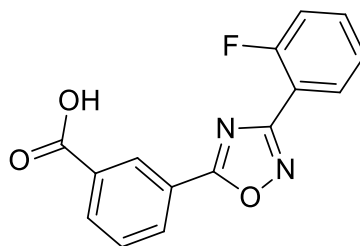


Figure 9. *Ataluren.*

Based on molecular modelling studies, a series of 3-(5-bromo-2,3-dimethoxyphenyl)-1,2,4-oxadiazoles has been recently synthesized and evaluated as potential dopamine agonists for the treatment of Parkinson's disease.⁴⁹ Once again, the choice of the 1,2,4-oxadiazole system was the result of its efficiency in replacing the amide group in a series of benzamide analogues with high affinity for dopamine receptors.

As neuroprotective agents, a series of 3,5-diaryl-1,2,4-oxadiazoles have been designed as potential probes for β -amyloid plaques occurring in the early state of Alzheimer disease.⁴⁸

The anti-inflammatory activity of 3,5-disubstituted oxadiazoles is among the most investigated. A similar activity to that of the phenylbutazone was shown by 5-methyl-3-phenyl-1,2,4-oxadiazole, and subsequently many examples of this heterocyclic compounds have been evaluated and reported as dual cyclooxygenase/5-lipoxygenase inhibitors, coumarin and 3-phenyl-1,2,4-oxadiazole-5-carbohydrazide derivatives.⁴⁸

Several 1,2,4-oxadiazoles are inhibitors of NF- κ B activity, whose activation mediates the expression of pro-inflammatory factors.⁵²

The use of compounds as polyphenols with anti-inflammatory and antioxidant properties consists also in a valid therapeutical approach.⁵³ The known properties of resveratrol, an antioxidant compound with stilbene structure, are due to the E configuration of ethylene bridge together with the hydroxy/methoxy substitution of aromatic. The E stilbene bridge has been replaced with 3,5-diphenyl-1,2,4-oxadiazoles to maintain the geometry of molecule obtaining a series of resveratrol derivatives with strongest anti-inflammatory and antioxidant activity than the lead.⁴⁸

The non-steroidal drugs (NSAIDs) are the most used in the anti-inflammatory therapy acting as inhibitors of COX enzymes responsible of metabolic transformation of acid arachidonic to prostaglandins.

Traditional NSAIDs have been shown to have the least amount of systemic side effects, particularly gastrointestinal toxicity due to the indifferent inhibition of all the COXs isoforms. Therefore, the selectivity between COX-1/COX-2 enzymes represents a research area of great interest.⁵⁴

Selective anti-inflammatory agents against COX-2 led to the generation of new NSAIDs.⁵⁵ In this frame, there are ketoprofen and naproxen analogues that acts as inhibitors of this enzyme, incorporating 1,2,4-oxadiazole motif.⁵⁶

CHAPTER 3

1,2,4-oxadiazoles as useful scaffolds for the development of new anti-inflammatory and antibacterial agents

3.1 Structure-based screening for the discovery of 1,2,4-oxadiazoles as promising hits for the development of new anti-inflammatory agents interfering with eicosanoid biosynthesis pathways

3.1.1 Overview on inflammatory response

The survival of all organisms depends on the removal of all external invading agents and damaged tissues. Such functions are mediated by inflammation, a complex host response which involves a variety of cells, signalling proteins, and other mediators.⁵⁷

This protective reaction is responsible for eliminating the initial cause of cell and tissue damage resulting from the initial insult, and for restoring the homeostasis through repairing processes.

Inflammatory condition is characterized by five cardinal signs used to make the diagnosis: pain (*dolor*), heat (*calor*), redness (*rubor*), swelling (*tumor*), and loss of function (*function lesa*). Such external manifestations are the consequence of vascular reactions and leukocyte recruitment, both activated by mediators derived from plasma proteins and various types of cells, serving as alarm signals. When the body encounters a foreign substance such as viruses, bacteria, or toxic chemicals, or suffers an injury, caused by physical or chemical insults, the presence of the damage or the infection is detected by resident cells. Dendritic cells, phagocytes, macrophages, monocytes, neutrophils, and other cells of the immune system can recognize and bind exogenous agents by expressing PRR (Pattern Recognition Receptors) proteins (Toll-Like Receptors, TLRs, are an example) leading to the production of several inflammatory mediators, including chemokines, cytokines, vasoactive amines, eicosanoids, and products of proteolytic cascades.⁵⁸

While the initial encounter between the harmful stimulus and these cells takes place in the connective tissue, the vascular reaction triggered by these interactions occurs immediately after and dominates the early responsive phase.

The main vascular reactions are a vasodilation that results in increased blood flow and a higher permeability of vessels, both aimed to bringing blood cells and proteins to the site of infection. The extravasation of leucocytes prevents the exit of erythrocytes through a selective mechanism that involves the inducible interaction of endothelial-cell selectins with integrins and chemokine receptors on leukocytes. Several cytokines produced in the inflammatory process promotes their migration through endothelial spaces, generating chemical gradients.⁵⁹

Once neutrophilic migration stops at the site, the direct contact with pathogens or the actions of cytokines released by tissue-resident cells allow them to be activated. The leucocytic activation results in the phagocytosis of microorganisms and their consequent intracellular destruction by releasing toxic contents such as reactive oxygen species (ROS) and reactive nitrogen species.⁵⁸

The removing of the insult's causes and the following resolution phase are crucial for a successful acute inflammatory response.⁶⁰

Before restoring the functional and structural homeostasis, the inflammatory mediation shall be terminated. This involves the neutralization of chemical mediators, the normalization of vascular permeability and the cessation of leukocyte migration with subsequent apoptosis of extravasated neutrophils. The transition from inflammation to resolution is mediated by both pro-inflammatory and anti-inflammatory pathways, in which several molecules

play the two different roles by the case in a balanced and controlled mechanism.⁶¹

Neutrophils start to produce mediators able to limit the inflammatory reaction, while necrotic debris and inflammatory cells are removed by phagocytes and lymphatic drainage. Cytokines are secreted by leucocytes to reorganize the tissue microanatomy and the formation of new vessels ensures the transport of nutrients and growth factors for the proliferation of fibroblasts and collagen deposition. The persistence of the foreign bodies, or some interferences with the normal healing process, generate a dysregulation of the repairing phase of acute inflammation leading to a chronic response. Depending on the extent of the initial tissue injury, or on its progression, chronic inflammation state may be followed by restoration of normal structure and function or may lead to scarring, a repairing tissue phase resulting from its destruction.⁵⁸

3.1.2 Inflammatory mediators and eicosanoids pathway: the role of PGE₂

A wide range of mediators coordinates the inflammatory state, acting as complex regulatory networks. As described in the previous paragraph, inflammatory mediators can be produced by different cells, particularly specialized leucocytes in the site of infection or derived from plasma precursors.⁵⁸

Mediators from the latter, such as complement fragments, coagulation systems components and kinins, are generated by proteolytic processing of inactive precursors from hepatic origins in the extracellular fluid. Their functions are related to different aspects of inflammatory response, in

particular granulocyte and monocyte recruitment and mast-cell degranulation, thereby affecting the vasculature.

Cells-derived mediators are normally stored in intracellular granules and released through cellular activation. This is the case of vasoactive amines, histamine and serotonin, which are secreted by mast cells, basophiles and platelets degranulation. Their effects cause respectively an increased vascular permeability and vasodilation, or vasoconstriction, depending on the context.

Other mediators are *de novo* synthesized and released in response to an appropriate stimulus by inducers of inflammation. Inflammatory cytokines are produced by activated macrophages and mast cells, aiming to activate the endothelium and leukocytes. The main cytokines of acute inflammation process are tumour-necrosis factor- α (TNF- α), IL-1, IL-6 and a group of chemotactic cytokines known as chemokines.

Other examples of molecules involved in this response are ROS, NO, proteolytic enzymes, neuropeptides, such as substance P, and platelet-activating factors (PAF) with diverse roles in inflammation process.⁶²

Noteworthy, among the main classes of pro-inflammatory mediators, there are lipid mediators derived from arachidonic acid (AA) metabolism, named eicosanoids.⁶³

The eicosanoids biosynthesis usually initiates from the activation of cytosolic phospholipase A2 (PLA2) induced by mechanical, physic or chemical stimuli, such as intracellular Ca^{2+} ions, in response to an extracellular signal. The mentioned activated lipase provides the oxidation of AA, characterized by a 20 carbons chains and released from cell membranes. The AA metabolism may be articulated into three different branches for the synthesis of inflammation mediators: cyclooxygenases

(COX) pathway, leading to the synthesis of prostaglandins (PG) and thromboxane (TX); lipoxygenases (LO) pathway, involved in the synthesis of leukotrienes (LT) and lipoxins (LX); and cytochrome P450 (CYP450) pathway, producing dihydroxyeicosatrienoic acids (DHETs).

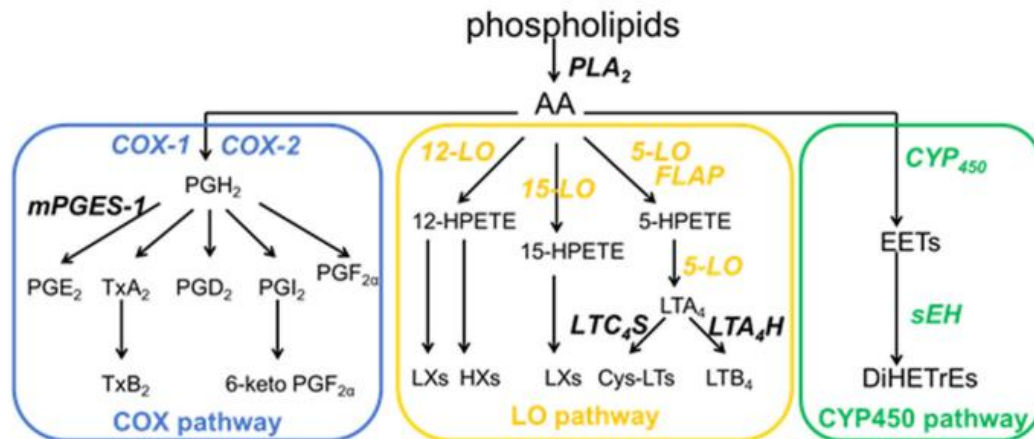


Figure 10. Three different pathways for the synthesis of inflammatory mediators from AA.

In details, the COX activities are induced by two isoforms of this enzyme: COX-1, constitutively expressed, and COX-2, the inducible isoform. The first step of this pathway is the initial oxidation of AA to an intermediate, prostaglandin G₂ (PGG₂), then reduced into the unstable peroxide intermediate prostaglandin H₂ (PGH₂).⁶⁴

Prostaglandin E₂ synthase is an inducible enzyme that catalyse the conversion of PGH₂ into prostaglandin E₂ (PGE₂) and involved also in the synthesis different prostanoids such as prostacyclin (PGI₂), prostaglandin D₂ (PGD₂), prostaglandin F_{2α} (PGF_{2α}) and thromboxane (TXA₂).⁶⁵

The aforementioned enzyme may be found in three different isoforms: *current expressed cytosolic prostaglandine E₂ syntase* (cPGES), *microsomal prostaglandin E₂ synthase 1 and 2* (mPGES-1 and mPGES-2).

The cPGES is a constitutive isoform involved in the basal production of PGE₂, functionally coupled to the activity of COX-1.

mPGES-1 is characterized by a reduced basal expression. Pro-inflammatory factors, rapidly induced this form by generating a massive production of PGE₂, with a subsequent increase of the inflammatory response, in conjunction with the activity of the enzyme COX-2.⁶⁶

mPGES-2 is a constitutive membrane enzyme expressed as integral membrane protein of the Golgi apparatus and is released as an active enzyme in the cytosol, even if its pathophysiological function is not entirely known. PGE₂ is released from the cell and express its actions through the link to specific G protein coupled receptors (EP1-4). The activation of these receptors triggers different transduction pathways involved in various biological functions as reported in Figure 11.⁶⁷

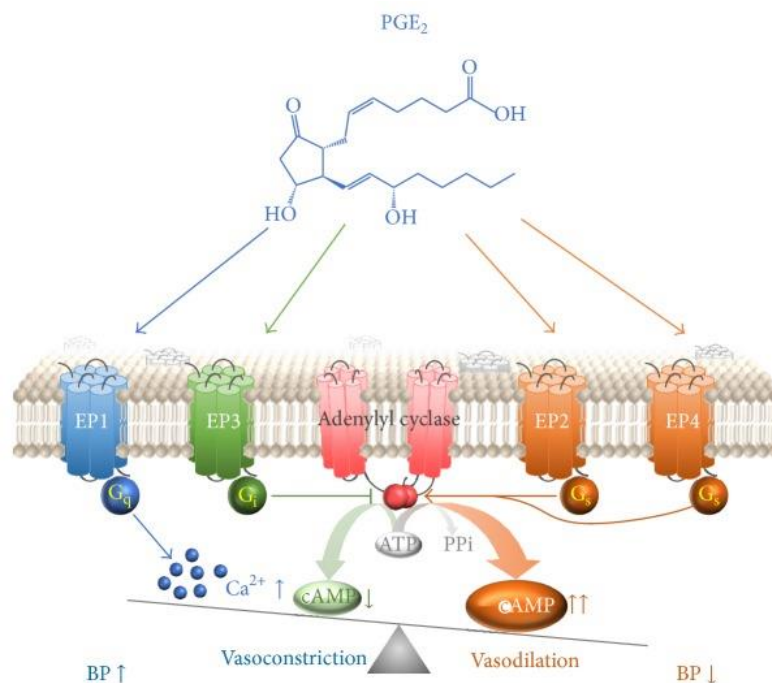


Figure 11. PGE₂ receptors.

Since PGE₂ plays a pivotal role in the evolution and progression of inflammatory and tumour diseases, many recent studies have reported the implication of the interference with PGE₂ biosynthesis as a therapeutic strategy.⁶⁸

Its production in higher concentration than homeostatic conditions, induces the main signs of flogosis such as oedema, redness, high temperature, both in the inflamed district and at central level as fever response and hypersensitivity of nociceptive fibres. Moreover, it is also involved in pro-carcinogenic processes, promoting cell proliferation, angiogenesis, and metastasis.⁶⁴

Several recent studies identified the isoform mPGES-1 as a promising target for inflammation and cancer state.^{69,70} Indeed, many pharmacological investigations reported an up-regulation of mPGES-1 induced by IL-1 β , LPS, TNF- α , and other inflammatory stimuli, and a connection between the concentration of PGE₂ and cancer progression.^{69,71} This research work takes place in this frame, with the aim to identify new chemical entities able to interfere with the activity of this enzyme involved in the synthesis of PGE₂. A brief description of mPGES-1 is here reported as follow.

3.1.3 Microsomal prostaglandin E₂ synthase-1 (mPGES-1)

Microsomal prostaglandine E₂ synthase-1 (mPGES-1) is an inducible membrane protein consisting of 152 amino acids, GSH-dependent, located in the endoplasmic reticulum. It was firstly reported in 1999 by Jakobsson et al.⁷² belonging to the superfamily of the "*Membrane-Associated Proteins involved in Eicosanoid and Glutathione metabolism*" (MAPEG family). Additionally, this family includes *5-lipoxygenase activating protein* (FLAP),

leukotriene C4 synthase and *microsomal glutathione transferases-1* (MGST-1) with which mPGES-1 presents 39% of structural homology.⁷³

As recently revealed by high resolution X-ray crystal structure,⁷⁴ mPGES-1 is a membrane homotrimer with three active sites partially occupied by the glutathione (GSH) as cofactor. Each monomer is characterized by four transmembrane helices with the active sites located toward the cytoplasmic region of the protein.

The folding structure of the enzyme is characterized by a cone-shaped cavity opened towards the cytoplasm giving the access to the catalytic site. The four helices are linked by several polar residues and two water molecules. Conformational modifications are mediated by helices I and IV leading the enzyme to change the inactive to the active form., so PGH₂ may be accommodated into the active pocket via its peroxofuran core.⁷⁵

GSH binds the protein in a U-shaped conformation through hydrogen bonds and π -stacking interactions in which different aminoacidic residues of helices are involved.

According to the proposed mechanism,⁷⁴ GSH cofactor mediates the conversion of PGH₂ into PGE₂. The thiol function of GSH is deprotonated by Ser127 to give the thiolate anion. The nucleophilic attack on the endoperoxide oxygen atom of PGH₂, destroying the peroxidic bond and giving the S-O bond. Subsequently, Asp49 mediates the abstraction of the proton at C-9 followed by the cleavage of S-O bond, which results in the regeneration of GSH and in the formation of PGE₂.⁷⁶

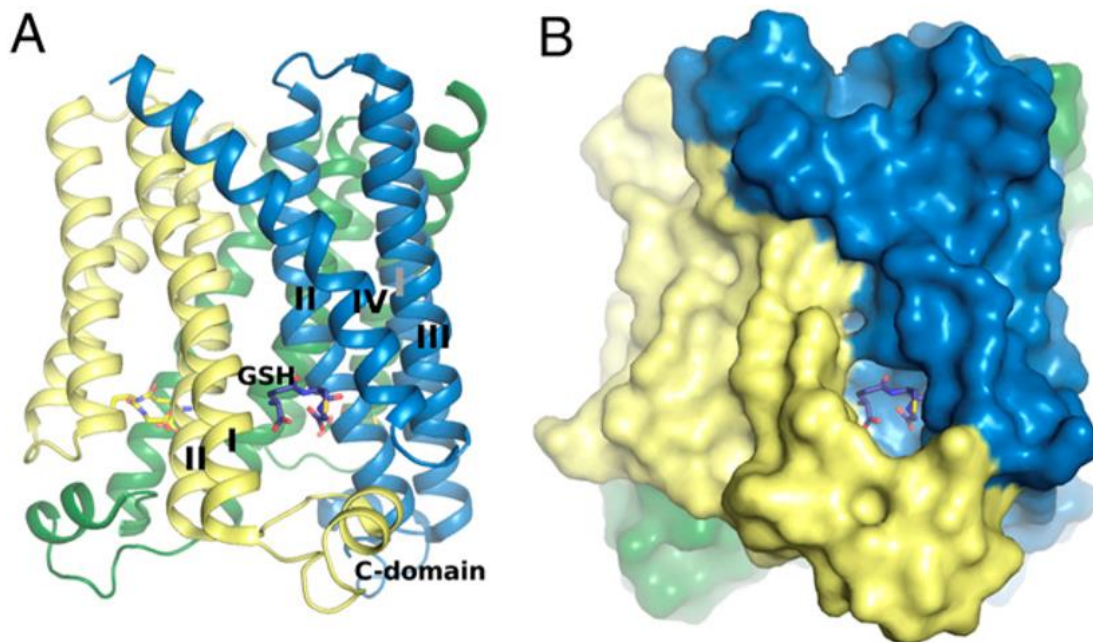


Figure 12. A) Crystal structure of mPGES-1 in presence of GSH cofactor; B) Representation of the trimeric surface.

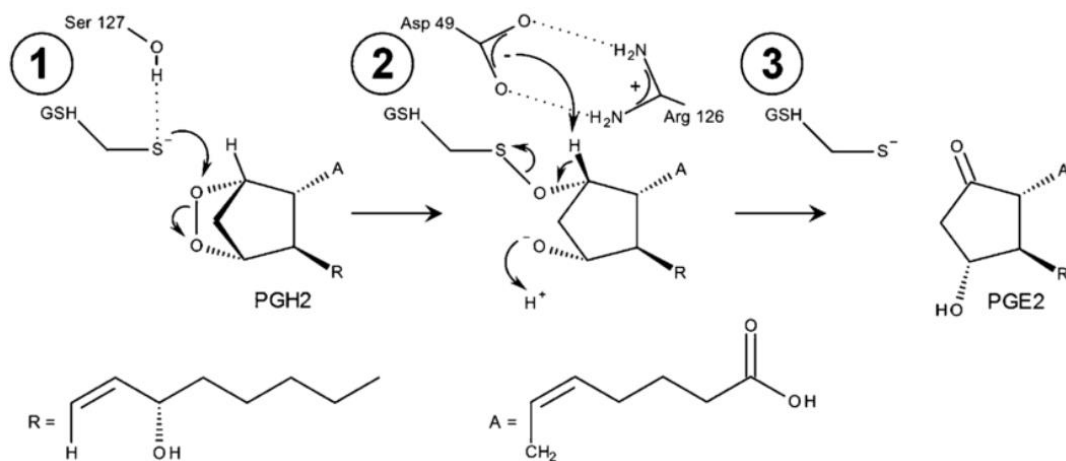


Figure 13. Proposed mechanism for the conversion of PGH₂ into PGE₂.⁷⁴

The current anti-inflammatory therapy includes the use of non-steroidal anti-inflammatory drugs (NSAIDs). Their mechanism is based on the non-

selective inhibition of COXs, leading to the inhibition not only of PGE₂'s production but also of other prostaglandins involved in important physiological roles.

Long-term treatment with this class of drugs causes severe side effects especially at gastro-intestinal level, such as haemorrhage and mucosal ulceration, arising from the inhibition of COX-1 activity.⁵⁶

Alternative strategies, in particular selective inhibitors of COX-2 (Coxib), were developed to overcome these undesirable effects and to improve the safety of anti-inflammatory therapy.⁷⁷ However, even if more tolerated at gastrointestinal level, they were shown to relate to increased vascular risk, including myocardial infarction, pulmonary and systemic hypertension, due to an unstable balance between PGI₂ and TXA₂.⁵⁴

mPGES-1 represent an interesting new target for the anti-inflammatory therapy: its inhibition allows to selectively reduce the production of PGE₂ released in response to inflammatory stimuli, without interfering with the basal production of other PGs. This mechanism reduces adverse effects caused by previously cited classes of drugs, ensuring a higher safety profile, and at the same time maintaining a comparable therapeutic efficacy.^{78,79,80}

Considering that mPGES-1 is placed downstream in the prostanoid biosynthetic pathway, its modulation induces an inhibition of PGE₂ synthesis and simultaneously the increase of other PGs, in particular PGI₂. From a safety point of view, this represents an important advantage as it reduces the cardiovascular risks of selective inhibitors of COX-2, and gastrointestinal side effects related with unselective COXs inhibition of traditional anti-inflammatory therapy.⁸¹

Starting from these observations, it's clear mPGES-1 represents an interesting and advantageous target involved in anti-inflammatory therapy since it results to be overexpressed in many chronic inflammatory diseases for which long-term treatment is required.

Moreover, its use is not limited to inflammatory condition. This enzyme plays a key role in several pathological conditions such as pain, fever, many neurologic disorders as Alzheimer's disease, multiple sclerosis, amyotrophic lateral sclerosis. Its overexpression is also relevant in a wide gamut of tumors, such as gastrointestinal, brain, thyroid, breast cancers, playing an important role in cancer progression.⁷⁰

The selective inhibition of mPGES-1 offers a wide range of opportunities for therapeutic application. Although mPGES-1 is considered a validated and promising therapeutic target for drug discovery, there are only a few published records of small-molecule inhibitors targeting the enzyme and exhibiting some *in vivo* activity. There are several examples of compounds that were identified and developed to target mPGES-1 that could be classified into three different groups: natural compounds; endogenous lipid, fatty acids and PGH₂ analogs; known anti-inflammatory drugs or inhibitors of leukotrienes biosynthesis.⁸² One of the most promising compounds belonging to the latter class is MK-886 which can inhibit FLAP (IC₅₀ = 26 nM) and mPGES-1 *in vitro* (IC₅₀ = 1.6 μM).^{83,84} This result reinforces the similarity among the members of MAPEG. Unfortunately, many studies have demonstrated that this compound is unlikely to serve as an mPGES-1 inhibitor *in vivo* to reduce PGE₂ production. Nevertheless, MK-886 has been used as a basis for the development of more potent and selective mPGES-1 inhibitors.⁸⁵ Although mPGES-1 is considered a validated and promising therapeutic target for anticancer drug discovery, there are only a few

published records of small-molecule inhibitors targeting the enzyme and exhibiting some *in vivo* activity. Since the large number of compounds targeting mPGES-1 developed so far is characterized by structural and pharmacokinetic properties with an extensive variability,^{86,87} this research project was driven by the application of several well-linked steps in a multidisciplinary approach aiming to find promising molecules targeting this protein in the frame of a drug design project.

3.1.4 Combinatorial Approach

This work was aimed to explore the potentiality of 1,2,4-oxadiazole as unprecedented chemical core for mPGES-1 inhibition.

In the introduction section, I extensively discussed both the rationale of the selection of this heterocyclic scaffold, as well as the relevance of mPGES-1 as established target for development of anti-inflammatory and anti-cancer agents.

For the design of a combinatorial library of 3,5-disubstituted 1,2,4-oxadiazoles, we selected the amidoxime route (Figure 7) since it offers many advantages over the alternative cycloaddition route (Figure 6) such as a lower number of synthetic steps, reducing time consuming, cost, and environmental impact, and first of all the high modularity of the process due to the commercial availability of a wide variety of nitriles and carboxylic acids that should maximize the potential chemodiversity around the heterocyclic scaffold.

The applied computational method is based on a sequence of techniques described as follow. Once the building blocks and the synthetic scheme were determined, CombiGlide software^{88,89} was used for the generation of all the possible compounds deriving from the combination of the commercially

available reagents, according to the chosen protocol. A wide combinatorial library was generated *in silico* combining 55 nitriles and 4888 carboxylic acids to obtain a final campaign of 273,728 novel compounds.

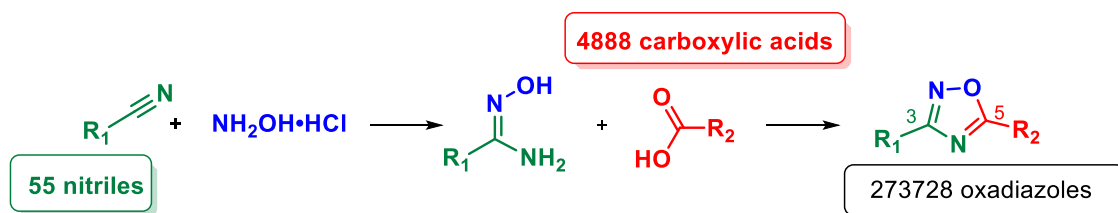


Figure 14. Generation of combinatorial library of 1,2,4-oxadiazoles using CombiGlide software.

All compounds were submitted to Ligprep software,⁹⁰ able to get energy minimization and provide many possible ionizations states and tautomers at physiological values of pH.⁹⁰

The relevant pharmaceutical properties of the designed molecules were calculated through Qikprop software,⁹¹ a module of Schrödinger LLC that accurately predicts the pharmacological profile of molecules. The prediction of pharmacokinetic parameters is strongly relevant to evaluate if a compound is a right candidate to become a drug, or if its properties are not appropriated to consider it in the frame of a drug design project.

In this way, only drug-like compounds are selected while the remaining compounds are discarded from the calculation.

The Lipinski's rule of five was applied as a filter used to estimate the absorption of the right hits, discarding in this way “non-drug like” compounds.⁹² The “five” refers to the limits, which are multiples of 5 and this prediction strategy consists of four important properties:

- a molecular weight no higher than 500 (MW <500)

- no more than 5 hydrogen bond donors
- no more than 10 hydrogen bond acceptors
- a logP less than 5 ($\log P < 5$)

The application of QikProp⁹³ and LigFilter⁹⁴ generated a final library of 150,512 compounds then submitted to structure-based molecular docking analysis on the 3D crystal structure of mPGES-1 (PDB code: 5TL9).⁹⁵ Glide software⁹⁶ was used to select a small molecules library with a potential activity on mPGES-1 by means of virtual screening workflow.

In detail, the applied VSW (Glide Software) consisted in three subsequent phases which operate with a gradually increasing precision. The *HighThroughput Virtual Screening* (HTVS) phase saves the top 60% of compounds ranked by docking score for the subsequent step. The next *Standard Precision* phase (SP) outperforms the first step in both sampling and scoring performances. Again, the 60% of top-ranked poses of HTVS were filtered according to docking score values, then submitted to the last phase of *Extra Precision* (XP), the most accurate step that save the top 70% of compounds ranked by docking score of the previous SP.

Consequently, the analysis of the docking poses through molecular docking calculations was carried out in order to select the most promising compounds, among a large collection of designed synthetically accessible 1,2,4-oxadiazole. The investigation of the binding mode of compounds leading to understand all the key interactions involved in the modulation of mPGES-1 in the binding sites, delimited by polar, charged, aliphatic and aromatic residues (Val24ChainC, Tyr28ChainC, Phe44ChainC, Arg52ChainC, His53ChainC, Pro124ChainA, Ser127ChainA,

Val128ChainA, Tyr130ChainA, Thr131ChainA, Leu132ChainA, Gln134ChainA).

A small library of 11 molecules was generated applying many specific filters on 4064 selected docking poses. The screened molecules were analysed considering docking score, binding mode and interactions established with the receptor required for the inhibition.

Considering also practical issues such as the chemicals costs, the actual commercial availability of reagents and the number of synthetic steps, all the selected compounds share the presence of 4-(thiophen-3-yl) phenyl substitution at position 3 and variable 5-substitution on the 1,2,4-oxadiazole ring.

A current problem in a drug design project is the presence of compounds that react in a non-specific way with numerous biological targets. The evaluation of these chemical entities belonging to “Pan-Assay Interference compounds”, was carried out with SwissADME⁹⁷ in order to avoid this issue. Furthermore, for each successfully processed compound, QikProp⁹³ performed a more detailed analysis of other pharmacological relevant features, producing several descriptors mainly related to ADME (absorption, distribution, metabolism, and excretion) and different types of reactive functional groups that may cause false positives in *high-throughput screening* (HTS) assays, or any problems in vivo such as decomposition, reactivity, or toxicity.

In Table 1 all the performed calculations according to QikProp software are summarized. The values of #stars in the second column indicates the number of property or descriptor values that fall outside the 95% range of similar values for known drugs (recommended values: 0-5). A vast number of stars suggests that compound is less drug-like than molecules with few stars.

Many descriptors are included in the determination of #stars that we have taken into account to generate our library of promising ligands:

- rfvFG, the number of reactive functional groups (range: 0-2)
- mol_MW, molecular weight of the compound (range: 130.0-725.0)
- SASA, total surface accessible solvent area, expressed in Angstrom (range: 300.0 – 1000.0)
- FOSA, hydrophobic component of the SASA (saturated carbon and attached hydrogen, range: 0.0 – 750.0)
- FISA, hydrophilic component of the SASA on N, O, H bound to hetero-atoms and carbonyl C (range: 7.0 – 300.0)
- PISA, π (carbon and attached hydrogen) component of the SASA (range: 0.0 – 450.0)
- WPSA, weakly polar component of the SASA (halogens, P, and S, range: 0.0 – 175.0)
- donorHB, number of hydrogen bonds that would be donated by the solute to water molecules in an aqueous solution (range: 0.0 – 6.0)
- accptHB, number of hydrogen bonds that would be accepted by the solute from water molecules in an aqueous solution (range: 2.0 – 20.0)
- QplogPC16, hexadecane/gas partition coefficient (range: 4.0 – 18.0)
- QplogPoct, octanol/gas partition coefficient (range: 8.0 – 35.0)
- QPlogPw, water/gas partition coefficient (range: 4.0 – 45.0)
- QplogPo/w, octanol/water partition coefficient (ranges: 2.0 – 6.5)
- QplogS, aqueous solubility, log S. S in mol dm⁻³ is the concentration of the solute in a saturated solution that is in equilibrium with the crystalline solid (range: 6.5 – 0.5)

- CIQPlogS, conformation-independent predicted aqueous solubility, $\log S$. S in mol dm^{-3} is the concentration of the solute in a saturated solution that is in equilibrium with the crystalline solid (range: -6.5 – 0.5)
- QPPCaco, apparent Caco-2 cell permeability in nm/sec . Caco-2 cells are a model for the gut-blood barrier. QikProp predictions are for non-active transport (range: <25 poor, >500 great)
- metab: number of likely metabolic reactions (range: 1 – 8)
- QplogKhsa, the predicted binding to human serum albumin (range: -1.5 – 1.5)
- PercentHumanOralAbsorption, human oral absorption on 0 to 100% scale. The prediction is based on a quantitative multiple linear regression model. This property usually correlates well with HumanOralAbsorption, as both measure the same property (range: >80% is high, <25% is poor)
- NandO, number of nitrogen and oxygen atoms (range: 2 – 15)
- RuleOfFive, number of violations of Lipinski's rule five (recommended values: maximum is 4)
- RuleOfThree, number of violations of Jorgensen's rule of three (the three rules are: QplogS > -5.7, QPPCaco > 22 nm/s , Primary Metabolites < 7, recommended values maximum is 3).

All these calculations describe the set of **11** compounds that match with promising features.

Table 1. Calculated properties and descriptors according to QikProp software of synthesized compounds **1-11**

Cmpd	#stars	#rtv FG	mol MW	SASA	FOSA	FISA	PISA	WPS A	donor HB*	acct HB*	QPlogP C16	QPlogP oct	QPlogP w	QPlog Po/w
1	0	0	348.4	641.6	87.2	105.0	393.6	55.8	1.0	3.8	12.6	17.4	9.2	4.6
2	0	0	348.4	657.2	69.4	112.7	419.3	55.8	1.0	3.8	13.0	17.4	9.2	4.7
3	0	0	348.4	650.7	93.9	106.6	394.3	55.8	1.0	4.7	12.8	17.7	9.9	4.3
4	0	0	320.4	591.3	0.0	105.9	429.6	55.8	1.0	3.8	11.8	16.6	9.7	4.0
5	1	0	374.3	609.4	0.0	98.7	341.0	169.7	1.0	3.8	10.8	17.2	9.2	4.6
6	0	0	355.4	631.2	195.3	127.9	252.2	55.8	1.0	7.7	11.7	19.4	15.1	1.9
7	2	0	343.4	613.2	0.0	77.1	480.3	55.8	1.0	3.0	12.5	17.2	9.4	4.9
8	0	0	335.4	600.9	0.0	152.3	392.8	55.8	2.5	4.8	12.5	19.5	12.8	2.9
9	0	0	349.4	630.2	15.1	154.2	405.0	55.8	3.0	4.8	13.3	20.4	13.3	2.8
10	0	0	363.4	650.4	52.3	149.1	393.2	55.8	3.0	4.8	13.6	20.7	13.0	3.2
11	0	0	377.5	661.8	103.0	125.9	377.1	55.8	3.0	4.8	13.8	21.0	12.7	3.6

* Values are averages taken over a number of configurations, so they can be non-integer

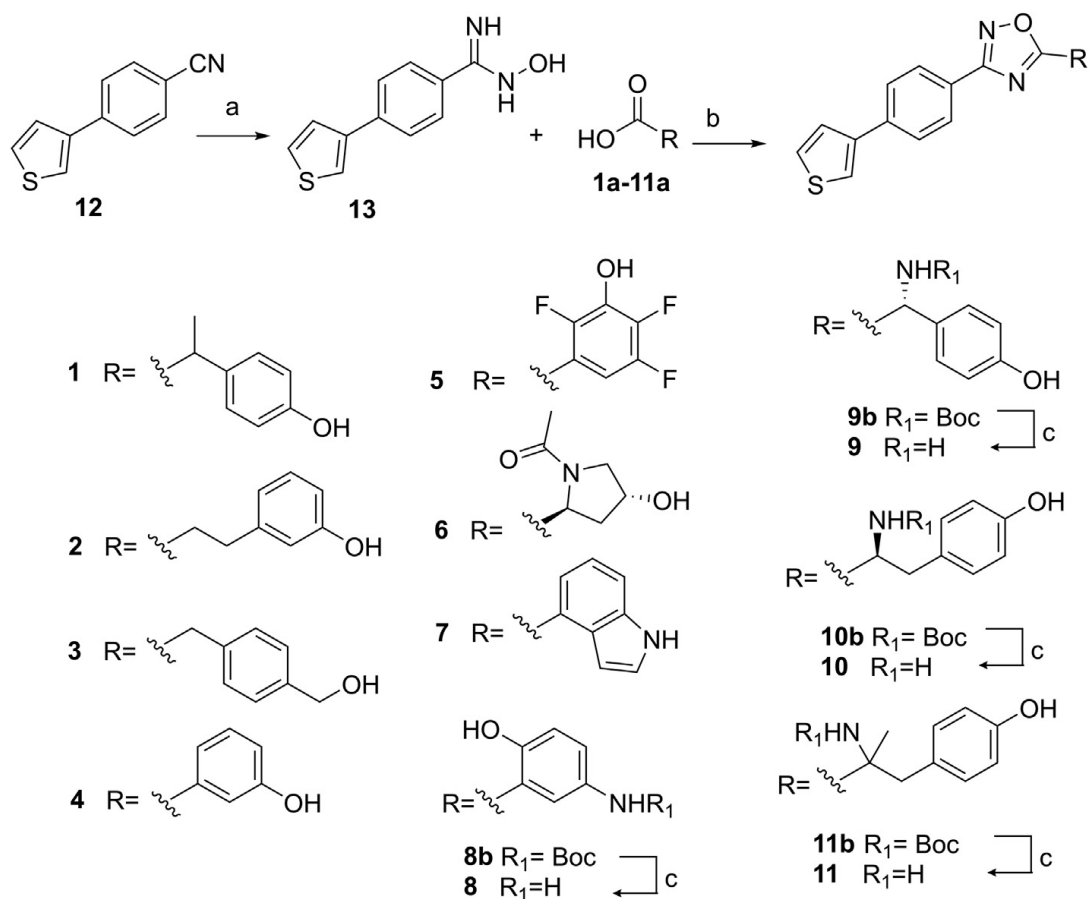
Cmpd	QPlogS	CIQPI ogS	QPPCaco	#metab	QPlogK hsa	PercentHumanO ralAbsorption	#NandO	RuleOf Five	RuleOf Three
1	-6.4	-6.1	1000.8	3	0.8	100.0	4	0	1
2	-6.5	-6.1	846.4	4	0.8	100.0	4	0	1
3	-6.0	-5.7	965.8	3	0.6	100.0	4	0	1
4	-5.8	-5.5	980.7	2	0.6	100.0	4	0	1
5	-6.6	-6.6	1149.0	2	0.7	100.0	4	0	1
6	-4.0	-3.7	334.0	3	-0.3	83.1	6	0	0
7	-6.6	-6.5	1840.1	1	0.9	100.0	4	0	1
8	-5.0	-5.3	356.1	3	0.3	89.9	5	0	0
9	-4.1	-4.5	85.1	5	0.3	78.0	5	0	0
10	-4.3	-4.8	95.2	6	0.4	80.8	5	0	0
11	-4.5	-5.1	158.1	4	0.5	87.1	5	0	0

3.1.5 Synthesis of compounds

The synthesis of oxadiazoles **1-11** has been performed starting from nitrile **12** through the formation of N'-hydroxy benzimidamide intermediate **13**. The following one-pot cyclization with several carboxylic acids was performed using as coupling reagents HBTU and DIPEA.

The presence of phenolic, benzylic and alcoholic functions on the carboxy moiety was proved to be tolerated, whereas in the case of compounds **8-11**, preventive Boc protection of the amine function of the corresponding acids **8a-11a** was need.

Boc removal was afforded with TFA in DCM as final step.



Scheme 2. Synthesis of compounds **1-11**

Reagents and conditions: a) $\text{NH}_2\text{OH HCl}$, K_2CO_3 in CH_3OH , reflux, 70% yield; b) Acids **1a-11a**, DIPEA, HBTU in DMF dry, 80 °C, 40-75% yield; c) TFA: CH_2Cl_2 1:1, 2 h, quantitative yield.

The structure of the synthesized compounds was confirmed by analysis of NMR data (^1H , ^{13}C and bidimensional NMR spectra) and ESI-MS.

3.1.6 Biological evaluation

The effects of 1–11 against mPGES-1 activity were tested at 10 μM by monitoring, through HPLC, the enzymatic conversion of the substrate PGH_2 to PGE_2 in a cell-free assay using microsomes of IL-1 β -stimulated A549 cells as a source of mPGES-1. Table 1 reports the residual activity expressed as percentage of control (100%): compound **5** was found to

reduce the enzyme activity approximately by 75%. Moreover, it showed a dose-response effect and displayed an IC_{50} value at the low micromolar range ($IC_{50} = 3.6 \pm 0.7 \mu\text{M}$) allowing to disclose the compound as a promising inhibitor of mPGES-1. The 3-hydroxy-2,4,5-trifluorophenyl substituent in 3 position was identified as the key fragment interfering with mPGES-1 activity.

As described before, mPGES-1 and FLAP are both members of the MAPEG superfamily.^{83,84} The activation of 5-lipoxygenase is fundamental for the leukotriene's production in the arachidonic acid cascade. FLAP acts as a membrane anchor for this enzyme, even if the mechanism of how they interact is not completely understood and this is the reason why a direct FLAP activity assay is not available. The antagonism towards FLAP has been indirectly investigated by testing all compounds (10 μM) to inhibit FLAP-dependent 5-LO product (LTB_4 and its isomers, and 5-H(P)ETE) in human intact neutrophils, where Ca^{2+} -ionophore was used to elicit 5-LO product formation, while exogenous addition of arachidonic acid largely circumvents the requirement of FLAP.⁹⁸ Interestingly, compounds **1**, **2** and **5**, showed a reduction of 5-LO products with compound **5** showing the most potent effects reducing the 5-LO products formation by more than 90% (100% vehicle control), especially in the absence of arachidonic acid, as reported in Table 2.

Table 2. Inhibition of compounds 1-11 on mPGES-1 activity and 5-LO product formation.

Cmpd	Residual activity of mPGES-1 (%) ± SEM^a	Residual 5-LO product (%) Stimulus: A23187^b	Residual 5-LO product (%) Stimulus: A23187^b plus AA
1	62.9 ± 5.6	6.02	7.54
2	76.4 ± 2.7	19.9	14.9
3	93.1 ± 5.7	73.6	65.2
4	84.1 ± 7.8	n.i. (>100%)	n.i. (>100%)
5	25.4 ± 2.7	1.7	18.5
6	82.2 ± 7.5	92.6	89.5
7	63.2 ± 10.01	59.7	99.3
8	81.9 ± 8.1	84.3	29.6
9	67.6 ± 2.1	47.5	50.3
10	82.7 ± 8.7	95	74.4
11	84.7 ± 5.8	78	61.3

^amPGES-1 residual activity of compounds **1-11** deriving from the cell-free assay. Data are expressed as percentage of control (100%) ± S.E.M., n = 3. ^b 5-LO product formation in intact human neutrophils after incubation with compounds 1-11. Stimulus: A23187 (Ca²⁺ ionophore, calcimycin) or A23187 plus arachidonic acid (AA). Data are expressed as percentage of control (100%).

At this stage, we wondered about the effect that these three compounds could have had directly on 5-LO, so we also analyzed the inhibition of 5-LO product formation in a “FLAP independent” cell-free 5-LO assay. A poor antagonism on the activity of 5-LO was showed by compounds **1** and **2** (Table 3), suggesting that the the inhibition of LO product formation in neutrophils might be due to interference with FLAP. On the other hand, compound **5** demonstrated a potent inhibition of 5-LO activity in the cell-

free assay. Dose-response curve disclosed an IC_{50} value in the micromolar range ($IC_{50} = 2.0 \pm 0.2 \mu M$). This suggests that inhibition of 5-LO and/or FLAP may account for the suppression of 5-LO product formation by compound **5** in intact cells.

Driven by the aim of identifying further activities involved in the anti-inflammatory pathway, compounds **1**, **2** and **5** were screened against soluble epoxide hydrolase (sEH) in another cell free assay. This enzyme is responsible to the hydration of epoxides of arachidonic acid into the corresponding 1,2-diols. Since these lipid mediators have been established to have very important biological functions, the activity of sEH plays a key role in inflammation.⁶³

None of compounds showed inhibitory activity (Table 2) towards sEH.

To complete and strengthen our analysis, a COX-1 and COX-2 cell-free assay was also performed. Interestingly, all these three candidates showed promising results. In particular, compounds **1** and **5** reduced the activity of COX-1 by >65% (100% vehicle control), and compound **2** inhibited COX-1 by >50%, while no activity have been shown on the inducible isoform COX-2, which acts together with mPGES-1.

The selectivity of compound **1**, **2** and **5** for COX-1 isoform could be considered for future investigations, since only few selective antagonists of this isoform are known. Indeed, recent reports displayed the involvement of COX-1 in several types of neoplastic diseases.⁹⁹

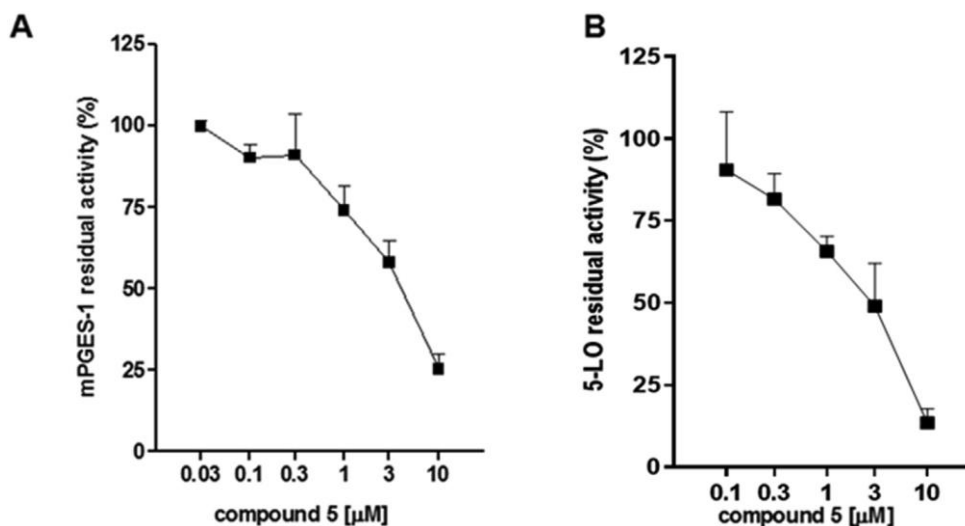


Figure 15. A) Concentration-response curve for inhibition of mPGES-1. The enzyme was incubated for 15 min with compound 5 at different concentrations (from 0.03 μM up to 10 μM) or vehicle (1% DMSO). Then, 20 mM PGH₂ was added as substrate, and the reaction was stopped after 1 min by adding FeCl₃. IC₅₀ = 3.6 \pm 0.7 μM .

B) Concentration-response curve of compound 5 for 5-LO inhibition in a cell-free assay. The purified 5-LO enzyme was pre-incubated 10 min on ice with compound 5 at different concentrations or vehicle (0.1% DMSO). Then, AA (20 μM) and CaCl₂ (2 μM) were added, and the mixture was incubated at 37 °C. After 10 min, the reaction was stopped by adding ice-cold methanol. IC₅₀ = 2.0 \pm 0.2 μM . Data are expressed as percentage of control (100%), means \pm S.E.M.; n = 3.

Table 3. Residual activity of compounds **1**, **2** and **5** at 10 μ M on isolated enzymes involved in the formation of pro-inflammatory eicosanoids. Data are expressed as a percentage of control (100%), $n = 3$.

Compd	5-LO residual activity (%)	sEH residual activity (%)	COX-1 residual activity (%)	COX-2 residual activity (%)
1	n.i (61.8)	n.i. (>50)	22.5	n.i. (>50)
2	n.i. (104.8)	n.i. (>50)	47.7	n.i. (>50)
5	10.3	n.i. (>50)	34.7	n.i. (>50)

The cytotoxic effects of compounds **1**, **2** and **5** at active concentration (10 μ M) were assessed by MTT assay on human monocytes (over 24 h) and human adenocarcinoma A549 cell line. Compounds **1**, **2** and **5** didn't significantly affect the viability of the cell population at 24h and no reduction was observed for compound **5** at 48h.

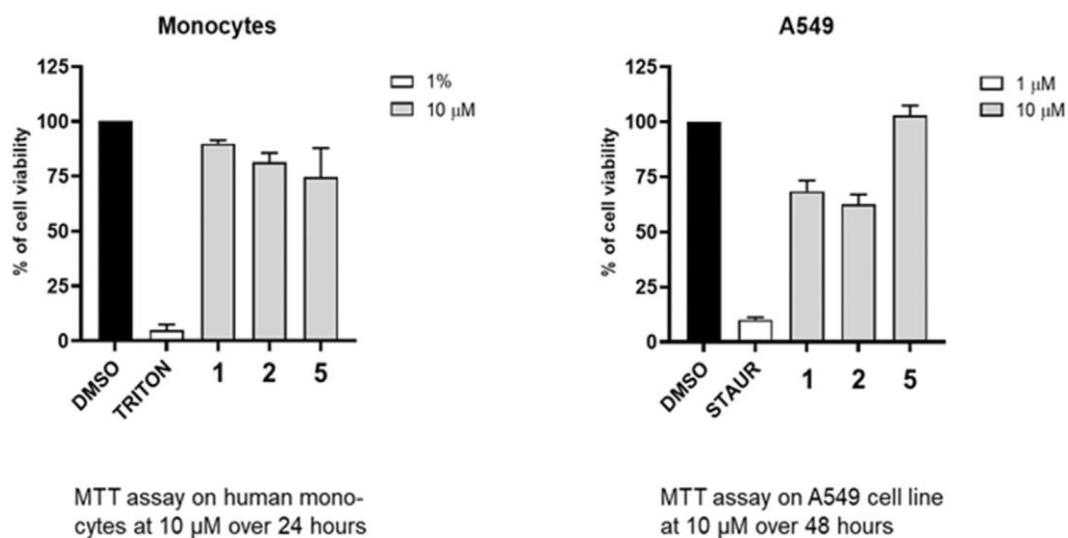


Figure 16. Cell viability assays were performed with human monocytes and A549 cells. **A)** Monocytes were treated with the test compounds **1**, **2** and **5** (10 μM), triton (1%, positive control) or vehicle (0.5% DMSO) for 24 h, and a MTT assay was performed; **B)** A549 cells were treated with the test compounds **1**, **2** and **5** (10 μM), staurosporine (1 μM, positive control) or vehicle (0.1% DMSO) for 48 h, and a MTT assay was performed. Data are expressed as percentage of control (100%), means, S.E.M., n =3.

Docking results highlighted the favourable accommodation of **5** in the mPGES-1 binding pocket and the establishment of a large set of interactions with key residues.

The aromatic ring on the C-3 interacts with the aromatic ring of the Tyr130_{chainC} establishing π - π stacking interaction. The thiophene ring as well is involved in π - π interactions with Tyr130_{chainC} and Tyr28_{chainA} orienting towards the key residue Gln134_{chainC}. The ring 2,3,6-trifluoro-5-phenolic linked to C-5 can form relevant interactions with several amino acid residues (Arg38, Leu39, Phe44, Asp49, His53, Ala123). Additionally, the phenolic group, that is in found to be in its dissociated form at physiological pH, forms a hydrogen bond with the side chain of Ser127.

The two residues of Tyr130 and Ser127 are considered the key amino acids in the active site of the enzyme as responsible for interaction with GSH. Van der Waals interactions with Ala31, Ile32 and Ala138 residues and polar interactions with Tyr28 and Gln36 residues further stabilize the ligand-enzyme complex. (Figure 17)

From a structural point of view, the mPGES-1 inhibitory activity of **5** with respect to the other compounds of this series, e.g., to its close congener (**4**), is ascribable to the presence of the hydroxytrifluorinated phenyl substituent, which also interacts with the Arg52 chainA. These data suggested the crucial role of the electronegative, small-sized fluorine atom for a specific ligand/target interaction. The presence of the hydroxypolyfluorinated phenyl substituent is crucial for the activity of the molecule, since it could be considered a bioisoster of several functional groups, confirming the versatility of the fluorine atom as decoration point in medicinal chemistry programs.¹⁰⁰

It was clear that the influence of fluorine substitution strongly affected the inhibition towards the target and this applied workflow stimulated further investigations towards the optimization of the identified hits, as I'll discuss in section 3.1.7.

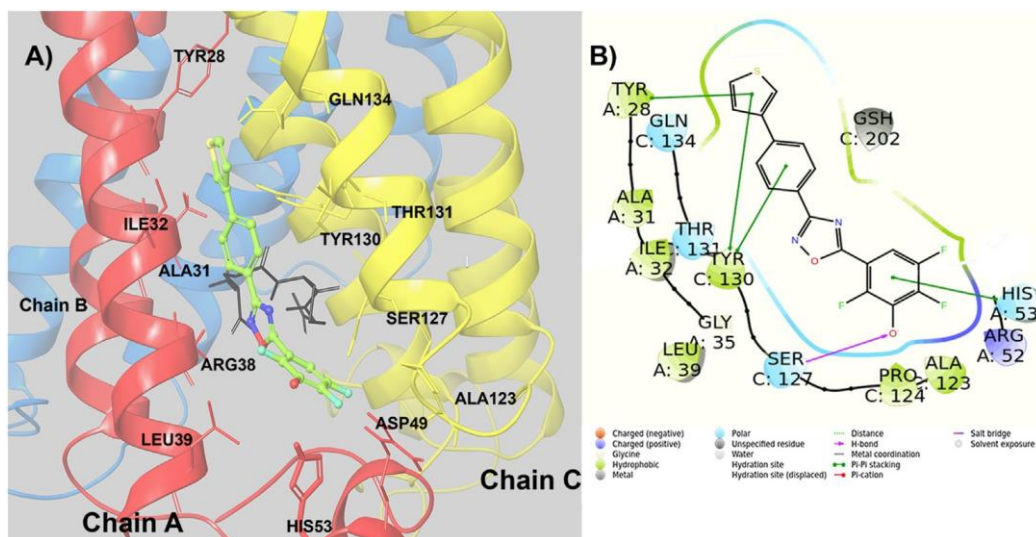


Figure 17. **A)** 3D representation of compound **5** (green sticks) in the binding site of mPGES-1 (pdb code: 5TL9); chain A is depicted in yellow, chain B in blue, and chain C in red ribbons; all the interactions are represented as dotted lines, green in hydrogen bonds, light blue in π - π interactions. **B)** 2D interactions diagram of compound **5** with mPGES-1 as counterpart (pdb code: 5TL9); H-bond interactions are reported as pink arrows, while π - π interactions as green lines; hydrophobic residues are depicted in green, polar residues in light blue, and positive charged residues in blue.

The interesting *in vitro* pharmacological results turned the attention of our pharmacological partner to an *in vivo* investigation on compound **5** effects in a model of inflammation that allows the characterization of leukocytes migration into the peritoneal cavity.

Intraperitoneal injection of zymosan, a polysaccharide cell wall component derived from *Saccharomyces cerevisiae*, has been largely used as a model to quantify the recruitment of monocytes and neutrophils

into the peritoneal cavity in order to study the potential effects of anti-inflammatory drugs.¹⁰¹ The zymosan-induced inflammation is known to be characterized by the migration of pro-inflammatory cytokines, such as IL-1 β , IL-6, TNF α and PGs with consequent cellular infiltration leading to a neutrophils, macrophages, and fibroblasts accumulation to the site of inflammation.^{102,103}

On the contrary, the release of IL-10, an anti-inflammatory cytokine, favours the suppression of the inflammatory response and inhibits the activation of T cells and monocytes.^{104,105,106}

Compound **5** demonstrated beneficial effects with a strong reduction of leucocytes recruitment at the dose of 10 mg/kg ($P \leq 0.01$) after 4h. On the contrary, its activity was less effective after 24h compared to zymosan + vehicle compound **5** group. Compound **5** at 10 mg/kg significantly reduced the levels of IL-1b and TNF-a, both at 4h and 24h without altering the level of IL-6 and IL-10.

Reducing the dose at 1 mg/kg ($P \leq 0.05$) at 4 h, compound **5** even showed a significant activity.

The zymosan-induced leukocytes migration was attenuated by treatment with compound **5**, starting from 4 h post model induction and the screening of the main pro-inflammatory cytokines has seen a significant reduction (IL-1 β and TNF- α) but not modulation in terms of IL-6 and IL-10 production. The difference in leukocytes accumulation and cytokines level observed between 4 and 24 h may be due to the route of administration and compound's bioavailability.

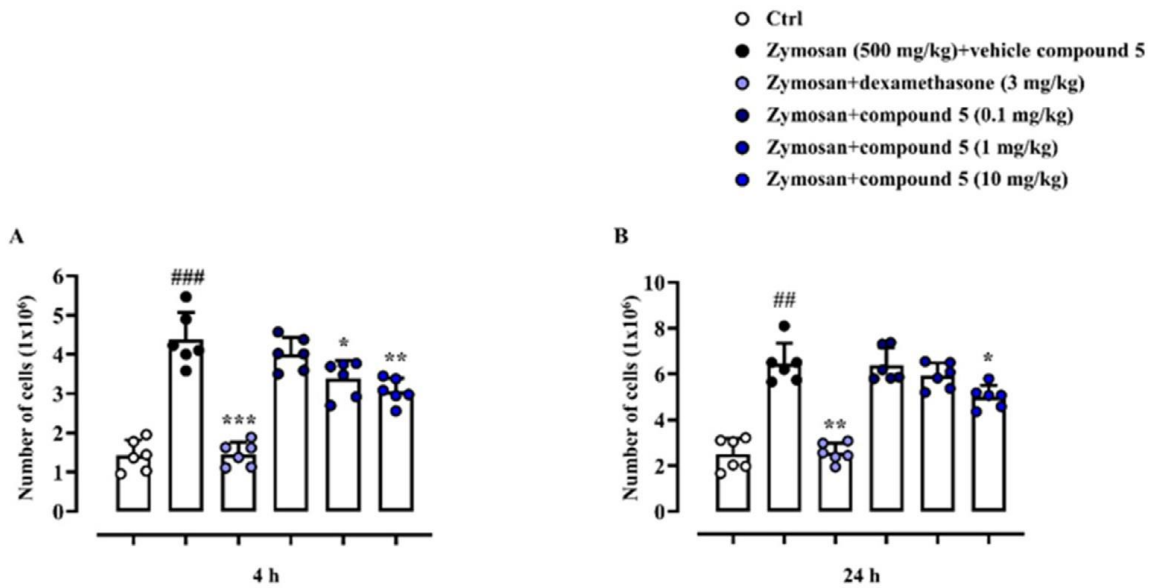


Figure 18. *Effect of compound 5 in zymosan-induced peritonitis in mice.* Mice were randomly divided into different experimental groups: control group (Ctrl), model group (zymosan + vehicle compound 5), zymosan + compound 5 (0.1, 1, and 10 mg/kg), and zymosan + dexamethasone (3 mg/kg) group. Animals received the selected compound or dexamethasone intraperitoneally (i.p.) 30 min after i.p. injection of zymosan (500 mg/kg). A) At 4 and B) 24 h after injection, peritoneal exudate from each mouse was recovered and total cell number (expressed as 10⁶ and normalized to exudate levels) was evaluated. Results are expressed as mean \pm S.D. Statistical analysis was performed by using one-way ANOVA followed by Bonferroni's for multiple comparisons. ##P \leq 0.01 and ###P \leq 0.005 vs Ctrl group, *P \leq 0.05, **P \leq 0.01 and ***P \leq 0.005 vs zymosan + vehicle compound 5-treated mice (n =6 per group).

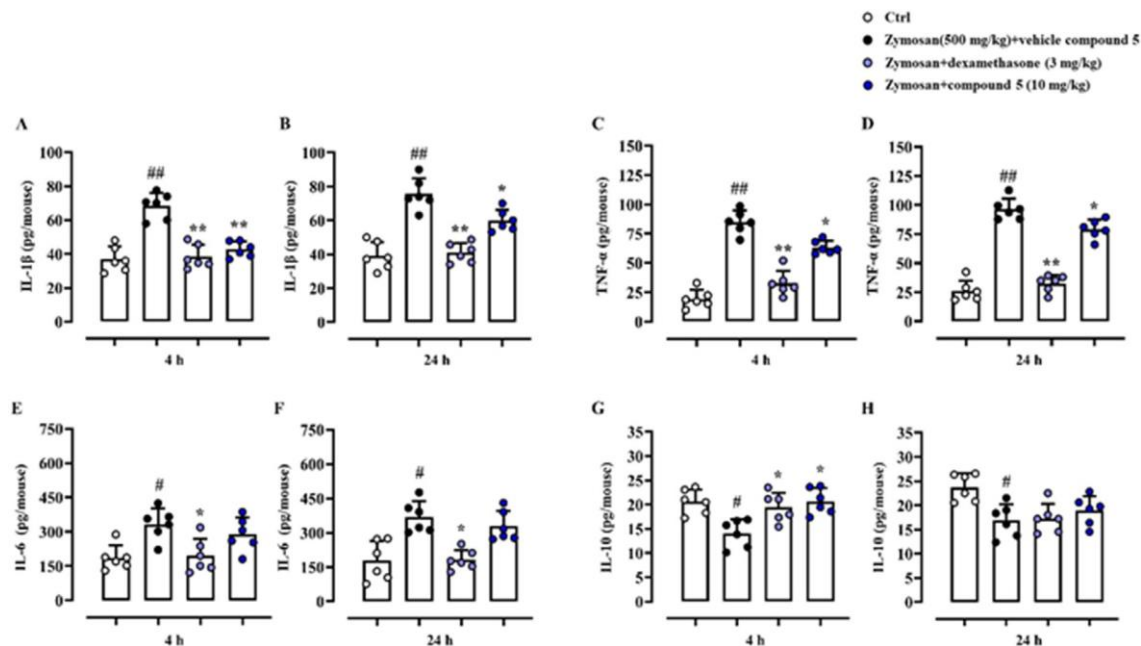


Figure 19. Cytokines analysis of the collected peritoneal exudate.

Analysis of the collected peritoneal exudate identified increased levels of the classical pro-inflammatory mediators. **A,B**) IL-1 β , **C,D**) TNF- α , **E,F**) IL-6, and decreased of **G,H**) IL-10 in the peritoneal cavity of mice from different experimental groups. Significant differences were found in relative levels after compound **5** administration. Results (normalized to exudate levels) are expressed as mean \pm S.D. Statistical analysis was performed by using one-way ANOVA followed by Bonferroni's for multiple comparisons. #P \leq 0.05 and ##P \leq 0.01 vs Ctrl group, *P \leq 0.05 and **P \leq 0.01 vs zymosan +vehicle compound **5** treated mice (n = 6 per group).

3.1.7 A new small-molecules library and future perspectives

A drug design project is more complex than just the development of the pharmacologically active compound. As well described by our research project, a lead compound needs to comply several features to be inserted among the best candidates as potential novel drugs. Most often, chemical modifications are required to improve the pharmacokinetic profile or to increase the affinity towards the selected target.

The applied multidisciplinary approach allowed not only to identify compound **5** as a multi-target inhibitor of arachidonic acid cascade

enzymes, even confirmed to have a strong activity *in vivo* model of zymosan-induced peritonitis, but also to establish the key role of the hydroxytrifluorinated linked to C-3 position.

The investigation around the chemical space of compound **5** encouraged a new optimization campaign in order to identify further promising compounds with a potent activity on mPGES-1 enzyme, characterized by an enhanced pharmacological profile. This challenge provides the opportunity to expand our library of anti-inflammatory compounds and a second research line was born considering the promising outcomes exhibited by compound **5** and the pivotal role played by the hydroxytrifluorinated phenyl substituent.

The main purpose has been to delineate a SAR and to identify the pharmacophoric portions for the inhibition of mPGES-1, also improving the pharmacodynamic and pharmacokinetic features.

The analysis performed on the active site of the crystal structure of the protein led us to increase the affinity towards the target through a repositioning of the substituents linked to C-5, while keeping fixed the hydroxytrifluorinated function at C-3.

Following the same well-linked steps of the previously applied workflow, a new library of 5 compounds was generated through computational tools. The same optimized protocol used for the synthesis of the previously discussed compounds, was applied to obtain a small library of 5 compounds. The synthesis of amidoximes **15a-e** has been performed starting from the correspondent nitrile **14a-e** and the subsequent coupling with 3-hydroxy-2,4,5-trifluorophenyl carboxylic acid allow to obtain the desired products. The structures of the newly designed compounds are depicted in Figure 20.

When tested at 1 and 10 μ M in a cell-free based mPGES1 assay, compounds **18** and **19** displayed significant inhibition of the enzyme. Planned ongoing experimentation involves further *ex vivo* experiments on the most active compounds **5**, **18** and **19** and *in vivo* experiments in order to evaluate the inhibitory activity in animal models of inflammation and cancer.

In the first step, a proteome profiler mouse cytokine array kit (a membrane-based sandwich immunoassay) will be used for the parallel determination of the relative levels of selected mouse cytokines, chemokines and acute phase proteins (\approx 40) modulated by the biological activity of active compounds. Afterwards, the levels of mPGES-1, mPGES-2, COXs, 5-LO, EP1 and EP4 will be monitored by western blot analysis. Moreover, the profile of lipid mediators will be devised in analogy to cytokines on peritoneal exudate. In the second phase of *ex vivo* experiments, other histological analyses will be planned to understand the distribution and localization of the selected biomarkers and of differentially expressed proteins in different parts of the collected biological tissue. This experimental model is preliminary to the next induction of colonic aberrant crypt foci (ACF) and tumors by azoxymethane (AOM) approved to Italian Ministry of Health (n $^{\circ}$ 200/2016-PR of 02/25/2016, related to the IG 17440).

The *in vivo* ability of our compounds as anti-inflammatory/anti-cancer agents will be estimated in animal model of acute inflammation (peritonitis)¹⁰⁷ and colorectal cancer (CRC), showing the pro-tumorigenic role of mPGES-1 Ps in chemical induced colon carcinogenesis. All experimental procedures have been already approved by Italian Ministry of Health and will be performed at the “Antonio Cardarelli” hospital

biotechnology center (Naples). Animal care will be in compliance with Italian (Decree 116/92) and European Community (E.C. L358/1 18/12/86) guidelines, including those of the D.Lgs. 26/2014 on the use and protection of laboratory animals. All efforts will be made to minimize animal suffering and to reduce the number of animals used

Effects of new mPGES-1 inhibitors in Zymosan-Induced Peritonitis in Mice

To investigate whether our mPGES-1 agents exhibit anti-inflammatory effectiveness and suppress PGE₂ biosynthesis *in vivo*, we will use the zymosan-induced peritonitis in Balb/c mice as a well-recognized model of acute inflammation.

Induction of colonic ACF and tumors by AOM treatment.

Induction of colonic aberrant crypt foci (ACF) and tumors by AOM (AOM) treatment will be performed in Balb/c mice (6–8 weeks old), a mouse strain that is sensitive to AOM-induced colon carcinogenesis.¹⁰⁸ The animals will be intraperitoneally injected with AOM. Mice will be killed 6 or 18 weeks after the last injection of AOM. After laparotomy, the entire colons will be dissected and then macroscopically divided into normal-appearing tissues and polyps as normal and tumor tissues, respectively. For microscopic analysis, the dissected colons will be filled with 10% neutral-buffered formalin and then opened longitudinally from the anus to the cecum. For analysis of ACF formation, each colon will be stained with 0.2% methylene blue in phosphate-buffered saline (PBS). Colon tissues will be scored under a light microscope for the number of ACFs or polyps per colon.

Evaluation of toxicity

The acute toxicity of tested compounds will be evaluated as described by Lorke *et al.*¹⁰⁹ according to the Italian (Decree 116/92) and European Community (E.C. L358/1 18/12/86) guidelines, including those of the D.Lgs. 26/2014 on the use and protection of laboratory animals.

Small animal imaging studies.

For small animal in vivo imaging, we will use three integrated, non-invasive, micro-US (ultrasound), micro-CT (computed tomography), and micro-MRI (magnetic resonance imaging). The multimodality imaging approach increases the results overcoming the limitations of each independent technique and will shed light on the specific local mechanisms involved in acute inflammation and carcinogenesis. The anti-inflammatory and anti-tumor effects of mPGES-1 inhibitors and EP antagonists will be directly verified measuring the anatomical and pathological peritonitis and carcinogenesis features. Micro-US will be employed thanks to the excellent safety profile and real-time dynamic visualization capacity, evaluating the wall thickening typically associated with a preliminary stage of acute inflammation. The increase of vascularity related to the inflammation will be evaluated using color-Doppler system; moreover, with micro-bubble contrast-US-imaging, we will also identify the level of wall membrane damage. Using micro-CT, a morphological in vivo intestinal wall analysis will be performed providing several descriptors such as wall thickness and multiple stratification parietal. MRI technique will be used to evaluate inflammatory infiltrates, wall thickening proliferation, submucosae edema, extra-parietal free fluid in experimental peritonitis animal models. MRI will be also used to accurately monitor tumor growth in mouse models of colorectal

carcinogenesis in a non-invasive way. Tumor volumes will be measured, and parameters relevant to the evaluation of therapeutic or preventive interventions (i.e., tumor initiation, tumor growth rates and regression, the time for tumors to reach a given size) will be calculated.

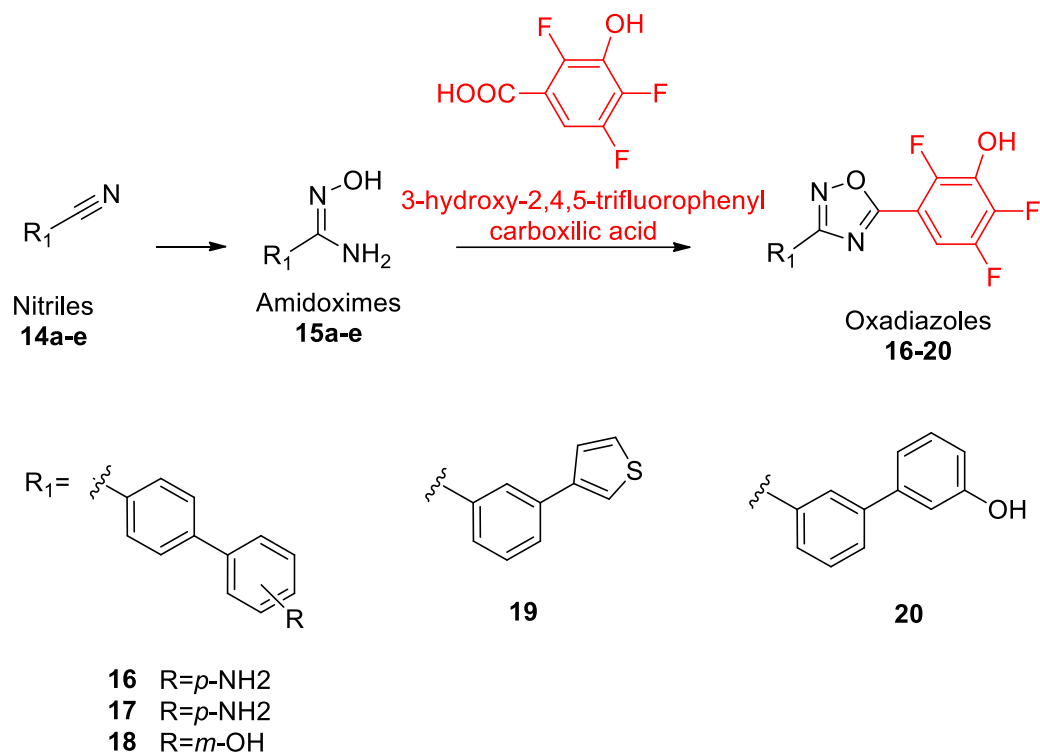


Figure 20. *New library of five compounds.*

3.2 Synergism of a novel 1,2,4-oxadiazole-containing derivative with oxacillin against methicillin-resistant *Staphylococcus aureus*

3.2.1 Drug-resistance: methicillin-resistant *S. aureus*

The discovery of antibiotics represents one of the most important events of the last century that changed the treatment of a wide range of infections in a significant way. The period between 1940 and 1962 is called “the golden era of antibiotics”, when most of the antibiotic classes were discovered and introduced into the market. Each class typically contains several antibiotics that have been discovered or are modified versions of previous types. Nowadays, antibiotics play an important role in the treatment of multiple diseases, but their efficacy is extremely compromised by the phenomenon of drug resistance. The spread of drug-resistant pathogens that have acquired new resistance mechanisms, reduces the possibility of intervention on several diseases, leading to an increased rate of morbidity and therapeutic failure. As a result of drug resistance, antibiotics and other antimicrobial medicines become ineffective and infections become increasingly difficult or impossible to treat, leading to extended hospitalisation times with a negative impact on healthcare costs.¹¹⁰

The discovery of novel active molecules with antibacterial activity on multi-drug resistant strains represents an emerging field of research since the phenomenon of drug-resistance is currently one of the main urgent priorities of the *World Health Organization (WHO)*.

Factors that contribute to the growth of bacterial resistance to antibiotics includes their inappropriate and indiscriminate use, and an improper prescribing of antimicrobial therapy. Moreover, a rapid evolution of the

bacterial genome under selective pressure exerted by the environment lead to emergence of resistant organisms.

Among Gram-positive bacteria, resistant *Staphylococcus aureus* represents the biggest threat to the global health.¹¹¹

S. aureus is a leading cause of health-related infections, and the diffusion of methicillin-resistant *S. aureus* (MRSA) has thwarted the efforts done in the discovery of antimicrobial agents. More than 80,000 severe methicillin-resistant *S. aureus* (MRSA) infections were diagnosed every year in USA, resulting in 11,285 annual deaths.¹¹²

Nowadays, MRSA has become epidemic not only in nosocomial infections but also in community-associated infections.¹¹³

Commonly, almost the 30% of the human population is colonized with *S. aureus*, which is part of human microbiota, in particular on external skin surfaces and the upper respiratory tract.¹¹⁴ However, is an opportunistic pathogen and under the right circumstances can cause more serious infections in humans and animals as skin or lung infections, mastitis, endocarditis, toxic shock syndrome, and bacteriemia.¹¹²

When the host barriers are broken, “commensal” *S.aureus* may invade deeper structures and produce these subsequent infections.¹¹⁵

S. aureus is also able to form biofilm on medical devices, resulting in further complication in the management of infections due to difficulties of antibiotics to penetrate the biofilm layer.¹¹⁶

The administration of a β -lactam antibiotic, Penicillin G (benzylpenicillin), was used for the treatment of *S.aureus* infections, before the resistance of this strain became a serious concern.^{117,118}

By the late 1950's was clear that the resistance to β -lactam antibiotics occurs through the synthesis of β -lactamases, enzymes that inactivate

these antibiotics by hydrolysing the amide bond of the β -lactam ring, that is crucial to the antimicrobial activity of these drugs.¹¹⁹ The synthesis of methicillin, in which the phenyl group of benzylpenicillin was decorated with methoxy groups allowed to produce a steric hindrance around the amide bond reducing its affinity for staphylococcal β -lactamases. As soon as methicillin was marketed and clinically used, methicillin-resistant *S. aureus* (MRSA) strains have been developed through a different resistance mechanism which includes the expression of a gene that encodes for a protein able to bind the drug and thus preventing the drug from killing the organism. In more details, the gene *mecA* encodes for a novel *penicillin binding protein 2a* (PBP2a), an enzyme responsible for crosslinking the peptidoglycans in the bacterial cell wall. PBP2a has a low affinity for β -lactams, resulting in the grow of bacterial cell even in the presence of these antibiotics, giving resistance to the entire antimicrobial class of drugs.¹²⁰

MRSA is one of the most successful modern pathogens and it has spread rapidly in the community. Many different pandemic strains have been identified, even though MRSA infection occurs globally. For instance, an emergent MRSA strain is represented by the health - care associated MRSA (HA-MRSA) clonal complex 30 (CC30) in North America and Europe, while livestock-associated MRSA (including ST398) and ST93 are the most spread in Australia.^{121,122,123,124}

MRSA colonization increases the risk of infection and can persist for long periods, especially within the home environment, complicating attempts at eradication. At the same time, colonization is not static, as strains have been found to evolve and even to be replaced within the same host.

The continuous emergence of resistant strains has created an enormous difficulty for the management of MRSA infections. Nowadays, MSRA

remains a prominent pathogen with increasingly high mortality, even with the ongoing development of new antibiotics and advances in infection prevention.¹²⁵

The search of novel antibiotics able to interfere with PBP2a, among other PBPs, is strongly supported by massive research efforts, aiming to control diseases by such resistant bacteria.

3.2.2 1,2,4-oxadiazoles as antimicrobial agents

One of the ways to front the antimicrobial resistance diffusion is the synthesis of new chemical compounds to which microorganisms are sensitive. Most often, newly synthesized molecules contain a heterocyclic moiety, and the motifs containing oxadiazole ring constitute a vast group of potential antimicrobial derivatives.¹²⁶

In the search of new antimicrobial agents, 1,2,4-oxadiazoles represent an emerging scaffold for drug design. Recent *in silico* screening proved 1,2,4-oxadiazole-derivatives to be a promising non β -lactam class of antibiotics as inhibitors of penicillin-binding protein 2a (PBP2a) of methicillin resistant *Staphylococcus aureus* (MRSA).

In more details, Chang *et al.*¹²⁷ reported in 2014 the bactericidal activity of this class of heterocycles against vancomycin and linezolid-resistant MRSA and other Gram-positive bacterial strains, performing a lead compound optimization, followed by *in vitro*, and *in vivo* evaluation.

The *in silico* screening was carried out on 1.2 million molecules derived from ZINC database,¹²⁸ all complexed to the X-ray structure of PBP2a of MRSA,¹²⁹ then scored to select the most promising complexes for further analysis leading to the synthesis of 29 compounds. Among these molecules, the evaluation of the minimum inhibitory concentrations

against *Escherichia coli* and ESKAPE panel bacteria,¹³⁰ disclosed compound **21** as promising lead compound due to its poor but reproducible activity against *S. aureus* and *E. faecium*.

Starting from these encouraging outcomes, an extensive investigation on the structure–activity relationship was performed, based on the presence of four interconnected aromatic rings (A–D). Further studies by the same research group led to modifications in the lead at the 5-position of the 1,2,4-oxadiazole (ring A), while keeping the 3-position constant as a 4-substituted diphenyl ether moiety. Interestingly, compounds containing a 5-indole ring A as compounds **21** and **22**, exhibited potent antimicrobial activity against MSRA strains, and were selected as the best candidates for their promising pharmacological features such as low toxicity, oral bioavailability, and *in vivo* activity in murine models of infection.^{131,78}

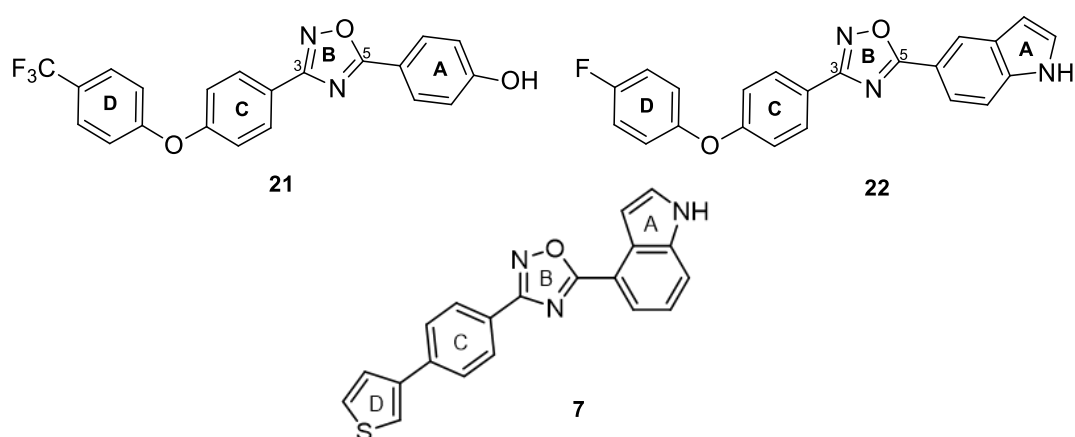


Figure 21. Structure antimicrobial 1,2,4-oxadiazoles.

The starting point of the present investigation is the purpose of repositioning of those 1,2,4-oxadiazoles compounds, described in the previous section, lacking enough anti-inflammatory activity.

Indeed, these compounds were already subjected to an extensive combinatorial assessment and pre-selection of relevant pharmacological features to ensure a promising and safer pharmacokinetic profile.¹³²

Drug repositioning process has become a promising approach for drug development in order to find new indications for existing drugs. As an advantage, it can reduce the risk of failure in the next phases of clinical investigations due to drug ineffectiveness or severe side effects.

The opportunity to find new potential antimicrobial indication of compounds having a lack in anti-inflammatory activity, drew our study to further explore the chemical space around the 1,2,4-oxadiazole scaffold.

Compound **7** of the previously synthesised library presents some analogies with compounds **21** and **22** as a regioisomeric 4-indole substituent at C-5 position of the 1,2,4-oxadiazole and the concatenation of four aromatic rings. The multidisciplinary computational protocol carried out for our previous study, allowed to define the pharmacological behaviour of the designed compounds as potential medicaments. Moreover, the cell viability assays already performed led to exclude any cytotoxic activity of the compounds.

Therefore, a small library of 1,2,4-oxadiazoles were obtained by maintaining a common 4-indole substituent at C-5, and by varying the aromatic ring in position 3. All the synthesized compounds were screened to test their antimicrobial activity against *S. aureus* 29213 and 43300 (MRSA), *P. aeruginosa*, and *K. pneumoniae*.

3.2.3 Compounds and chemistry

Compound **7** belonging to the previously synthesized library, was screened for the analysis of the antimicrobial activity against two strains of *S. aureus* (ATCC 29213 and MRSA ATCC 43300). As reported in Table 4, the compound was found to possess a very good activity against both strains.

Encouraged by these promising outcomes, we decided to build a small library of 15 1,2,4-oxadiazoles based compounds, only modifying the aromatic functions in position 3 as rings C and D, while keeping fix 4-indolyl function in position 5 as ring A.

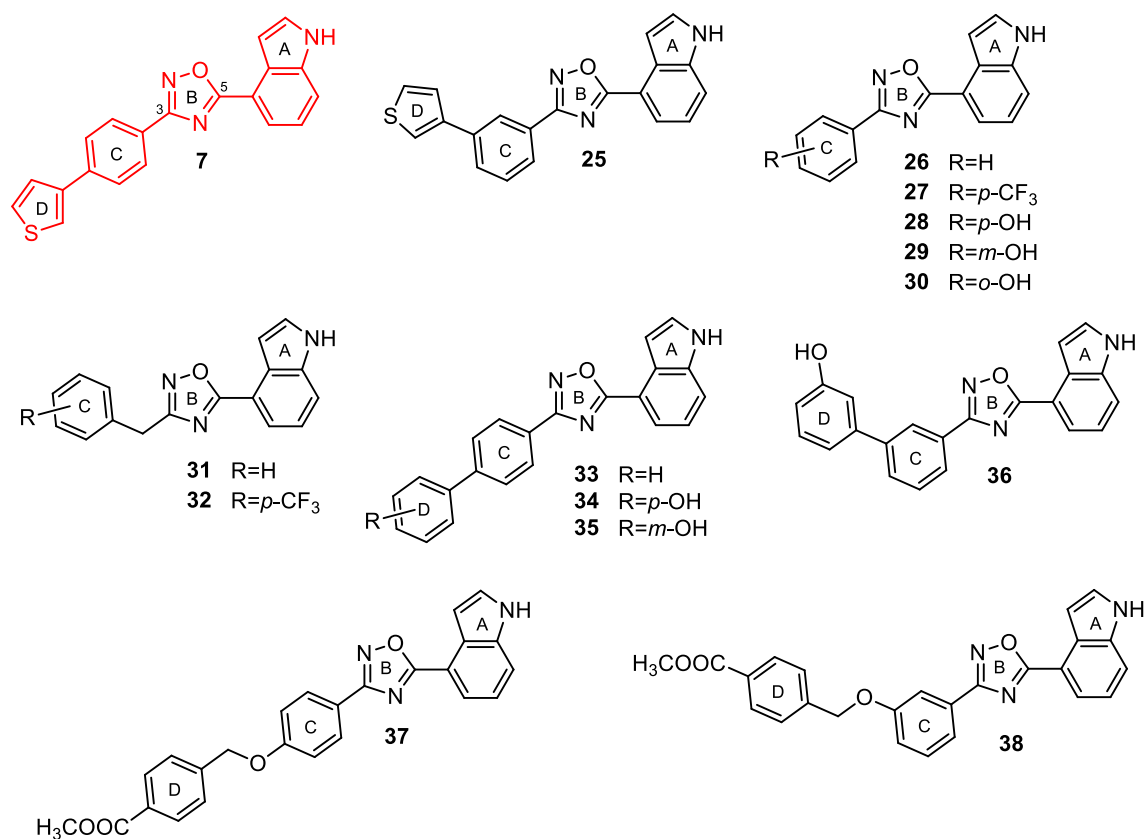


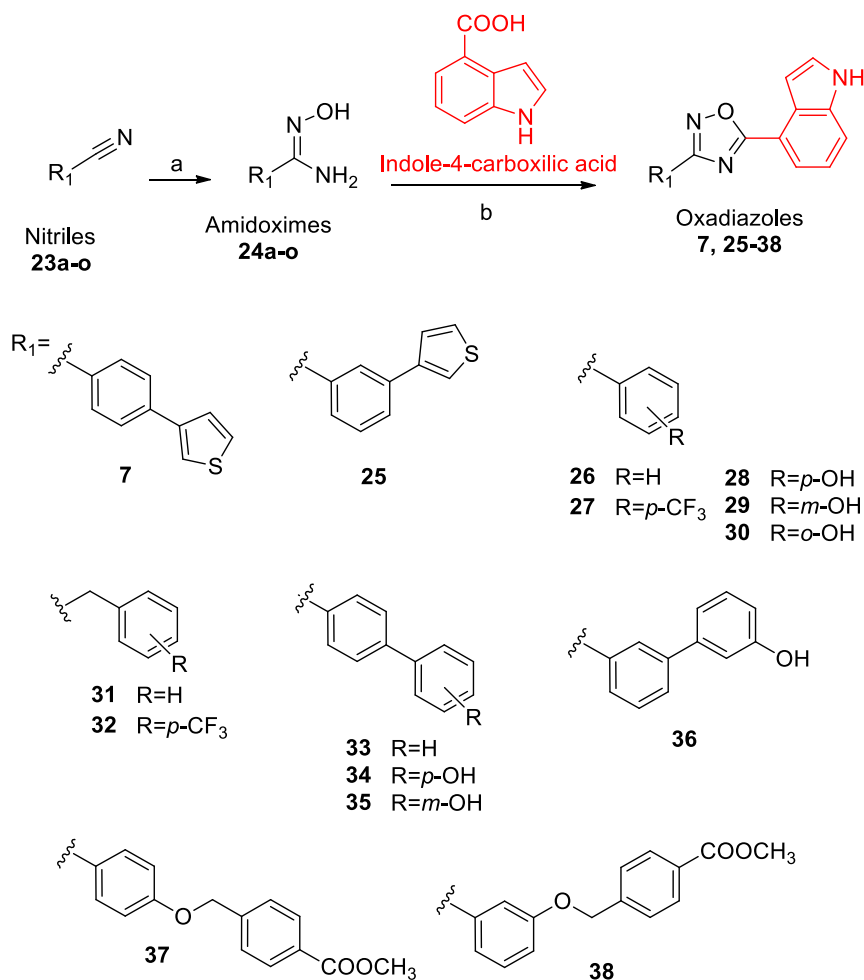
Figure 22. 1,2,4-oxadiazoles synthesized in this research.

As shown in Figure 22, compounds **26-32** have no ring D, while different substituents have been added on ring C. In the other remaining molecules, the diphenyl ether portion (rings C and D) have been replaced with different benzyl, biphenyl, thienyl, or benzyloxyphenyl functions substituted at different positions.

As in previous study, the compounds were synthesized via amidoxime route. Amidoximes **24a-o** (prepared by reaction of corresponding nitriles **23a-o** with hydroxylamine hydrochloride) were reacted with indole-4-carboxylic acid, using HBTU as coupling agent to afford compounds **25-38**. (Scheme 3)

Nitriles **23n** and **23o** are not commercially available and had to be synthesized following Williamson reactions between 4-cyanophenol and methyl 4-(bromomethyl) benzoate or methyl 3-(bromomethyl)benzoate, respectively.

The structures of synthesized compounds were confirmed by analysis of NMR data (^1H and ^{13}C NMR spectra) and ESI-MS, as reported in the next experimental section.



Scheme 3. General procedure for the synthesis of 1,2,4-oxadiazoles derivatives.

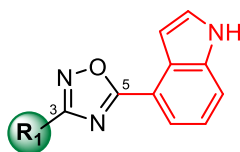
Reagents and conditions: a) NH₂OH HCl, K₂CO₃ in CH₃OH, reflux; b) indole-4 carboxylic acid, DIPEA, HBTU in DMF dry, 140 °C.

3.2.4 Antimicrobial Activity

The antimicrobial activity of synthesized compound **7**, **25-38** was evaluated against *S. aureus* ATCC 29213 and *S. aureus* ATCC 43300, and two Gram negative, *P. aeruginosa* ATCC 27853 and *K. pneumoniae* ATCC 13883. Table 4 summarizes all the obtained results and the strongest antimicrobial activity against the two Staphylococcal strains was shown by compounds **27**, **32**, **34** and **35** reporting a MIC value of 6.25

μM . Compound **28** showed its activity at 100 μM , while compound **33** resulted to be active at a lower MIC value of 2 μM . Compounds **25**, **29**, **31**, **37** and **38** were not active, while none of them were active against *P. aeruginosa* ATCC 27853 and *K. pneumoniae*.

Table 4. *In vitro* antimicrobial activity of compounds 7,25-38. MIC values are expressed as μM .



Cmpds	<i>S. aureus</i> ATCC 29213	<i>S. aureus</i> ATCC 43300
7	4	4
25	>100	>100
26	25	12.5
27	6.25	6.25
28	100	100
29	>100	>100
30	25	25
31	>100	>100
32	6.25	6.25

33	2	2
34	6.25	6.25
35	6.25	6.25
36	12.5	12.5
37	>100	>100
38	>100	>100
Vancomycin^a	2	2
Oxacillin^a	2	10

^aAntibiotic concentrations are expressed as $\mu\text{g/mL}$ (2 $\mu\text{g/mL}$ corresponds to 1.35 μM for vancomycin and 4.72 μM for oxacillin; 10 $\mu\text{g/mL}$ of oxacillin corresponds to 23.6 μM).

Among the fifteen synthesized and screened molecules, compounds **7** and **33** displayed the best activity since the minimum bactericidal concentration (MBC) resulted 4 and 2 μM , respectively. This initial screening led us to establish the SAR considering the strong influence exerted by the C-3 functionalization. In particular, para-biaryl unsubstituted systems of compounds **7** and **33** displayed the highest activity.

Since compound **33** resulted the most active of the library, a time-kill assay¹³³ was performed to determine its bactericidal or bacteriostatic activity over time on *S. aureus* ATCC 29213 and *S. aureus* ATCC 43300

at the MIC value. As reported in the following graph, compound **33** exhibited bactericidal effect, reducing the starting $\log_{10}\text{CFU/mL}$ by greater than $3\log_{10}$ after 3 h, while any cell growth was detected at 24 h.

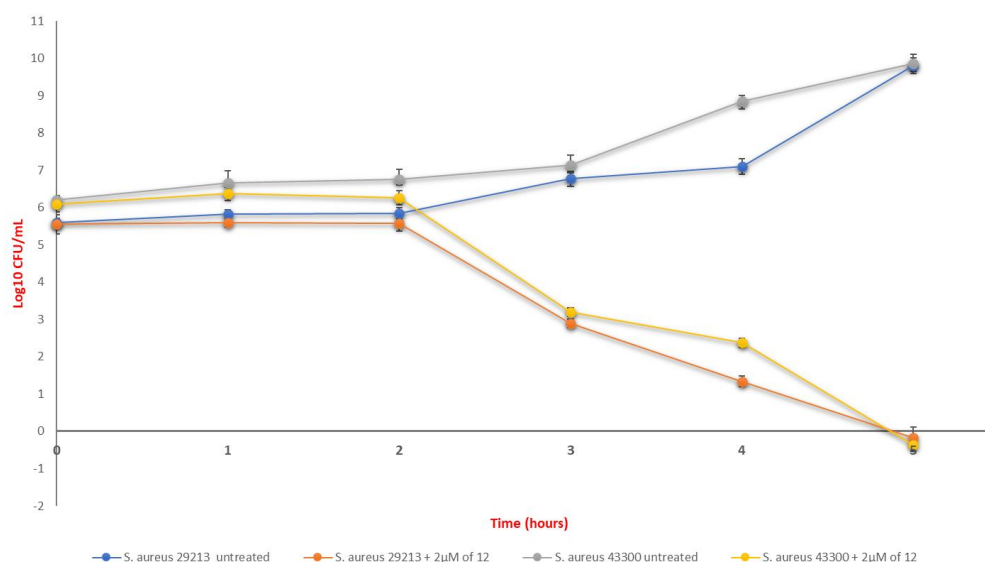


Figure 23. Time-kill assay of compound **33** against *S. aureus* ATCC 29213 and *S. aureus* ATCC 43300.

Each experiment is the result of three independent experiments performed in triplicate.

In these obtained results, is worth mentioning that compound showed antimicrobial activity at a lower concentration rather than the already reported values in previous studies for the oxadiazoles class as antimicrobial agents. Moreover, the presence of para-biphenyl system in position 3 give the compound greater effectiveness rather than the para-diphenyl ether function in compounds **21** and **22** reported by Chang's group.

3.2.5 Synergistic study

Novel approaches of great interest in antibiotics research field involve the synergism between traditional antibiotics and new agents to minimize the spread of antibiotic-resistant pathogens. The clinical benefit of antimicrobial synergism has been appreciated considering the possibility to restore or improve the activity of existing antibiotics well-known for their pharmacokinetic features.

Compound **33** demonstrated antibacterial activity and also synergy when combined with and oxacillin against MRSA.

Synergy measurement between **33** and oxacillin was evaluated by checkerboard analysis. The Fractional Inhibitory Concentration (FIC) index value represents the combination of antibiotics compared to their individual activities. The most impressive synergistic interaction was obtained with the combination values of 0.78 μM for compound **33** and 0.06 $\mu\text{g/mL}$ for oxacillin. The FIC index value of 0.396, confirmed the synergistic effect of compound **33** and oxacillin.

3.2.6 Molecular analysis

The major cause of resistance in MRSA is the *mecA* gene, contained in a sequencing region named the staphylococcal cassette chromosome *mec* (SCC*mec*), which is absent in methicillin susceptible *S. aureus*.¹³⁴

The *mecA* gene encodes for a novel penicillin-binding protein, PBP-2a, that displays a low affinity for methicillin and favours an undisturbed biosynthesis of bacterial cell-wall. The expression of PBP-2a is controlled by two genes, *mecRI* and *mecI*, located upstream from *mecA*. Normally, *mecA* transcription is repressed by *mecI* bound to its promoter region, while in presence of β -lactams, detected by the sensory domains in *mecR*,

the repression of *mecA* transcription by *mecI* is completely inhibited. This mechanism leads to *mecA* transcription and PBP2a translation, conferring the methicillin resistance.¹³⁵

In this study we analyzed how compound **33** can modulate the expression of *mecA*, *mecI*, *mecR1*.¹³⁶ The treatment with sub-inhibitory concentration of **33** (1 μ M and 0.39 μ M) for 30 min induced a reduced expression of all *mec* operon genes, whereas oxacillin strongly induced them both at sub-inhibitory (0.03 μ M g/mL) than MIC values (10 μ M g/mL) (Figure 24). On the contrary, the synergic interaction between **33** and oxacillin, used at sub-inhibitory concentrations, counteracts the effect of oxacillin restoring the level of expression of all genes (*mecA*, *mecI*, and *mecR1*) to value comparable to **33** treated cells.

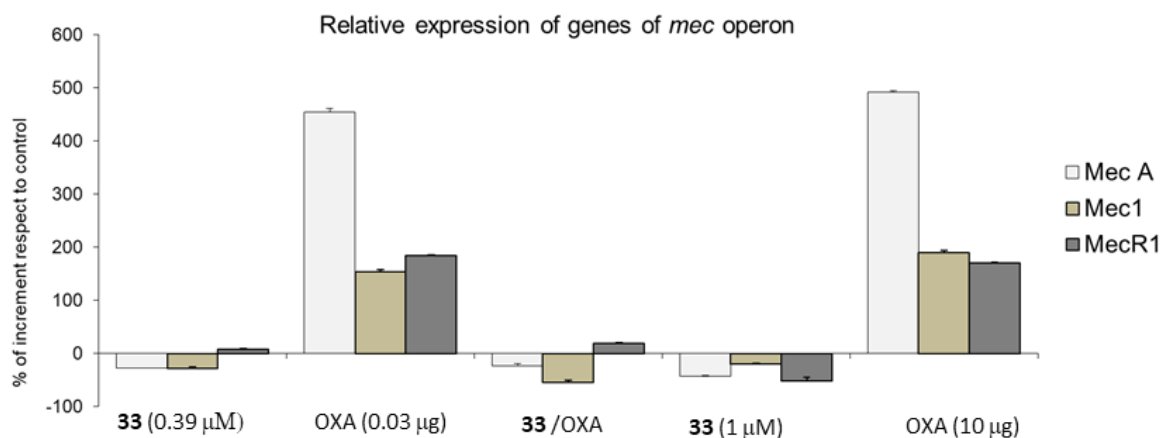


Figure 24. Relative expression of genes of *mec* operons.

S. aureus ATCC 43300 was treated with sub-inhibitory concentrations of **33** (0.39 μ M) and oxacillin (OXA) (0.03 μ g/mL) for 30 min. Transcript levels were monitored by RT-PCR. The data are presented as the fold change in gene expression normalized to an endogenous reference gene (16 S) and relative to the untreated. Values represent the mean \pm SD for three independent experiments.

The treatment of MRSA with compound **33** induced a decreased expression of genes included in the *mec* operon. Compound **33** interestingly contrasts the protective response of bacteria to oxacillin treatment, namely the strong induction of *mecA* gene and related genes of the operon, re-sensitising MRSA to beta-lactam antibiotics.

3.2.7 Cytotoxic assays

Cytotoxicity of **33** was analyzed in HaCaT isolated keratinocytes as human model *in vitro*. The bioscreen revealed that **33** is able to inhibit cell proliferation only at higher concentrations.

Specifically, after 48 hours of incubation at ≤ 25 μM concentration, compound **33** does not show any interference with cells viability. However, at higher concentrations more than 35 μM , compound **33** exhibited a cytotoxic activity on HaCaT cells line. Figure 25 A represents the curve-concentration in which can be noted a typical concentration-dependent sigmoid trend yielding IC_{50} values in the low micromolar range (Figure 25 B). DMSO was used as negative control to exclude any effect of the vehicle. As reported in Figure 25 A, there is no interfering with cell viability following incubation with DMSO, even at higher concentrations.

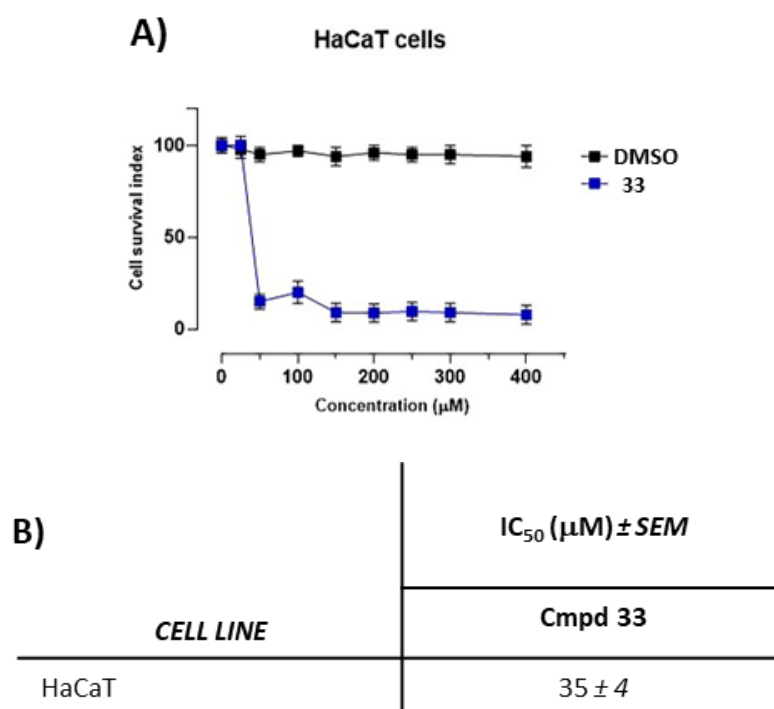


Figure 25. **A)** Cell survival index, evaluated by the MTT assay and monitoring of live/dead cell ratio relative for the compound **33** for HaCaT cell line following 48 h of incubation with the indicated concentration (the range 1 → 400 µM), as indicated in the legend. Data are expressed as percentage of untreated control cells and are reported as mean of five independent experiments ± SEM (n = 30); **B)** IC₅₀ values (µM), relative to the compound **35** for HaCaT cell line following 48 h of incubation. The IC₅₀ value is reported as mean values ± SEM (n = 30).

CHAPTER 5

Design and synthesis of compounds from natural source inspiration as potential anticancer agents

5.1 The importance of natural compounds in drug discovery

Nature has been always recognized as an invaluable source of inspiration in discovering new drugs and the use of natural products as therapeutical agents has been described through history since the earliest human civilization. Extracts derived from plants, microorganisms, fungi, and minerals have been represented for many years the only available medical treatment in forms of oils, potions, or remedies.²²⁴

Since they have evolved over millions of years, natural products represent relevant privileged scaffolds due to their unique chemical diversity and structural variability which result in several biological activities and drug-like properties that have gained considerable attention.²²⁵ Indeed, the research on natural compounds and secondary metabolites relies on a wide a variety of lead structures, which may be used as templates for the development of new potential drugs by both academic laboratories and pharmaceutical industry.²²⁵

The world of drug discovery has been revolutionized by new powerful innovations able to accelerate this long and complex process.²²⁶ Therefore, increasing interest has recently been paid to natural products in the search for novel drugs in combination with new technology, such as high-throughput selection and combinatorial chemistry. The exhibition of a wide range of pharmacophores is expected to contribute to the ability of such collections to provide hits. Thus, the generation of many libraries of compounds is based on the strong relevance of natural products as platforms for new drug candidates' development.

Even considering these advances, natural compounds and derivatives and their potential in speeding up the drug discovery process is still underexplored.

Approximately 40 % of the developed drugs approved by the FDA during the last decades were natural products, their derivatives, or synthetic mimetics related to natural products.²²⁷

This supports the growing efforts of medicinal and organic chemists in pursuing chemical modification and derivatization of active natural product skeletons towards the generation of novel therapeutical agents. A deeper knowledge of the selected targets, through the auxiliary of developmental computational techniques and *in silico* studies, suggests the optimization to be made on the scaffold to guarantee the best interactions towards the protein.

5.2 Bromodomains as epigenetic targets

The research on cancer's treatment has been focused for many years on the identification of gene mutations such as amplifications, deletions, and point mutations.

The role of epigenetic alterations has known to become increasingly relevant in the insurgence of tumor or other age-related diseases.²²⁸ The word "epigenetics" was originally coined by Conrad Waddington in 1939,²²⁹ who wanted to define the study of heritable changes in gene expression not related to alterations in the nucleotide sequence of DNA. In human cancers, epigenetic changes such as DNA methylation, histone modifications, micro RNAs and nucleosome remodelling, control the gene expression harming the homeostatic functions of cells.²³⁰ Among them, lysine acetylation represents one of the main post-translational modifications (PTMs) occurring in histone tails and it has been largely investigated for the important role displayed in the epigenetic landscape.²³¹ Acetyl groups are inserted on lysine residues due to the

activity of the histone acetyltransferases (HATs), while histone deacetylases (HDACs) are responsible their removal.²³² The acetylation status of lysine residues regulates the chromatin structure, and it is largely responsible for the functional diversity of the proteome by varying the affinity of histones towards DNA by covalent additions.

Another class of molecules known as “readers” is able to recognize *N*-acetylated lysine (KAc) residues on histones tails, and this is the important function played by bromodomains (BRDs).²³³

BRDs are evolutionary conserved epigenetic proteins with several relevant functions in gene transcription and chromatin remodeling, gene splicing, protein scaffolding and signal transduction.²³⁴ Firstly, they have been elucidated as a new structural pattern by J.W. Tamkun, who studied the gene *Brahma* (*brm*) of *Drosophila* and identified sequence similarity with genes involved in transcriptional activation.²³⁵

Acetylated lysins are recognized by bromodomain readers, which recruit complexes of remodelling and transcriptional factors, determining the functional outcome derived from the post-translational changes.

The human proteome presents 46 bromodomain containing proteins (Bcps), for a total of 61 different bromodomains, divided into eight distinct families according to their structural homology.^{236,237}

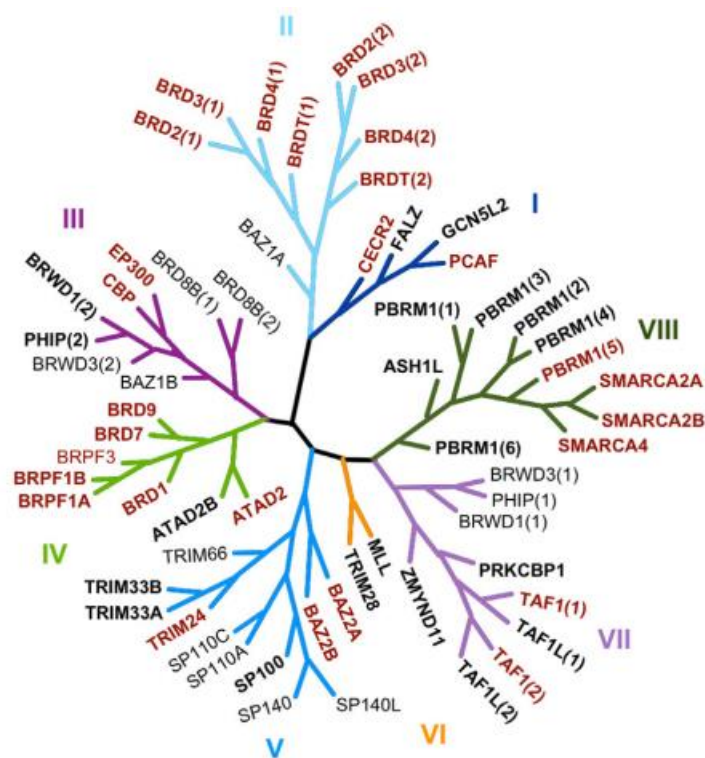


Figure 31. *Phylogenetic tree of humans bromodomains.*²³⁶

The structural organization of the bromodomains provides a left-handed bundle of four α -helices named αZ , αA , αB , αC . The hydrophobic pocket responsible of the interaction with acetylated lysine residues consists in a flexible loop region between αZ and αA (ZA loop) and a smaller one formed by αB and αC (BC loop).²³⁸ The four helices form a deep cavity between the two loops creating the binding site for the acetylated lysine. Structural studies suggest that the main interaction responsible of the correct orientation of *N*-acetyl lysine involves the oxygen of the acetylated carbonyl group and the amidic nitrogen of a residue of asparagine (Asn) at the end of the ZA loop, and a water-mediated interaction with a residue of tyrosine (Tyr). Indeed, despite the variations in various bromodomains, the amino acid residues in the binding site are highly conserved.

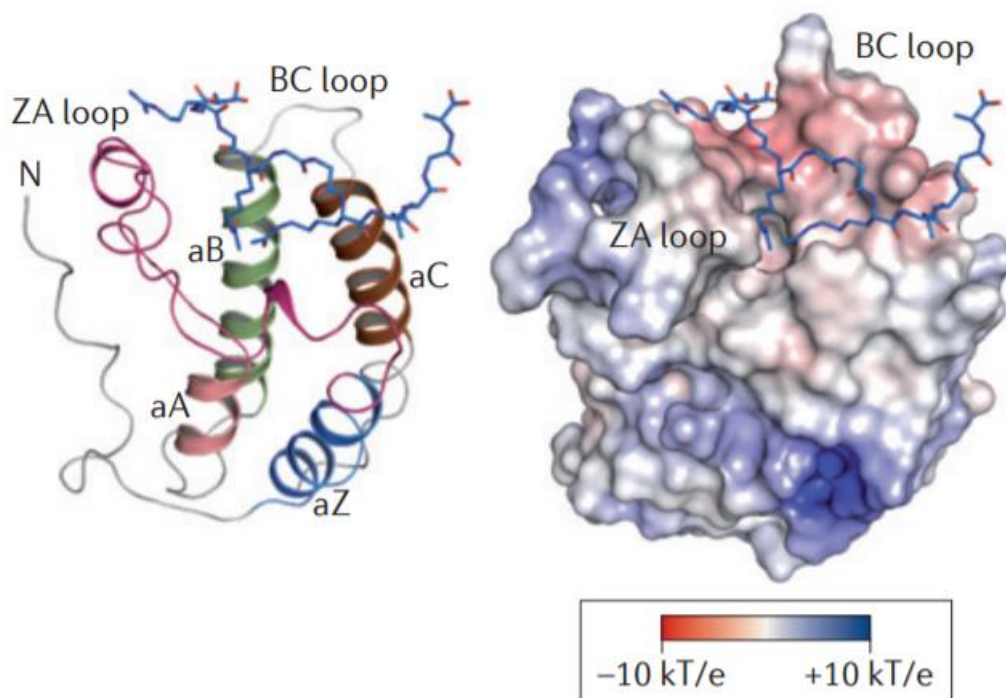


Figure 32. Four α -helices (αZ , αA , αB , αC) linked by ZA and BC loops. In figure is shown BRD4 in complex with a di-acetylated histone H4 peptide. The electrostatic potential highlights the charged nature of the surface lining the acetyl-lysine recognition site.²³⁸

Some bromodomains have shown to bind simultaneously two *N*-acetyl lysine residues and this is a typical feature of all members of the BET subclass (BRD2, BRD3, BRD4 and BRDT).²³⁶ The presence of a bromodomain at the N-terminal end and a C-terminal ET (extra-terminal) domain is responsible for the recognition of multi-acetylate histone tails.²³⁹

The presence of hydrophobic and aromatic residues characterizes the hydrophobic nature of the binding site, and this makes BRDs druggable targets of interest for the development of molecules able to inhibit protein-protein interaction.²³⁸

Considering that bromodomain-containing proteins are involved in the regulation of transcriptional process, also playing a key role in the development of several aggressive types of cancer, their activity has been investigated in many studies over the years.

Several computational tools, such as quantitative structure–activity relationship, virtual screening and machine learning, have been used for the prediction of bromodomain inhibitors and especially the members of BET family have been the protagonists of many investigations in the last decade, allowing to obtain different ligands with high affinity involved in autoimmune diseases, haematological cardiovascular diseases and cancers.²³³

Recent studies have also been devoted to the exploration of the structural features and the activity of the remaining non-BET domains, representing the most part of BRDs.

5.2.1 BRD9: a promising target for the treatment of cancer

ATP-dependent chromatin remodelling complexes (CRCs) are a group of epigenetic regulators. Their remodelling activity facilitates the accessibility of transcriptional factors by regulating gene expression and repression, as well as DNA replication, recombination and repairing processes.

These factors are divided into four distinct groups: SWI/SNF (*switching defective/sucrose non-fermenting*), ISWI (*imitation SWI*), NuRD (*nucleosome remodelling and deacetylation*)/Mi-2/CHD (*chromodomain, helicase, DNA binding*) e INO80 (*inositol requiring 80*). Despite the ATP-domain is very similar, the main difference among the four families is

represented by the domains involved in the interaction with chromatin (bromine, chromium and SANT domini).²³⁰

In more than 20% of cancers the components of SWI/SNF CRC appears to be mutated, supporting the role of epigenetic regulators in the development and progression of various types of cancers such as renal carcinoma, breast cancer, acute myeloid leukaemia (AML), cervical carcinoma, hepatocellular carcinoma.²⁴⁰

The SWI/SNF CRC changes chromatin accessibility by chromatin repositioning, nucleosome ejection, and histone dimer eviction. It is one of the most investigated not only for its involvement in oncogenesis, but also for its role in the regulation of pro-inflammatory genes. Two major subtypes of SWI/SNF have been identified in mammals, determined by their subunit composition: BAF (*BRG1-or BRM-associated factors*) and PBAF (*factors associated with Polybromo-BAF*).²⁴¹

In more details, BRD9 (*Bromodomain-containing protein 9*), which is part of BAF complex and member of the fourth family of bromodomains, has recently shown to play a relevant role in cancers development as a subunit of SWI/SNF. This protein is involved in the recognition of acetylated lysine residues on histone tails, even if the mechanism beyond this function is nowadays poorly understood despite many advances in epigenetic field.²⁴²

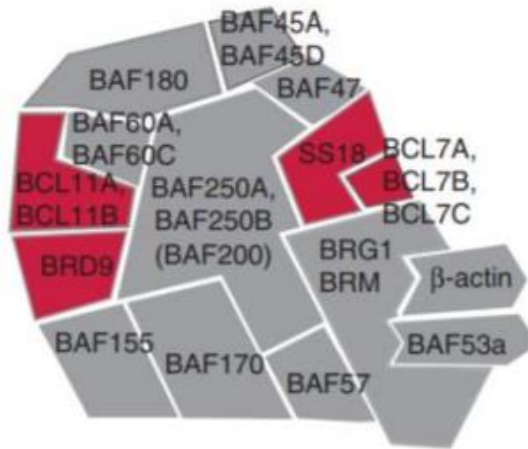


Figure 33. Recent model of BAF SWI/SNF complex. In red are highlighted the most recently identified subunits, among them BRD9.²⁴⁰

The gene encoding BRD9 is located on the 5p arm of chromosome 5, and although its biological function and exhaustive mechanism remains still undefined, this protein appears to be overexpressed in different pathological tissues. Moreover, BRD9 is part of a newly characterized non-canonical complex of mammalian SWI/SNF (ncBAF), which lacks several subunits compared with canonical BAF (e.g., BAF47, ARID1A).²⁴³ ncBAF complex maintains proliferation of AML cells while exhibiting increasing responses to the BRD9 subunit perturbation during the origin of hematologic neoplasms. Recent studies showed that SWI/SNF complex results altered even in paediatric malignant rhabdoid tumors (RTs), driven by a biallelic inactivation of SMARCB1, due to a lack in BRD9 of this core subunit.²⁴⁴ The same kind of mutation has been reported also for myoepithelial tumors and hepatoblastomas. A significant increase of BRD9's copy number has been shown in cervical cancer as well as non-small-cell lung cancer.^{245,246,245}

Overall, these outcomes indicate that BRD9 plays a critical role in the development and progression of several human cancers. Therefore, selectively targeting BRD9 displays a promising potential as an innovative therapeutic option against cancer.²³⁸

Since bromodomains have emerged as compelling targets for cancer treatment, the development of selective and potent BET inhibitors, especially in the last years, have rapidly translated into clinical studies and have strongly motivated the drug development aiming to target non-BET BRDs.

In this contest, Bromosporine represents one of the first report of multi-bromo-domain inhibitor, which acts as a broad-spectrum inhibitor. This promiscuous compound presents a triazolopyridazine dicyclic scaffold and has proven to be very useful in the exploration of physiological and pathological processes in which these domains are involved.²⁴⁷

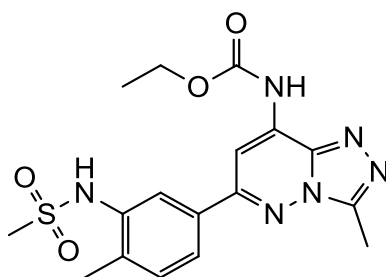


Figure 34. *Bromosporine.*

Other examples of most potent inhibitors known to target all eight bromodomains of the BET family are I-BET762,²⁴⁸ JQ1,²⁴⁹ I-BET151,²⁵⁰ I-BET726,²⁵¹ PFI-1.²⁵²

The high similarity found between the different bromodomain subfamilies, especially in the KAc binding site, makes very difficult the development of their selective inhibitors. Nevertheless, some detectable differences in the amino acid sequence allow to define a greater selectivity between BET and non-BET, and also within the same entire subfamily.

The tertiary structure of BRD9 shares with other bromodomains the same left-handed bundle of four α -helices connected by ZA and BD loops. An important structural feature consists in a sequence of three amino acids adjacent to the ZA loop that appears to be stored especially among the members of BET subfamily. Since not all bromodomains present this structural motif, this region can be taken into account to obtain a selective activity, especially between BET and non-BET inhibitors.

In more details, in the BET members, of which BRD4 BD1 is the main exponent, this region is named *WPF shelf* for presence of the amino acids Trp81 (W), Pro82 (P) and Phe83 (F); in BRD9 the correspond hydrophobic pocket is the *GFF shelf* due to the presence of Gly43 (G), Phe44 (F) and Phe45 (F).^{253,254} The analysis of their crystallographic structures allowed to elucidate important differences in the active site.²⁵⁵ In particular, a residue of Tyr106 (coloured in blue in Figure 35 D) plays the role of “gate keeper” preventing the access to the GFF region and blocking the accommodation of a second molecule of acetylated lysine. Thus, the hydrophobic pocket is less large than the same correspondent in the BET bromodomains, making more complex the development of suitable inhibitors. Indeed, the same role in BET is played by Ile146 (coloured in blue in Figure 35 C) allowing the WPF shelf to be wider and more accessible. Another key difference is given by the presence of a residue of Alanine (Ala54, in red in figure 35 D) rather than a Leucine (Leu94, in red

in Figure 35 C) in BRD4 BD1, which shows basic properties when protonated, that makes less hydrophobic the binding site of BRD9. Additionally, the ZA channel's architecture is different between BRD9 and BRD4, since in BRD9 the residues of Ala46, Phe47, Pro48, Thr50 e Ile53 amplify this region forming a wide hydrophobic cavity.

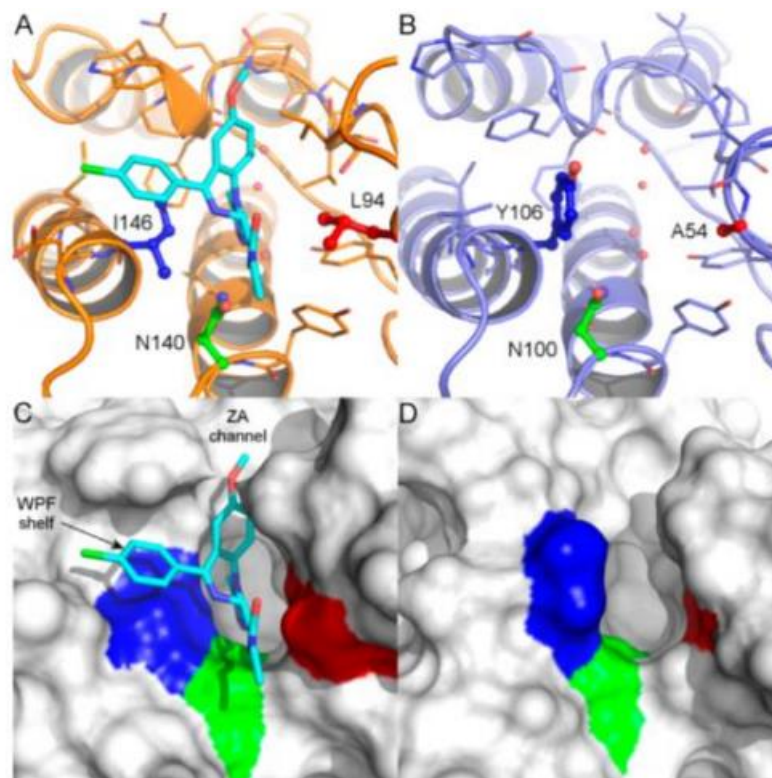


Figure 35. X-ray crystal structures of BRD4 BD1 and BRD9.

A) BRD4 BD1 bromodomain with I-BET762; B) BRD9 bromodomain; C) BRD4 BD1 surface; D) BRD9 surface.²⁵⁵

An interesting structural similarity has been noted between the active site of BRD9 and BRD7, a bromodomain-containing protein which is part of PBAF subclass of SWI/SNF and belongs to the same subfamily of BRD9.²⁵⁶ Despite their bromodomains are highly homologous, their roles in tumor progression are quite different since BRD9 plays a role in cancer

promotion as previously described, while BRD7 acts as a tumor suppressor, whose expression is mutated in several types of cancer.²⁵⁷

Due to the close homology between BRD9 and BRD7, many co-inhibitors exist, and the first known example is LP99 reported in 2015 as a valid modulator of pro-inflammatory cytokine secretion towards the selective inhibition of both bromodomains.²⁵⁸

Recently, an iterative structure-based design has been described the 9H-purine scaffold as bromodomain template to further explore the investigation around BRD9 inhibition.²⁵⁹

I-BRD9 has been reported as the first selective inhibitor of BRD9, with a 700-fold selectivity greater than the BET subfamily and more than 200-fold selectivity over its homologous BRD7.²⁵⁵ Its structure presents a thienopyridone ring in which the carbonyl moiety makes a hydrogen-bond with Asn100, a very important residue for KAc recognition. The carbonylic function also forms a shorter hydrogen-bond bridge with a conserved water molecule and Tyr57. Moreover, the N-methylpyridone methyl group acts as a structural analogue of KAc.²⁵⁵

Two other BRD9 inhibitors, BI-7273 and BI-9564, have been shown an antitumor activity in an AML xenograft model.²⁶⁰

TP-472 has recently demonstrated suitable inhibition towards both BRD9/7 bromodomains *in vivo* studies.²⁶¹

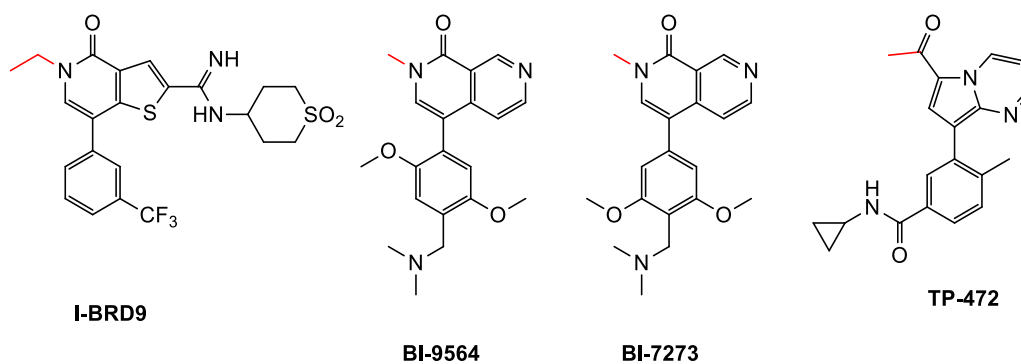


Figure 36. *Examples of BRD9 inhibitors.*
 In red are shown the mimicking groups of acetyl lysines.

Despite the great advances made by several investigations in this emerging target area, BRD9 still remains an ambiguous target not yet fully elucidated. Moreover, the high structural homology between BRD7 and BRD9 (62% of the amino acid sequence) and the similar distance between the two opposite sides of the binding site, makes more complex and also challenging the search of new selective ligands against BRD9.

The present research work takes place in this frame with the main purpose to synthesize novel potential BRD9 modulators driven by a combination of structure-guided and computational approaches.

5.3 Viridicatin derivatives as potential inhibitors of BRD9

5.3.1 Viridicatin and viridicatol

Viridicatin (3-Hydroxy-4-phenyl-1H-quinolin-2-one) and viridicatol (3-hydroxy-4-(3-Hydroxyphenyl)-1H-quinolin-2-one) are two fungal metabolites produced by several species of *Penicillium* known for their antimicrobial and anti-inflammatory properties. A recent study also reports their inhibitory effect towards matrix metalloproteinases (MMPs), enzymes involved in the extracellular matrix degradation, that appeared to increase in tumorigenesis.²⁶²

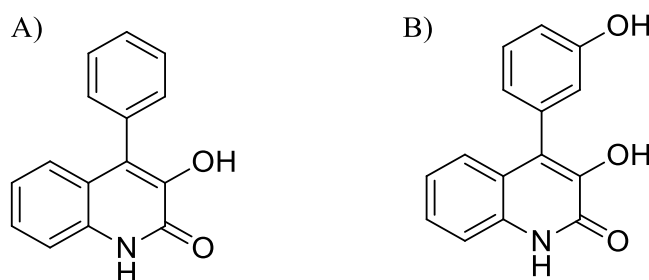


Figure 37. Structures of viridicatin (A) and viridicatol (B).

The structural features of these natural alkaloids make them ideal candidates for the design of novel compounds able to target BRD9.

The main purpose of this research project is to investigate the ability of viridicatin and viridicatol and their semi-synthetic derivatives to interact with this promising target, starting from a preliminary *in silico* analysis of the binding of the two molecules in the active site of BRD9 performed by our computational partners from the University of Salerno.

We also envisaged that further functionalization of viridicatol and viridicatin skeletons could lead to suitably decorated compounds bearing

the essential acetyl-lysine mimetic moiety in their structures. First of all, since both compounds are commercially available, we sought to investigate their binding to BRD9 at different concentrations. This preliminary investigation revealed a moderate and dose-depending binding to BRD9 worthy of further investigation.

5.3.2 *In silico* studies

With the aim of identifying a new KAc mimetic chemotype, an *in silico* study has been performed in order to investigate the binding mode of viridicatin and viridicatol's scaffolds in the active pocket of BRD9.

The results of docking calculations showed remarkably convergent binding modes. The quinolone scaffold is positioned in an amphipatic pocket, where it establishes cation π and π - π stacking interaction with Asn100 (Figure 38 A) and Tyr106. Moreover, the nitrogen H-bonds the Phe44 backbone. The binding mode of viridicatin results further stabilized by an additional stacking interaction between its phenolic ring and the aromatic chain of Tyr106.

The designed derivatives have been characterized by a mono or double alkylation of nitrogen in position 1 and enolic oxygen in position 3. The rational introduction of these structural elements is based on their ability to mimic acetylic groups of histone lysines, responsible for bromodomain's recognition. A recent discovery made by Clegg and co-workers,²⁶³ in which they disclosed the possibility of increasing the selectivity of inhibitors against BRD9/7 by replacing the classical methyl with a n-butyl group, supported the introduction of these functions on the chemical core. Indeed, the predicted binding mode of the substituted analogues showed to further stabilize the accommodation within the active

site of BRD9. Another element of variability is represented by the introduction of different substituents on the aromatic ring in position 4, to clarify its role in the interaction towards the target.

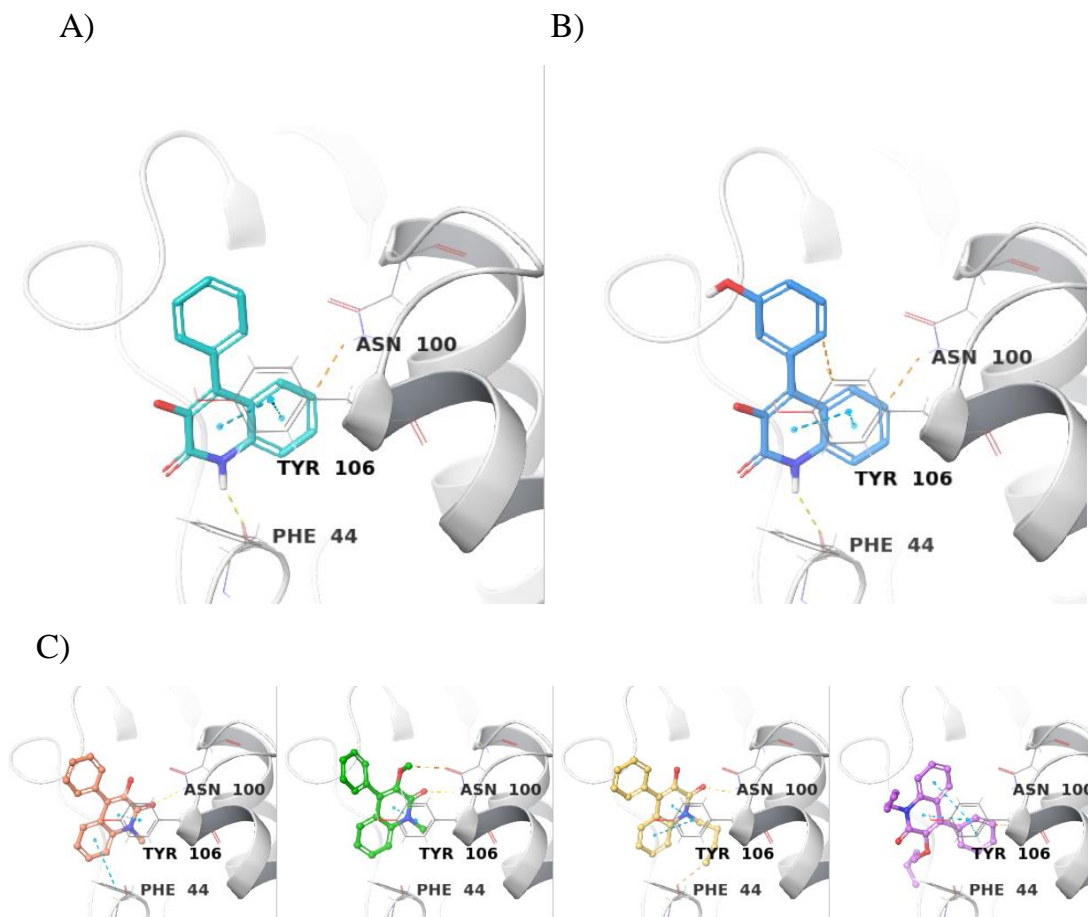


Figure 38. A) *binding mode of viridicatin*; B) *binding mode of viridicatol*; C) *representative examples of the binding mode of derivatives*.

A small focused library of analogues was thus generated following a recently published synthetic strategy allowing the fast and diversity-oriented generation of viridicatin derivatives through one-pot ring-expansion on isatin derivatives.²⁶⁴

Accordingly, the quinolone core of the compounds deriving from the one-pot protocol were on the N- or O- alkylated in position 1 and/or 3, respectively. Moreover, in order to boost our SAR analysis, we also

synthesized dialkyl derivatives. Beyond the classical alkylation with methyl group to obtain acetyl lysine mimetics, we also designed butyl derivatives, in line with recent literature reports.

Finally, a library of 12 compounds has been synthesized and fully characterized. Others derivatives are planned to be further obtained, in particular the mono-alkylated compounds in position 3. Moreover, we will further explore other substitutions on the phenyl ring in position 4, as promising modulators of the receptor, accordingly to the study of BRD9 crystallographic's structure.

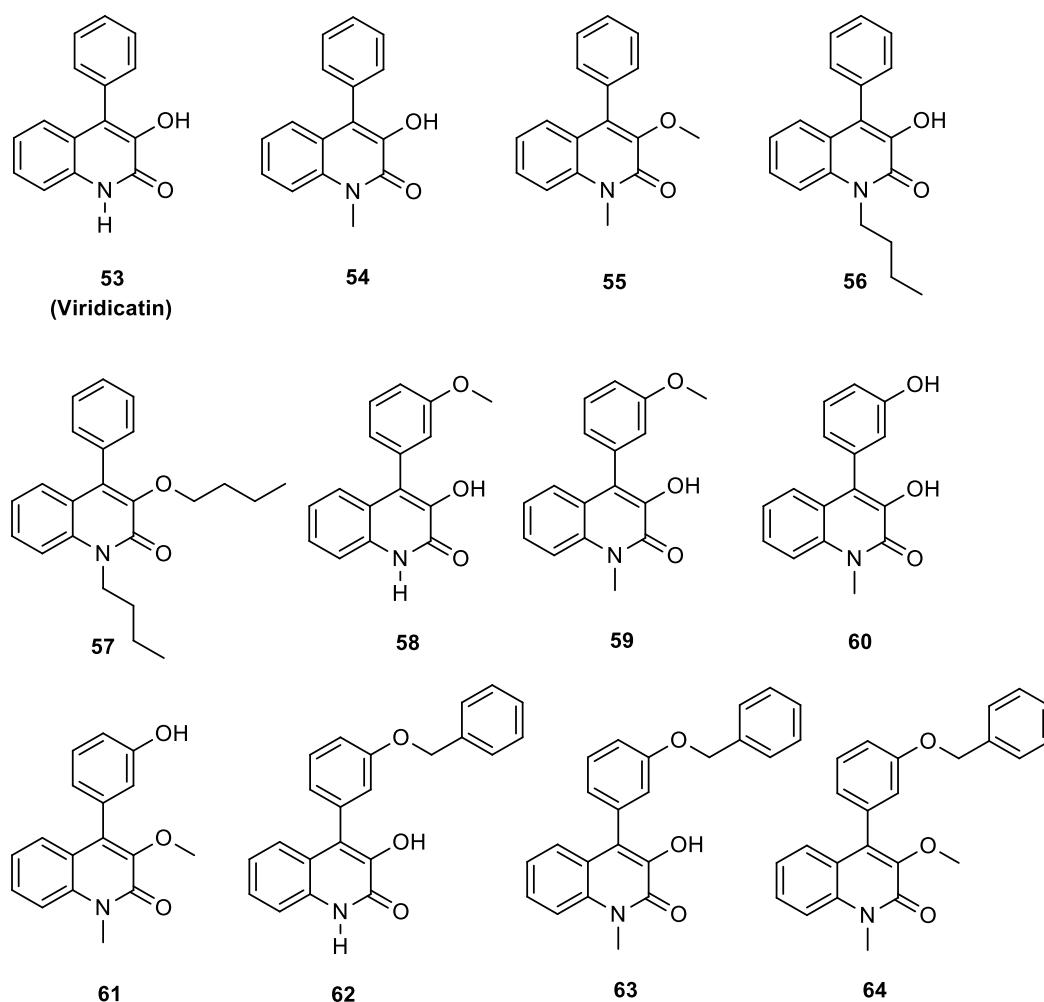
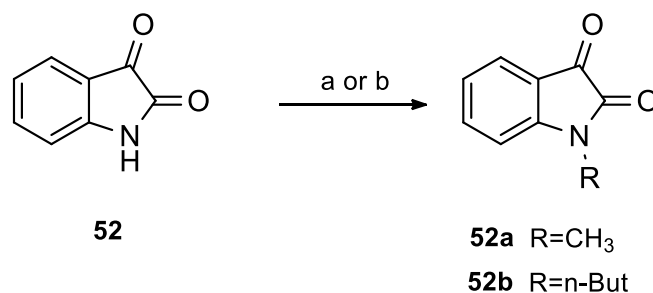


Figure 39. Library of viridicatin and derivatives.

5.3.3 Synthesis of viridicatin and derivatives

Compounds **53-64** have been synthesized using isatin as raw material. This scaffold is considered an important building block in organic synthesis, and a wide range of reactions is based on the use of isatin in the synthesis of heterocyclic compounds.²⁶⁵

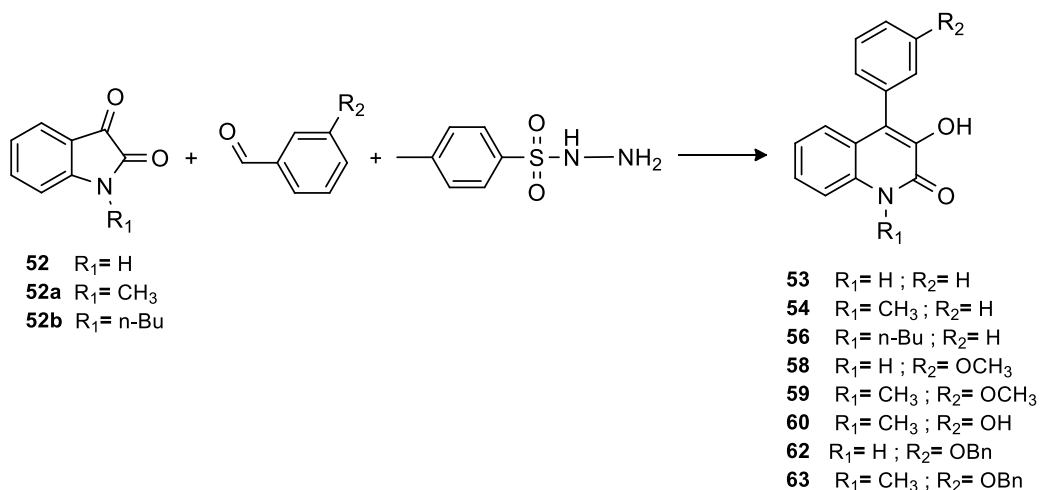
An initial N-alkylation of isatin has been required for the synthesis of compounds **54**, **56**, **59**, **60** and **63**, all characterized by the presence of N-methyl or N-butyl substitution. This modification is performed on the isatin **52**, deprotonated in presence of NaH with CH₃I or 1-Bromobutane.



Scheme 5. Synthetic procedure for the synthesis of intermediates **52a** and **52b**

Reagents and conditions: a) NaH, CH₃I in DMF dry, 0 °C, yield 80%; b) NaH, 1-Bromobutane, in DMF dry, 0 °C, yield 80%.

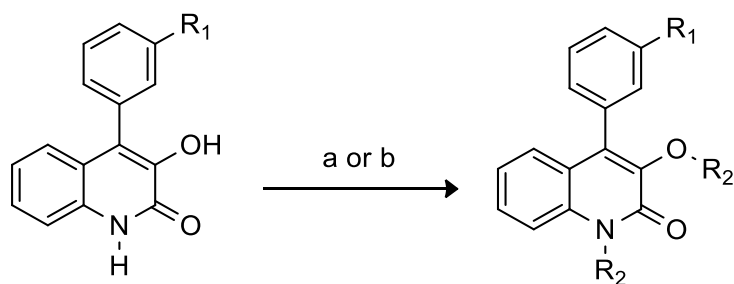
The quinolone nucleus has been synthesized through a regioselective one-pot ring expansion. This protocol involves the use of 3 reactant components: a) isatin **52** or its alkylated derivatives **52a** and **52b**, b) one arylaldehyde and c) p-toluenesulfonylhydrazide. α -aryldiazomethane formed *in situ* by reaction of aldehyde and p-toluenesulfonylhydrazide, followed by base treatment, regioselectively attacks 3-carbonyl of isatine with subsequent ring expansion to afford derivatives **53**, **54**, **56**, **58**, **59**, **60**, **62** and **63**.



Scheme 6. One-pot ring-expansion for the synthesis of chinolonic nucleus-

Reagents and conditions: a) isatin, pTs-hydrazide, aryl-aldehyde, K₂CO₃ in EtOH, reflux o/n, yield 60-80%.

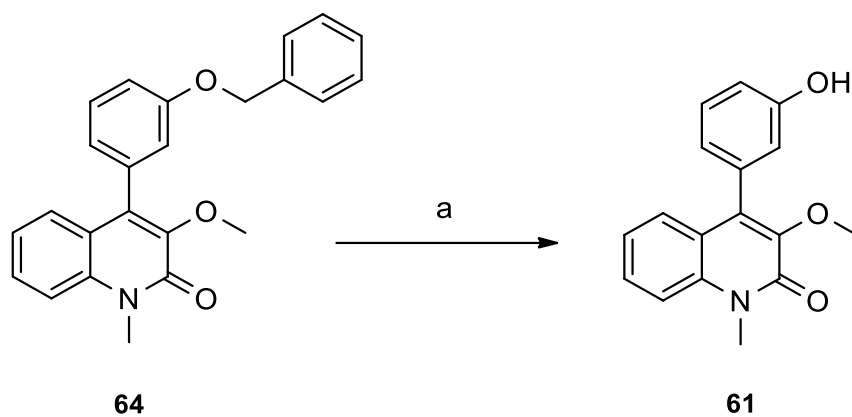
Double alkylated compounds **55**, **57**, and **64** were obtained from compounds **53** and **62** by N,O-dimethylation, or dibutylation, as described before.



Scheme 7. Synthetic procedures for compounds **55**, **57** and **64**.

Reagents and conditions: a) NaH, CH₃I in DMF dry, 0 °C, 1h; b) NaH, 1-Bromobutane, in DMF dry, 0°C, 1h, yield 70-80%.

Finally, compound **61** has been synthesised from **64** by a hydrogenolysis reaction with H₂ and Pd/C (10 %), which favoured the deprotection of the etheric aryl-bound benzyl group at position 4.



Scheme 8. Deprotection of benzylic function on compound **64** to afford compound **61**.

Reagents and conditions: a) H₂, Pd/C (10 %) in MeOH dry, 2 h, yield 97%.

5.3.4 Biological evaluation and future plans

All the synthesized compounds have been sent to the Reaction Biology Company (Malvern, PA), in order to evaluate their ability to interact against BRD9. Unfortunately, the obtained result did not match with our predictions since the performed *in vitro* assay revealed poor inhibition of the selected target. Nevertheless, the drug-like properties of our molecules make them suitable candidates to interact with biological targets of significant interest.

The quinolone moiety offers an easily accessible and well-understood scaffold for designing new drugs. Thus, an extension of our library can be planned on the basis of the structural activity relationship, since many anti-cancer activities of these motifs have been outlined.

Further studies will be carried out to exploit these properties as promising pharmacophores in the landscape of cancer therapy.

CONCLUSIONS

In my PhD research activity, different heterocyclic motifs have been explored as privileged scaffolds, obtaining wide libraries of compounds characterized by many interesting pharmacological properties.

The accurate selection of the best drug-like candidates has been carried out by an extensive *in silico* study, since the analysis of ligand-macromolecule interactions and the evaluation of possible binding modes are the starting points in a drug design project.

In the challenging process to find new promising and powerful drugs, I afforded to the identification of many active compounds, in particular 1,2,4-oxadiazoles-based hits disclosing very promising anti-inflammatory outcomes as compounds **1**, **2** and **5**. Interestingly, compound **5** displays its ability to interfere with the biosynthesis of prostanoids and leukotrienes with a horizontally and vertically multi- inhibitory activity on both COX and 5-LO pathways (COX-1, mPGES-1, and 5-LO), exhibiting IC₅₀ values at the low micromolar range. Moreover, *in vivo* studies confirmed its anti-inflammatory properties since can interfere with leukocytes migration in a model of zymosan-induced peritonitis and modulate the release of IL-1 β and TNF- α .

The elucidated multi-inhibition character can ensure an optimal safety profile that does not compromise the basal production of eicosanoids involved in physiological functions.

The concept of multi-target therapy has seen a rapid advance, becoming one of the hottest topics in drug discovery supporting the evidence that in some cases single-target drugs are inadequate to achieve a therapeutic effect in many complex pathologies. In this contest, the obtained results are of great interest considering that moderate interference with multiple targets might have advantages in re-adjusting homeostasis.

The application of computational tools allows to amplify the future prospective through a drug repositioning process carried out to optimize the search of new active compounds characterized by a promising and safer pharmacological profile.

An intense research activity has also favoured a repositioning study without the auxiliary of computational chemists, but only with a comprehensive exploration of the available literature that allowed to find a new application of a previously synthesized compound **7** with a lack in anti-inflammatory activity.

Thus, I investigated also the antimicrobial potential of this class of valuable heterocycle by exploring their chemodiversity. The most promising MIC value was exhibited by compound **33** of a newly designed library of molecules, when tested for the treatment of MRSA infections. Moreover, a typical pattern of synergistic interactions with oxacillin was shown by this active hit, identifying these outcomes as a great point of interest in light of the increasing widespread antibiotic resistance, considered by *WHO* one of the highest priorities for the global safety.

In the complex process of drug discovery, organic chemistry plays the key role to materialize the designed molecule after the intensive study of the most optimal synthetic strategies. Thus, the methodological aspect is also fundamental to gain the best performance and thanks to my abroad experience, I took the opportunity to explore a new frontier of organic synthesis represented by photocatalysis. In this contest, the emerging applications of carbon materials as catalyst supports in many catalytic pathways, allowed me to also approach the interesting field of nanotechnologies by investigating a new graphene-based carbocatalyst able to yield valuable heterocyclic cores as 1,3,4-oxaziazole based

molecules. The rational heterogenization of GA precursor makes possible the chemical reactions in a more sustainable fashion accordingly to the basic principles of green chemistry.

In this thesis, I followed an interesting approach consisted in different well-linked experimental steps to find novel chemical entities as active compounds. The multidisciplinary aspect that characterizes my research project has proved to be extremely useful to enrich the arsenal of molecules to be used in the treatment of important human disorders.

EXPERIMENTAL SECTION

Computational studies

The structures of 55 nitriles and 4888 carboxylic acids commercially available at Merck database, were used for building the novel library of 1,2,4-oxadiazoles. The reagents were converted from 2D to 3D structures using LigPrep and prepared using Reagent Preparation: the cyano group and the acidic moiety were removed in order to retain only the useful building blocks. The final.bld files were combined with 1,2,4-oxadiazole scaffold obtaining a novel library of 273,728 compounds. LigPrep⁹⁰ performed calculation increased the number to 303,618 molecules. QikProp⁹³ and LigFilter⁹⁴ were applied and a final library of 150,512 was obtained and submitted to docking studies.

The human crystal structure released in 2017 (PDB code: 5TL9)⁹⁵ of mPGES-1 was used to perform structure-based molecular docking experiments. The three-dimensional model of the protein was prepared using the Schrodinger Protein Preparation Wizard:²⁶⁶ hydrogens and cap termini were added, bond orders were assigned, water molecules were removed. Then, the combinatorial library was submitted to the virtual screening workflow (VSW) using Glide⁹⁶ software. The receptor grid adopted for molecular docking calculation was focused onto the co-crystallized ligand binding site⁹⁵ characterized from inner- and outer-box dimensions of 10 x 10 x 10 and 27.6 x 27.6 x 27.6, respectively. VSW consisted of three rounds of experiments: 1) High-Throughput Virtual Screening (HTVS) precision mode of Glide for a first enrichment from the starting library of compounds with a high fastness; 2) Standard Precision (SP) for the analysis of the 60% top-ranked poses of HTVS filtered according to docking score values; 3) Extra-Precision (XP) for the analysis of the 70% top-ranked poses of SP using the Glide mode experiment, the

final and most accurate docking step. Finally, specific filters on 4064 selected docking poses were applied using the pose filter tool of Maestro,⁹⁴ setting the key interactions as a qualitative filter. Furthermore, the final selection of the most promising molecules was also optimized considering computational tools: a) SwissADME,⁹⁷ for filtering the compounds displaying the features of “*Pan-Assay Interference Compounds*”; b) detailed analysis of the other specific pharmaceutically relevant properties obtained by QikProp software.⁹³

Chemistry

General experimental procedures

1D and 2D NMR spectra were recorded on Bruker Avance NEO 400 and 700 spectrometers equipped with an RT-DR-BF/1H-5 mm-OZ SmartProbe (¹H at 400 MHz, ¹⁹F at 376 MHz and ¹³C at 100 MHz; ¹H at 700 MHz and ¹³C at 175 MHz).

Coupling constants (J values) are given in Hertz (Hz), chemical shifts were reported in δ (ppm) and referred to the residual CH₃OD, CDCl₃ and CD₃SOCD₃ as internal standards ($\delta_{\text{H}} = 3.31$ and $\delta_{\text{C}} = 49.0$ ppm; $\delta_{\text{H}} = 7.26$ and $\delta_{\text{C}} = 77.0$ ppm; $\delta_{\text{H}} = 2.50$ and $\delta_{\text{C}} = 39.6$ ppm). All the recorded signals were in accordance with the proposed structures. Spin multiplicities are given as *s* (singlet), *br s* (broad singlet), *d* (doublet), or *m* (multiplet). ESI-MS analysis was carried out on a mass spectrometer LTQ-XL.

Specific rotations were measured on a PerkinElmer 243 B polarimeter. HPLC was performed with a Waters Model 510 pump equipped with Waters Rheodine injector and a differential refractometer, model 401.

Reaction progress was monitored via thin layer chromatography (TLC) on Alugram silica gel G/UV254 plates. The silica gel MN Kiesel gel 60

(70e230 mesh) of Macherey Nagel was used for flash chromatography. The purity of compounds was determined to be always greater than 95% by HPLC analysis or by NMR analysis according to the reported literature. All chemical solvents and reagents are commercially available from Sigma Aldrich® and TCI, with the following exception. Methanol was anhydri-fied from magnesium methoxide as follow. Magnesium turnings (5 g) and iodine (0.5 g) are refluxed in a small amount of methanol (50-100 mL), until all magnesium has reacted. The mixture was diluted (up to 1 L) with methanol, refluxed for 2-3 h and then distilled under argon. All reactions were carried out under argon atmosphere using flame-dried glassware

Acids **1a** (2-(4-hydroxyphenyl) propionic acid), **2a** (3-(3-hydroxyphenyl)propionic acid), **3a** (4-hydroxymethylphenylacetic acid), **4a** (3-hydroxybenzoic acid), **5a** (3-hydroxy-2,4,5-trifluorobenzoic acid) **6a** [(2S, 4R)-1-acetyl-4-hydroxypyrrolidine2-carboxylic acid], **7a** (indole-4-carboxylic acid) and **10a** (Boc-L-Tyr-OH) are commercially available and are purchased from Sigma Aldrich®.

Boc-protected acids **8a** (5-(tert-butoxycarbonyl) amino-2-hydroxybenzoic acid), **9a** [(2R)-2-(tert-butoxycarbonyl) amino-2-(4-hydroxyphenyl)acetic acid] and **11a** (α-methyl-(DL)-Boc-Tyrosine) were synthesized according to the reported methods.

Synthetic procedure for compound 13

Potassium carbonate (1.5 mol eq.) and hydroxylamine chloridrate (2.5 mol eq.) were added to a solution of 4-(3-thiophenyl) benzonitrile **12** (1 mol eq.) in dry methanol. The mixture was refluxed for 8 h in inert atmosphere. The reaction was concentrated under vacuum, diluted with water, and extracted three times with DCM. The organic phases were dried with

anhydrous Na₂SO₄, filtrated, and concentrated under vacuum to obtain the correspondent amidoxime **13** (70% yield). The product was subjected to the next steps without any purification.

Synthetic procedures for compounds 1-7

DIPEA (1.8 mol eq.) was added to a solution of carboxylic acids 1a-7a (1.2 mol eq.) dissolved in DMF dry. HBTU (1.5 mol eq.), was added to the mixture at room temperature as coupling reagent. Amidoxime **13** (1 mol eq.) was added 10 min later. The mixture was stirred at 140 °C for 12 h, then fractionated in water and ethyl acetate for three times. The organic layer was cooled and washed three times with a saturated solution of LiBr, then with a saturated solution of NaHCO₃ and distilled water. The organic layer was dried over anhydrous Na₂SO₄, filtered and concentrated under reduced pressure (40 - 75% yield).

Procedure for Boc protection of acids 8a and 11a

5-amino-2-hydroxybenzoic acid (0.653 mmol, 1 eq) and a methyl-DL-tyrosine (0.512 mmol, 1 eq) were respectively treated with Boc₂O (2eq) in 10% TEA in MeOH (5 ml) and stirred at rt overnight. Then the reaction solution was concentrated under reduced pressure, and the residue was extracted with H₂O /DCM for three times.

Purification on silica gel (DCM:MeOH) afforded Boc-protected acids **8a** and **11a**.

Procedure for Boc protection of acid 9a

D-4-hydroxyphenylglycine (0.597 mmol, 1 eq) was dissolved in a solution of NaHCO₃ (1 M) and Boc₂O (2.5 eq) in 1,4-dioxane at 0 °C. The solution was stirred overnight, and after the pH was adjusted until 2 - 3 using HCl 2 N, it was extracted with H₂O / Ethyl Acetate for three times to give Boc-protected acid **9a**.

Synthetic procedure for compounds 8-11

The compounds **8b-11b** were prepared treating the Boc-protected acids **8a, 9a** and 11a and the Boc-L-tyrosine **10a** with amidoxime **13** using the same synthetic procedure followed for compounds **1 - 7**.

Boc deprotection using a solution of DCM:TFA (1:1) at rt for 2h afforded the final compounds **8 - 11**.

Synthetic procedure for amidoximes 15a-e

The applied synthetic protocol was the same previously described to afford compound **13**.

Synthetic procedure for compounds 16-20

The applied synthetic protocol was the same previously described to afford compounds **1-11**.

Synthetic procedure for nitriles 23n and 23o

Methyl 4-(bromomethyl)benzoate and methyl 3-(bromomethyl)benzoate (1.2 mol eq.) were respectively added to a solution of 4-cyanophenol (1 mol eq.) and K₂CO₃ (2 mol eq.) in DMF dry at 100 °C. The reaction was stirred at 25 °C overnight, then fractionated in water and ethyl acetate for three times. The organic layers were dried over anhydrous Na₂SO₄, filtrated and concentrated under vacuum to obtain the correspondent nitriles methyl 4-[(4-cyanobenzyl)oxy]benzoate (**23n**) and methyl 3-[(4-cyanobenzyl)oxy]benzoate (**23o**).

Synthetic procedure for amidoximes 24a-o

The applied synthetic protocol was the same previously described to afford compound **13**.

Synthetic procedure for compounds 25-38.

The applied synthetic protocol was the same previously described to afford compound **1-11**.

Synthetic procedure for compounds 44a and 44b

NaH (1.16 mol eq) was added at 0° C in a solution of isatin (1 mol eq) in DMF *dry*. Iodomethan (1.16 mol eq.)/1-Bromobuthan (1.16 mol eq.) was added after 5 minutes, and the mixture was stirred at 0° C for 1 h in inert atmosphere. The reaction was then submitted to a quenching procedure with NH₄Cl and then concentrated under vacuum, diluted with water, and extracted three times with Ethyl Acetate. The organic phases were dried with anhydrous Na₂SO₄, filtrated and concentrated under vacuum to obtain the crude extract.

Sytnthetic procedure for compounds 53, 54, 56, 58, 59, 60, 62 and 63

A mixture of aldehyde (1 mol eq) and p-toluensulfonil hydrazide (1 mol eq) in ethanol was stirred at room temperature until the consumption of the starting materials (monitored by TLC). Isatin or its derivatives were added (1 mol eq) with K₂CO₃ (2 mol eq) was stirred to reflux for 8 h. The crude reaction was then concentrated under vacuum, diluted with water, and extracted three times with ethyl acetate. The organic phases were dried with anhydrous Na₂SO₄, filtrated and concentrated under vacuum to obtain the crude extract.

Synthetic procedure for compound 55 and 64

The applied synthetic protocol was the same previously described to afford compound **53a**, using 2 mol eq of CH₃I.

Synthetic procedure for compound 57

The applied synthetic protocol was the same previously described to afford compound **53b**, using 2 mol eq of 1-Bromobuthane.

Synthetic procedure for compound 61

Compound **64** has been dissolved in MeOH dry in a dry-flask with a small quantity of Pd/C (10%) under H₂. The reaction was stirred at rt for 2h and

then filtered on celite. The solvent was removed under vacuum to afford compound **61**.

5-(1-(4-hydroxyphenyl)ethyl)-3-(4-(thiophen-3-yl)phenyl)-1,2,4-oxadiazole (1). An analytic sample of crude reaction was purified by HPLC using a Luna Column C-18 (10 μ m, 250 mm x 10 mm) with MeOH/H₂O (80:20) as eluent (flow rate 3.00 mL/min) affording compound **1** (t_R = 13.5 min). ¹H NMR (400 MHz, CD₃OD): δ_H 8.10 (2H, d, J = 8.5 Hz), 7.83 (2H, d, J = 8.5 Hz), 7.78 (1H, dd, J = 2.7, 1.6 Hz) 7.52 (2H, ovl), 7.22 (2H, d, J = 8.6 Hz), 6.79 (2H, d, J = 8.6 Hz) 4.46 (1H, q, J = 7.2 Hz), 1.76 (3H, d, J = 7.2 Hz); ¹³C NMR (100 MHz, CD₃OD): δ_C 184.0, 169.2, 158.1, 142.5, 139.7, 132.5, 129.7 (2C), 128.8 (2C), 128.0 (3C), 127.4, 126.9, 123.0, 117.0 (2C), 38.8, 20.2; ESI-MS m/z 349.1 [M + H]⁺.

5-(2-(3-hydroxyphenyl)ethyl)-3-(4-(thiophen-3-yl)phenyl)-1,2,4-oxadiazole (2). An analytic sample of crude reaction was purified by HPLC using Luna Column C-18 (10 μ m, 250 mm x 10 mm) with MeOH/H₂O (80:20) as eluent (flow rate 3.00 mL/min) to give compound **2** (t_R = 23.5 min). ¹H NMR (400 MHz, CD₃OD): δ_H 8.07 (2H, d, J = 8.5 Hz), 7.83 (2H, d, J = 8.5 Hz), 7.78 (1H, m), 7.54 (2H, ovl) 7.11 (1H, t, J = 7.9 Hz), 6.71 (1H, d, J = 7.9 Hz), 6.70 (1H, s), 6.63 (1H, d, J = 7.9 Hz), 3.27 (2H, t, J = 7.7 Hz), 3.13 (2H, t, J = 7.7 Hz); ¹³C NMR (100 MHz, CD₃OD): δ_C 181.4, 169.2, 159.0, 142.6 (2C), 140.1, 130.5, 129.1 (2C), 127.9 (3C), 127.2, 126.9, 122.8, 120.5, 116.4, 114.7, 33.5, 28.9; ESI-MS m/z 349.1 [M + H]⁺.

5-(4-(hydroxymethyl)benzyl)-3-(4-(thiophen-3-yl)phenyl)-1,2,4-oxadiazole (3). An analytic sample of crude reaction was purified by HPLC using Luna Column C-18 (10 μ m, 250 mm x 10 mm) with

MeOH/H₂O (80:20) as eluent (flow rate 3.00 mL/min) to give compound **3** (*t_R* = 15.5 min). ¹H NMR (400 MHz, CD₃OD): δ_H 8.08 (2H, d, *J* = 8.4 Hz), 7.83 (2H, d, *J* = 8.4 Hz), 7.78 (1H, dd, *J* = 2.5, 1.6 Hz), 7.54 (2H, ovl), 7.38 (4H, s), 4.61 (2H, s), 4.36 (2H, s); ¹³C NMR (100 MHz, CD₃OD): δ_C 180.0, 169.3, 142.5, 142.2, 140.0, 134.3, 130.0 (2C), 128.7 (2C), 128.5 (2C), 127.7 (3C), 126.9, 126.4, 122.6, 64.4, 33.4. ESI MS *m/z* 349.1 [M + H]⁺.

5-(3-hydroxyphenyl)-3-(4-(thiophen-3-yl)phenyl)-1,2,4-oxadiazole (4).

An analytic sample of crude reaction was purified by HPLC using Luna Column C-18 (10 μm, 250 mm x 10 mm) with MeOH/H₂O (90:10) as eluent (flow rate 3.00 mL/min) to give compound **4** (*t_R* = 8.0 min). ¹H NMR (400 MHz, CD₃OD): δ_H 8.17 (2H,d, *J* = 8.4 Hz), 7.86 (2H, d, *J* = 8.4 Hz), 7.80 (1H, dd, *J* = 2.7, 1.3 Hz), 7.69 (1H, d, *J* = 7.7 Hz), 7.62 (1H, br t, *J* = 2.0 Hz), 7.56 (1H, dd, *J* = 5.0, 1.3 Hz), 7.53 (1H, dd, *J* = 5.0, 2.7 Hz), 7.43 (1H, t, *J* = 7.7 Hz), 7.09 (1H, dd, *J* = 7.7, 2.0 Hz); ¹³C NMR (100 MHz, CD₃OD): δ_C 177.4, 169.9, 159.6, 142.5, 140.1, 131.6, 129.0 (2C), 127.7 (3C), 127.0, 126.6, 126.4, 122.7, 121.3, 120.1, 115.5. ESI-MS *m/z* 321.1 [M + H]⁺.

5-(2,4,5-trifluoro-3-hydroxyphenyl)-3-(4-(thiophen-3-yl)phenyl)-1,2,4-oxadiazole (5).

An analytic sample of crude reaction was purified by HPLC using Luna Column C-18 (10 μm, 250 mm x 10 mm) with MeOH/H₂O (92:8) as eluent (flow rate 3.00 mL/min) to give compound **5** (*t_R* = 10.5 min). ¹H NMR (400 MHz, CD₃OD): δ_H 8.14 (2H, d, *J* = 8.4 Hz), 7.84 (2H, d, *J* = 8.4 Hz), 7.77 (1H, dd, *J* = 2.8, 1.3 Hz), 7.54 (1H, dd, *J* = 5.0, 1.3 Hz), 7.53 (1H, dd, *J* = 5.0, 2.8 Hz), 7.49 (1H, m); ¹³C NMR (100 MHz, CD₃OD): δ_C 173.2, 169.4, 150.1, 147.6, 144.1, 142.4, 140.2, 138.8, 128.7 (2C), 127.9 (2C), 127.5, 127.0, 126.4, 122.4, 109.0,

106.3.19F (376 MHz): ^1F 134.4 (m); 142.5 (m); 150.7 (m). ESI-MS m/z 375.0 $[\text{M} + \text{H}]^+$.

5-((2*S*-4*R*)-1-acetyl-4-hydroxypyrrolidin-2-yl)-3-(4-(thiophen-3-yl)phenyl)-1,2,4-oxadiazole (6). An analytic sample of crude reaction was purified by HPLC using Luna Column C-18 (10 μm , 250 mm x 10 mm) with MeOH/H₂O (68:32) as eluent (flow rate 3.00 mL/min) to give compound **6** (t_{R} = 11.5 min). ^1H NMR (400 MHz, CD₃OD): δ_{H} 8.05 (2H, d, J $\frac{1}{4}$ 8.4 Hz), 7.81 (2H, d, J = 8.4 Hz), 7.77 (1H, dd, J = 2.5, 1.5 Hz), 7.54 (2H, ovl), 5.34 (1H, t, J = 8.1 Hz), 4.63 (1H, m), 4.00 (1H, dd, J = 11.0, 4.4 Hz) 3.69 (1H, br d, J = 11.0 Hz), 2.46 (1H, m), 2.28 (1H, m), 2.15 (3H, s); ^{13}C NMR (100 MHz, CD₃OD): δ_{C} 181.5, 172.7, 169.3, 142.4, 141.1, 128.9 (2C), 127.7 (3C), 127.0, 126.3, 122.7, 70.7, 57.0, 53.6, 40.6, 22.3. $[\alpha]_{\text{D}}^{25}$ 30.7 (c = 0.22 in MeOH). ESI-MS m/z 356.1 $[\text{M} + \text{H}]^+$.

5-(1*H*-indol-4-yl)-3-(4-(thiophen-3-yl)phenyl)-1,2,4-oxadiazole (7). An analytic sample of crude reaction was purified by HPLC using Luna Column C-18 (10 μm , 250 mm x 10 mm) with MeOH/H₂O (95:05) as eluent (flow rate 3.00 mL/min) to give compound **7** (t_{R} = 9.0 min). ^1H NMR (400 MHz, CD₃OD): δ_{H} 8.24 (2H, d, J = 8.5 Hz), 8.04 (1H, dd, J = 7.8, 0.7 Hz), 7.88 (2H, d, J = 8.5 Hz), 7.80 (1H, dd, J = 2.8, 1.3 Hz), 7.73 (1H, br dd, J = 7.8, 1.3 Hz), 7.57 (1H, dd, J = 5.0, 1.3 Hz), 7.55 (1H, d, J = 3.0 Hz), 7.53 (1H, d, J = 3.0 Hz), 7.33 (1H, d, J = 7.8 Hz) 7.30 (1H, d, J = 5.0, 0.7 Hz); ^{13}C NMR (100 MHz, CD₃OD): δ_{C} 182.2, 169.7, 142.6, 139.9, 138.6, 129.0 (2C), 128.7, 127.8 (2C), 127.7, 127.4, 127.1, 127.0, 122.7, 122.6, 122.0, 117.5, 115.9, 103.3. ESI-MS m/z 344.1 $[\text{M} + \text{H}]^+$.

5-(5-amino-2-hydroxyphenyl)-3-(4-(thiophen-3-yl)phenyl)-1,2,4-oxadiazole (8). An analytic sample of crude reaction was purified by HPLC using Luna Column C-18 (10 μm , 250 mm x 10 mm) with

MeOH/H₂O (68:32) + 0.1% TFA as eluent (flow rate 3.00 mL/min) to give compound **8** ($t_R = 17.0$ min). ¹H NMR (400 MHz, CD₃OD): δ_H 8.20 (2H, d, $J = 8.6$ Hz), 8.00 (1H, dd, $J = 2.7$ Hz), 7.91 (2H, d, $J = 8.6$ Hz), 7.84 (1H, dd, $J = 2.7$ and 1.5 Hz) 7.58 (1H, dd, $J = 5.1$ and 1.5 Hz), 7.57 (1H, dd, $J = 5.1$ and 2.7 Hz), 7.52 (1H, dd, $J = 8.9, 2.7$ Hz), 7.28 (1H, d, $J = 8.9$ Hz); ¹³C NMR (100 MHz, CD₃OD): δ_C 175.2, 169.1, 158.5, 142.6, 140.8, 139.3, 129.8, 129.0 (2C), 127.9 (2C), 127.7, 126.9, 126.0, 122.9, 122.8, 122.4, 120.3. ESI-MS m/z 336.1 [M + H]⁺.

(R)-5-(amino(4-hydroxyphenyl)methyl)-3-(4-(thiophen-3-yl) phenyl)-1,2,4-oxadiazole (9). An analytic sample of crude reaction was purified by HPLC using Luna Column C-18 (10 μ m, 250 mm x 10 mm) with MeOH/H₂O (70:30) + 0.1% TFA as eluent (flow rate 3.00 mL/min) to give compound **9** ($t_R = 5.0$ min). ¹H NMR (400 MHz, CD₃OD): δ_H 8.16 (2H, d, $J = 8.3$ Hz), 7.86 (2H, d, $J = 8.3$ Hz), 7.80 (1H, dd, $J = 2.5, 1.5$ Hz), 7.55 (2H, ovl), 7.37 (2H, d, $J = 8.5$ Hz), 6.91 (2H, d, $J = 8.5$ Hz), 6.01 (1H, s); ¹³C NMR (100 MHz, CD₃OD): δ_C 176.8, 169.4, 160.9, 142.3, 140.6, 130.9 (2C), 129.1 (2C), 127.8 (3C), 127.0, 125.5, 122.9, 122.7, 117.4 (2C), 52.2. [a]_D 25 ρ 17 (c $\frac{1}{4}$ 0.76 in MeOH). ESI-MS m/z 350.1 [M + H]⁺.

(S)-5-(1-amino-2-(4-hydroxyphenyl)ethyl)-3-(4-(thiophen-3-yl) phenyl)-1,2,4-oxadiazole (10). An analytic sample of crude reaction was purified by HPLC using Luna Column C-18 (10 μ m, 250 mm x 10 mm, flow rate 3.00 mL/min) using as mobile phase Buffer A (0.1% TFA in water) and Buffer B (0.1% TFA in acetonitrile), with the following gradient: the initial solvent condition was 20% solvent B for 3 min; the gradient was then gradually increased from 20% to 95% solvent B over 18 min; solvent B was increased to 100% and was kept at 100% of B for 10 min. The purification afforded compound **10** ($t_R = 14.0$ min). ¹H NMR

(400 MHz, CD₃OD): δ_{H} 8.11 (2H, d, $J = 8.4$ Hz), 7.86 (2H, d, $J = 8.4$ Hz), 7.78 (1H, dd, $J = 2.5, 1.7$ Hz), 7.55 (2H, ovl), 7.04 (2H, d, $J = 8.5$ Hz), 6.78 (2H, d, $J = 8.5$ Hz), 5.05 (1H, t, $J = 7.3$ Hz), 3.35 (2H, d, $J = 7.3$); ¹³C NMR (100 MHz, CD₃OD): δ_{C} 177.4, 170.6, 159.5, 142.9, 141.2, 131.0 (2C), 129.6 (2C), 128.3, 128.0 (2C), 127.2, 126.0, 125.5, 122.8, 117.4 (2C), 50.8, 38.4. $[\alpha]_{\text{D}}^{25} = 38$ ($c = 0.15$ in MeOH). ESI-MS m/z 364.1 $[\text{M} + \text{H}]^+$.

5-(1-amino-1-methyl-2-(4-hydroxyphenyl)ethyl)-3-(4-(thiophen3-yl)phenyl)-1,2,4-oxadiazole (11). An analytic sample of crude reaction was purified by HPLC using Luna Column C-18 (10 μm , 250 mm x 10 mm) with MeOH/H₂O (50:50) + 0.1% TFA as eluent (flow rate 3.00 mL/min) to give compound **11** ($t_{\text{R}} = 6.0$ min). ¹H NMR (400 MHz, CD₃OD): δ_{H} 7.92 (2H, d, $J = 8.4$ Hz), 7.91 (1H, ovl), 7.84 (2H, d, $J = 8.4$ Hz), 7.57 (2H, ovl), 7.00 (2H, d, $J = 8.5$ Hz), 6.61 (2H, d, $J = 8.5$ Hz), 3.13 (1H, d, $J = 13.9$ Hz), 3.07 (1H, d, $J = 13.9$ Hz), 1.63 (3H, s); ¹³C NMR (100 MHz, CD₃OD): δ_{C} 185.1, 169.2, 159.4, 142.9, 142.7, 131.9 (2C), 129.9 (2C), 128.2, 128.0 (2C), 126.9, 126.8, 125.5, 124.5, 115.8 (2C), 70.7, 44.0, 22.6. ESI-MS m/z 378.1 $[\text{M} + \text{H}]^+$.

***N'*-hydroxy-4-(thiophen-3-yl) benzimidamide (13)** ¹H NMR (400 MHz, CD₃OD): δ_{H} 7.91 (2H, d, $J = 8.5$ Hz), 7.77 (2H, d, $J = 8.5$ Hz), 7.69 (2H, m), 7.52 (1H, d, $J = 1.9$ Hz); ¹³C NMR (100 MHz, CD₃OD): δ_{C} 161.5, 141.9, 141.8, 133.7 (2C), 128.2, 128.0 (2C), 127.0, 123.7. ESI-MS m/z 219.1 $[\text{M} + \text{H}]^+$

3-(4'-amino-[1,1'-biphenyl]-4-yl)-5-(2,4,5-trifluoro-3-hydroxyphenyl)-1,2,4-oxadiazole (16). An analytic sample of crude reaction was purified by HPLC using Luna Column C-18 (10 μm , 250 mm x 10 mm) with MeOH / H₂O (80:20) + 0.1% TFA as eluent (flow rate 3.00 mL/min) to

give compound **14** ($t_R = 9,0$ min). ^1H NMR (400 MHz, CD_3OD): δ_{H} 8.24 (2H, d, $J = 8.4$ Hz), 7.84 (2H, d, $J = 8.4$ Hz), 7.82 (2H, d, $J = 8.4$ Hz), 7.62 (1H, m), 7.37 (2H, d, $J = 8.4$ Hz); ^{13}C NMR (100 MHz, CD_3OD): δ_{C} 173.1, 169.5, 150.1, 146.7, 144.5, 144.2, 139.2, 138.7, 136.2, 129.4 (2C), 129.0 (2C), 128.3 (2C), 127.1, 122.5 (2C), 109.3, 106.9. ESI-MS m/z 383.09 [$\text{M} + \text{H}$] $^+$.

3-(3'-amino-[1,1'-biphenyl]-4-yl)-5-(2,4,5-trifluoro-3-hydroxyphenyl)-1,2,4-oxadiazole (17). An analytic sample of crude reaction was purified by HPLC using Luna Column C-18 (10 μm , 250 mm x 10 mm) with $\text{MeOH} / \text{H}_2\text{O}$ (80:20) + 0.1% TFA as eluent (flow rate 3.00 mL/min) to give compound **15** ($t_R = 8,5$ min). ^1H NMR (400 MHz, CD_3OD): δ_{H} 8.24 (2H, d, $J = 8.6$ Hz), 7.82 (2H, d, $J = 8.6$ Hz), 7.62 (1H, m), 7.48-7.41 (2H, ovl), 7.17 (1H, m); ^{13}C NMR (100 MHz, CD_3OD): δ_{C} 173.1, 169.5, 150.1, 146.7, 144.7, 144.5, 143.1, 140.2, 138.7, 131.3, 129.0 (2C), 128.3 (2C), 127.5, 124.0, 120.3, 119.2, 109.3, 106.7. ESI-MS m/z 383.09 [$\text{M} + \text{H}$] $^+$.

3-(3-hydroxy-[1,1'-biphenyl]-4-yl)-5-(2,4,5-trifluoro-3-hydroxyphenyl)-1,2,4-oxadiazole (18). An analytic sample of crude reaction was purified by HPLC using Luna Column C-18 (10 μm , 250 mm x 10 mm) with $\text{MeOH} / \text{H}_2\text{O}$ (80:20) + 0.1% TFA as eluent (flow rate 3.00 mL/min) to give compound **18** ($t_R = 8,0$ min). ^1H NMR (400 MHz, CD_3OD): δ_{H} 8.14 (2H, d, $J = 8.4$ Hz), 7.72 (2H, d, $J = 8.4$ Hz), 7.60 (1H, m), 7.27 (1H, t, $J = 8.0$), 7.13 (1H, m), 7.10 (1H, m), 6.81 (1H, ddd, $J = 8.0, 2.4, 0.8$ MHz); ^{13}C NMR (100 MHz, CD_3OD): δ_{C} 173.1, 169.4, 159.1, 150.1, 147.9, 144.5, 144.2, 142.6, 138.8, 131.0, 128.8 (2C), 128.4 (2C), 126.6, 119.3, 116.0, 114.6, 109.3, 106.9. ESI-MS m/z 384.07 [$\text{M} + \text{H}$] $^+$.

3-(3-thiophen-3-yl)phenyl[1,1'-biphenyl]-4-yl)-5-(2,4,5-trifluoro-3-hydroxyphenyl)-1,2,4-oxadiazole (19). An analytic sample of crude

reaction was purified by HPLC using Luna Column C-18 (10 μ m, 250 mm x 10 mm) with MeOH / H₂O (92:8) + 0.1% TFA as eluent (flow rate 3.00 mL/min) to give compound **19** (t_R = 7,5 min). ¹H NMR (400 MHz, CD₃OD): δ_H 8.40 (1H, s), 8.07 (1H, d, J = 8.4 Hz), 7.88 (1H, d, J = 8.4 Hz), 7.75 (1H, dd, J = 2.8, 1.3 Hz), 7.60 (1H, m) 7.58 (1H, m), 7.54 (1H, dd, J = 5.0, 1.3 Hz), 7.53 (1H, dd, J = 5.0, 2.8 Hz); ¹³C NMR (100 MHz, CD₃OD): δ_C 173.1, 169.4, 150.1, 146.7, 144.5, 142.4, 140.2, 138.8, 130.9, 130.5, 128.7, 127.4 (2C), 127.1, 126.2, 122.3, 109.3, 106.9. ESI-MS m/z 375.0 [M + H]⁺.

3-(3-hydroxy-[1,1'-biphenyl-3-yl]-5-(2,4,5-trifluoro-3-hydroxyphenyl)-1,2,4-oxadiazole (20). An analytic sample of crude reaction was purified by HPLC using Luna Column C-18 (10 μ m, 250 mm x 10 mm) with MeOH / H₂O (80:20) + 0.1% TFA as eluent (flow rate 3.00 mL/min) to give compound **20** (t_R = 9,0 min). ¹H NMR (400 MHz, CD₃OD): δ_H 8.33 (1H, t, J = 1.6 Hz), 8.09 (1H, d, J = 7.8 Hz), 7.78 (1H, d, J = 7.8 Hz), 7.60 (1H, m), 7.59 (1H, t, J = 7.6), 7.29 (1H, t, J = 7.8 Hz), 7.15 (1H, d, J = 7.8 Hz), 7.11 (1H, s), 6.81 (1H, d, J = 7.7 Hz); ¹³C NMR (100 MHz, CD₃OD): δ_C 173.1, 169.5, 159.1, 150.1, 149.7, 146.7, 143.4, 142.8, 138.8, 131.1, 131.0, 130.7, 128.2, 127.2, 126.9, 119.3, 115.9, 114.8, 109.3, 106.9. ESI-MS m/z 384.07 [M + H]⁺.

5-(1H-indol-4-yl)-3-(3-(3-thienyl)phenyl)-1,2,4-oxadiazole (25). An analytic sample of crude reaction was purified by HPLC using a Luna Column C-18 (10 mm, 250 mm x 10 mm) with MeOH / H₂O (80:20) as eluent (flow rate 3.00 mL/min) affording compound **25** (t_R = 9.0 min). ¹H NMR (700 MHz, CD₃OD): δ_H 8.20 (1H, s), 7.99 (1H, d, J = 7.4 Hz), 7.3 (1H, d, J = 7.8 Hz), 7.77 (1H, m), 7.75 (1H, d, J = 7.8 Hz), 7.69 (1H, d, J = 7.8 Hz), 7.58 (1H, dd, J = 5.0, 1.2 Hz), 7.51 (1H, d, J = 3.1 Hz), 7.45

(1H, d, $J = 3.1$ Hz), 7.25 (1H, t, $J = 7.8$ Hz) 7.13 (1H, d, $J = 3.0$ Hz); ^{13}C NMR (175 MHz, CD_3OD): δ_{C} 167.8, 160.0, 142.8, 138.7, 137.7, 133.6, 130.3, 129.8, 129.1, 128.4, 127.6, 127.3, 126.8, 126.4, 123.8, 122.2, 121.6, 121.1, 117.8, 103.5. ESI-MS m/z 344.2 $[\text{M} + \text{H}]^+$.

5-(1H-indol-4-yl)-3-phenyl-1,2,4-oxadiazole (26). An analytic sample of crude re-action was purified by HPLC using a Luna Column C-18 (10 mm, 250 mm x 10 mm) with MeOH / H_2O (80:20) as eluent (flow rate 3.00 mL/min) affording compound **26** ($t_{\text{R}} = 21.0$ min). ^1H NMR (700 MHz, CD_3OD): δ_{H} 8.20 (2H, d, $J = 7.7$ Hz), 8.01 (1H, d, $J = 7.4$ Hz), 7.71 (1H, d, $J = 7.8$ Hz), 7.56 (3H, ovl), 7.51 (1H, d, $J = 3.1$ Hz), 7.31 (1H, t, $J = 7.8$ Hz), 7.28 (1H, d, $J = 3.1$ Hz); ^{13}C NMR (175 MHz, CD_3OD): δ_{C} 178.7, 170.1, 138.7, 132.5, 130.4 (3C), 128.9, 128.6 (2C), 127.6, 122.4, 122.2, 117.4, 116.1, 103.6. ESI-MS m/z 262.1 $[\text{M} + \text{H}]^+$.

5-(1H-indol-4-yl)-3-(4-(trifluoromethyl)phenyl)-1,2,4-oxadiazole (27). An analytic sample of crude reaction was purified by HPLC using a Luna Column C-18 (10 μm , 250 mm x 10 mm) with MeOH / H_2O (90:10) as eluent (flow rate 3.00 mL/min) affording compound **27** ($t_{\text{R}} = 17.5$ min). ^1H NMR (700 MHz, CD_3OD): δ_{H} 8.29 (2H, d, $J = 8.0$ Hz), 7.95 (1H, d, $J = 7.7$ Hz), 7.79 (2H, d, $J = 8.0$ Hz), 7.67 (1H, d, $J = 7.7$ Hz), 7.48 (1H, d, $J = 3.0$ Hz), 7.26 (1H, t, $J = 7.8$ Hz) 7.24 (1H, d, $J = 3.0$ Hz); ^{13}C NMR (175 MHz, CD_3OD): δ_{C} 178.5, 165.7, 138.5, 133.5 (q, $J = 32.7$ Hz), 132.2, 128.9 (2C), 128.7, 127.4, 126.8 (2C, q, $J = 3.5$ Hz), 125.4 (q, $J = 271.2$ Hz), 122.2, 121.9, 117.6, 115.3, 103.3. ESI-MS m/z 330.1 $[\text{M} + \text{H}]^+$.

5-(1H-indol-4-yl)-3-(4-(hydroxy)phenyl)-1,2,4-oxadiazole (28). An analytic sample of crude reaction was purified by HPLC using a Luna Column C-18 (10 μm , 250 mm x 10 mm) with MeOH / H_2O (80:20) as eluent (flow rate 3.00 mL/min) affording compound **28** ($t_{\text{R}} = 10.0$ min).

^1H NMR (400 MHz, CD_3OD): δ_{H} 8.03 (2H, d, $J = 8.7$ Hz), 7.99 (1H, d, $J = 7.8$ Hz), 7.70 (1H, d, $J = 7.8$ Hz), 7.51 (1H, d, $J = 3.1$ Hz), 7.30 (1H, t, $J = 7.8$ Hz) 7.26 (1H, d, $J = 3.1$ Hz), 6.94 (2H, d, $J = 8.7$ Hz); ^{13}C NMR (100 MHz, CD_3OD): δ_{C} 178.0, 169.8, 161.7, 138.5, 130.2 (2C), 130.1, 128.5, 127.4, 122.0 (2C), 119.5, 117.3, 116.7, 116.0, 103.35. ESI-MS m/z 278.1 $[\text{M} + \text{H}]^+$.

5-(1H-indol-4-yl)-3-(3-(hydroxy)phenyl)-1,2,4-oxadiazole (29). An analytic sample of crude reaction was purified by HPLC using a Luna Column C-18 (10 μm , 250 mm x 10 mm) with MeOH / H_2O (80:20) as eluent (flow rate 3.00 mL/min) affording compound **29** ($t_{\text{R}} = 11.5$ min). ^1H NMR (700 MHz, CD_3OD): δ_{H} 8.00 (1H, d, $J = 7.6$ Hz), 7.71 (1H, d, $J = 8.0$ Hz), 7.67 (1H, d, $J = 7.6$ Hz), 7.64 (1H, d, $J = 1.6$ Hz), 7.51 (1H, d, $J = 3.0$ Hz), 7.37 (1H, t, $J = 8.0$ Hz), 7.31 (1H, t, $J = 7.6$ Hz), 7.28 (1H, d, $J = 3.0$ Hz), 6.97 (1H, dd, $J = 8.0, 1.6$ Hz); ^{13}C NMR (175 MHz, CD_3OD): δ_{C} 178.3, 169.9, 159.2, 138.5, 131.1, 129.7, 128.6, 127.4, 122.1, 122.0, 119.6, 119.3, 117.4, 115.9, 115.1, 103.3. ESI-MS m/z 278.1 $[\text{M} + \text{H}]^+$.

5-(1H-indol-4-yl)-3-(2-(hydroxy)phenyl)-1,2,4-oxadiazole (30). An analytic sample of crude reaction was purified by HPLC using a Luna Column C-18 (10 μm , 250 mm x 10 mm) with MeOH / H_2O (80:20) as eluent (flow rate 3.00 mL/min) affording compound **30** ($t_{\text{R}} = 19.0$ min). ^1H NMR (400 MHz, CD_3OD): δ_{H} 8.14 (1H, d, $J = 7.7$ Hz), 8.05 (1H, d, $J = 7.4$ Hz), 7.76 (1H, d, $J = 8.0$ Hz), 7.56 (1H, d, $J = 3.0$ Hz), 7.45 (1H, t, $J = 8.0$ Hz), 7.35 (1H, t, $J = 7.7$ Hz), 7.22 (1H, d, $J = 3.0$ Hz), 7.07 (1H, d, $J = 8.0$ Hz) 7.05 (1H, d, $J = 7.7$ Hz); ^{13}C NMR (100 MHz, CD_3OD): δ_{C} 177.1, 168.6, 158.4, 138.6, 134.1, 129.6, 129.0, 127.3, 122.6, 122.0, 120.9, 118.4, 118.0, 115.1, 112.6, 103.0. ESI-MS m/z 278.1 $[\text{M} + \text{H}]^+$.

3-benzyl-5-(1H-indol-4-yl)-1,2,4-oxadiazole (31). An analytic sample of crude reaction was purified by HPLC using a Luna Column C-18 (10 μ m, 250 mm x 10 mm) with MeOH / H₂O (80:20) as eluent (flow rate 3.00 mL/min) affording compound **31** (t_R = 13.5 min). ¹H NMR (400 MHz, CD₃OD): δ_H 7.92 (1H, dd, J = 7.5, 0.8 Hz), 7.70 (1H, d, J = 8.0 Hz), 7.49 (1H, d, J = 3.2 Hz), 7.43 (2H, d, J = 7.5 Hz), 7.36 (2H, t, J = .5 Hz), 7.33 (2H, ovl), 7.15 (1H, dd, J = 3.2, 0.8 Hz); ¹³C NMR (175 MHz, CD₃OD): δ_C 178.5, 171.3, 138.6, 137.5, 130.2 (2C), 128.9 (2C), 128.7, 128.1, 127.4, 122.2, 122.0, 117.5, 115.9, 103.2, 33.0. ESI-MS m/z 276.1 [M + H]⁺.

5-(1H-indol-4-yl)-3-(4-(trifluoromethyl)benzyl)-1,2,4-oxadiazole (32). An analytic sample of crude reaction was purified by HPLC using a Luna Column C-18 (10 μ m, 250 mm x 10 mm) with MeOH / H₂O (80:20) as eluent (flow rate 3.00 mL/min) affording compound **32** (t_R = 18.0 min). ¹H NMR (700 MHz, CD₃OD): δ_H 7.90 (1H, d, J = 7.5 Hz), 7.68 (2H, d, J = 8.0 Hz), 7.65 (2H, d, J = 8.0 Hz), 7.61 (2H, d, J = 8.0 Hz), 7.47 (1H, d, J = 3.1 Hz), 7.26 (1H, t, J = 7.8 Hz) 7.13 (1H, d, J = 3.1 Hz), 4.28 (2H, s); ¹³C NMR (175 MHz, CD₃OD): δ_C 178.6, 170.6, 142.0, 138.5, 130.8 (2C), 130.3 (q, J = 32.2 Hz), 128.7, 127.3, 127.0 (2C, q, J = 3.7 Hz), 126.1 (q, J = 271 Hz), 122.1, 121.9, 117.5, 115.7, 103.1, 32.9. ESI-MS m/z 344. [M + H]⁺.

3-([1,1'-biphenyl]-4-yl)-5-(1H-indol-4-yl)-1,2,4-oxadiazole (33). An analytic sample of crude reaction was purified by HPLC using a Luna Column C-18 (10 μ m, 250 mm x 10 mm) with MeOH / H₂O (80:20) as eluent (flow rate 3.00 mL/min) affording compound **33** (t_R = 10.0 min). ¹H NMR (700 MHz, CD₃OD): δ_H 8.27 (2H, d, J = 8.3 Hz), 8.03 (1H, d, J = 7.4 Hz), 7.82 (2H, d, J = 8.3 Hz), 7.71 (3H, ovl), 7.53 (1H, d, J = 3.0 Hz), 7.48 (2H, t, J = 7.4 Hz), 7.39 (1H, t, J = 7.4 Hz), 7.32 (1H, d, J = 7.4 Hz),

7.30 (1H, d, $J = 3.1$ Hz); ^{13}C NMR (175 MHz, CD_3OD): δ_{C} 178.4, 169.7, 145.3, 141.3, 138.4, 130.0 (2C), 129.0, 128.9 (2C), 128.5, 128.4 (2C), 128.0 (2C), 127.3 (2C), 122.1, 121.9, 117.4, 115.8, 103.3. ESI-MS m/z 338.2 $[\text{M} + \text{H}]^+$.

3-(4'-hydroxy-[1,1'-biphenyl]-4-yl)-5-(1H-indol-4-yl)-1,2,4-oxadiazole

(34). An analytic sample of crude reaction was purified by HPLC using a Luna Column C-18 (10 μm , 250 mm x 10 mm) with MeOH / H_2O (85:15) as eluent (flow rate 3.00 mL/min) affording compound **34** ($t_{\text{R}} = 11.5$ min). ^1H NMR (400 MHz, CD_3OD): δ_{H} 8.23 (2H, d, $J = 8.5$ Hz), 8.03 (1H, d, $J = 7.5$ Hz), 7.77 (2H, d, $J = 8.5$ Hz), 7.72 (1H, d, $J = 8.0$ Hz), 7.57 (2H, d, $J = 8.5$ Hz), 7.53 (1H, d, $J = 3.1$ Hz), 7.33 (1H, t, $J = 7.8$ Hz), 7.30 (1H, d, $J = 3.1$ Hz), 6.90 (2H, dd, $J = 8.5$ Hz); ^{13}C NMR (100 MHz, CD_3OD): δ_{C} 178.8, 170.2, 159.4, 145.7, 139.0, 133.0, 129.6 (2C), 129.3 (2C), 129.1, 128.2 (2C), 127.8, 126.8, 122.5, 122.4, 117.8, 117.2 (2C), 116.4, 103.6. ESI-MS m/z 354.1 $[\text{M} + \text{H}]^+$.

3-(3'-hydroxy-[1,1'-biphenyl]-4-yl)-5-(1H-indol-4-yl)-1,2,4-oxadiazole

(35). An analytic sample of crude reaction was purified by HPLC using a Luna Column C-18 (10 μm , 250 mm x 10 mm) with MeOH / H_2O (85:15) as eluent (flow rate 3.00 mL/min) affording compound **35** ($t_{\text{R}} = 12.0$ min). ^1H NMR (700 MHz, CD_3OD): δ_{H} 8.22 (2H, d, $J = 8.2$ Hz), 8.01 (1H, d, $J = 7.3$ Hz), 7.75 (2H, d, $J = 8.2$ Hz), 7.70 (1H, d, $J = 8.0$ Hz), 7.51 (1H, d, $J = 3.0$ Hz), 7.28 (3H, ov), 7.13 (1H, d, $J = 3.0$ Hz), 7.12 (1H, d, $J = 1.8$ Hz), 6.82 (1H, dd, $J = 8.0, 1.8$ Hz); ^{13}C NMR (175 MHz, CD_3OD): δ_{C} 178.3, 169.6, 159.5, 145.3, 142.8, 138.5, 131.0, 128.8 (2C), 128.6, 128.4 (2C), 127.4, 127.3, 122.1, 122.0, 119.1, 117.4, 116.2, 115.9, 115.0, 103.4. ESI-MS m/z 354.1 $[\text{M} + \text{H}]^+$.

3-(3'-hydroxy-[1,1'-biphenyl]-3-yl)-5-(1H-indol-4-yl)-1,2,4-oxadiazole (36). An analytic sample of crude reaction was purified by HPLC using a Luna Column C-18 (10 μ m, 250 mm x 10 mm) with MeOH / H₂O (85:15) as eluent (flow rate 3.00 mL/min) affording compound **36** (t_R = 12.0 min). ¹H NMR (700 MHz, CD₃OD): δ_H 8.39 (1H, s), 8.12 (1H, d, J = 7.7 Hz), 8.02 (1H, d, J = 7.5 Hz), 7.77 (1H, d, J = 7.9 Hz), 7.70 (1H, d, J = 7.9 Hz), 7.59 (1H, t, J = 7.7 Hz), 7.51 (1H, d, J = 3.0 Hz), 7.30 (1H, t, J = 7.7 Hz), 7.29 (1H, d, J = 3.0 Hz), 7.24 (1H, d, J = 7.9 Hz), 7.09 (1H, d, J = 1.8 Hz), 7.04 (1H, d, J = 7.5 Hz), 6.78 (1H, dd, J = 8.0, 1.8 Hz); ¹³C NMR (175 MHz, CD₃OD): δ_C 178.1, 169.7, 161.9, 143.6, 142.4, 138.3, 130.6, 130.5, 130.1, 128.6, 128.4, 127.1, 126.6, 126.5, 121.9, 121.7, 117.3, 117.1, 116.8, 116.0, 115.6, 103.1. ESI-MS m/z 354.1 [M + H]⁺.

5-(1H-indol-4-yl)-3-(4-((4-methoxycarbonylbenzyl)oxy)phenyl)-1,2,4-oxadiazole (37). An analytic sample of crude reaction was purified by HPLC using a Luna Column C-18 (10 μ m, 250 mm x 10 mm) with MeOH / H₂O as eluent (flow rate 3.00 mL/min) affording compound **37** (t_R = 14.0 min). ¹H NMR (400 MHz, CDCl₃): δ_H 8.47 (1H, br s, NH), 8.21 (2H, d, J = 8.8 Hz), 8.10 (3H, ovl), 7.66 (1H, d, J = 8.0 Hz), 7.55 (2H, d, J = 8.1 Hz), 7.46 (2H, d, J = 2.2 Hz), 7.36 (1H, t, J = 8.0 Hz), 7.12 (2H, d, J = 8.8 Hz), 5.23 (2H, s), 3.95 (3H, s); ¹³C NMR (175 MHz, CDCl₃): δ_C 176.1, 168.3, 166.8, 160.6, 141.7, 136.5, 130.0 (2C), 129.8, 129.2 (2C), 127.0 (2C), 126.6, 126.0, 121.9, 121.8, 120.4, 115.8, 115.6, 115.1 (2C), 103.6, 69.6, 52.4. ESI-MS m/z 426.1 [M + H]⁺.

5-(1H-indol-4-yl)-3-(4-((3-methoxycarbonylbenzyl)oxy)phenyl)-1,2,4-oxadiazole (38). The crude reaction was purified by flash chromatography using a gradient from 9:1 to 8:2 Hexane/Ethyl Acetate affording 30 mg of compound **38** (54% yield). ¹H NMR (400 MHz, CDCl₃): δ_H 8.54 (1H, s,

NH), 8.22 (2H, d, $J = 8.7$ Hz), 8.17 (1H, s), 8.12 (1H, d, $J = 7.6$ Hz), 8.06 (1H, d, $J = 7.6$ Hz), 7.70 (2H, ovl), 7.52 (2H, ovl), 7.38 (1H, t, $J = 7.6$ Hz), 7.30 (1H, s), 7.13 (2H, d, $J = 8.7$ Hz), 5.22 (2H, s), 3.96 (3H, s); ^{13}C NMR (100 MHz, CDCl_3): δ_{C} 175.5, 168.4, 166.3, 160.5, 137.0, 136.5, 131.9, 130.6, 129.4, 129.2 (2C), 128.7, 128.6, 126.6, 126.0, 121.8 (2C), 120.4, 115.8, 115.5, 115.1 (2C), 103.8, 69.3, 52.1. ESI-MS m/z 426.1 [$\text{M} + \text{H}$] $^+$.

1-methy-isatin (52a) The crude reaction was purified by flash chromatography using a gradient of Petroleum Ether/Ethyl Acetate as eluent (80:20). The purity of the compound was confirmed by NMR analysis corresponding to the reported data.²⁶⁷

1-butyl-isatin (52b) The crude reaction was purified by flash chromatography using a gradient of Petroleum Ether/Ethyl Acetate as eluent (80:20). The purity of the compound was confirmed by NMR analysis corresponding to the reported data.²⁶⁷

3-Hydroxy-4-phenylquinolin-2(1H)-one (53) The crude mixture was purified by flash chromatography using a gradient of Petroleum Ether/Ethyl Acetate (20:80). The purity of the compound was confirmed by NMR analysis corresponding to the reported data.²⁶⁴

3-Hydroxy-1-methyl-4-phenylquinolin-2(1H)-one (54) The crude mixture was purified by flash chromatography using a gradient of Petroleum Ether/Ethyl Acetate as eluent (70:30). The purity of the compound was confirmed by NMR analysis corresponding to the reported data.²⁶³

3-Methoxy-1-methyl-4-phenylquinolin-2(1H)-one (55) The crude mixture was purified by flash chromatography using a gradient of

Petroleum Ether/Ethyl Acetate (70:30); The purity of the compound was confirmed by NMR analysis corresponding to the reported data.²⁶⁴

1-Butyl-3-hydroxy-4-phenylquinolin-2(1H)-one (56) The crude mixture was purified by flash chromatography using a gradient of Petroleum Ether/Ethyl Acetate as eluent (99:1). ¹H NMR (400 MHz, CDCl₃): δ_H 7.34-7.39 (2H, m), 7.32-7.23 (5H, m), 6.99-7.03 (2H, m), 4.30 (2 H, t, *J* =7.8 Hz), 1.70 (2H, m), 1.42 (2 H, m), 0.88 (3 H, t, *J* =7.4 Hz); ¹³C NMR (100 MHz, CDCl₃): δ_C 158.7, 140.6, 133.5, 133.07, 129.9 (2 C), 128.5 (2C), 128.1, 127.2, 126.4, 123.2, 122.7, 122.4, 114.2, 43.3, 29.7, 20.3. ESI-MS *m/z* 294.1488[M+H]⁺.

3-Butoxy-1-butyl-4-phenylquinolin-2(1H)-one (57) The crude mixture was purified by flash chromatography using a gradient of Petroleum Ether/Ethyl Acetate as eluent (99:1); ¹H NMR (400 MHz, CDCl₃): 7.51-7.43 (4H, m), 7.39(d, 1H), 7.34 (1H, d, *J* =1.69 Hz), 7.32 (1 H, d, *J* =1.19 Hz), 7.28 (1H, d, *J* =1.44 Hz), 7.1 (1H, t, *J* =7.56), 4.38 (2 H, t, *J* =7.82 Hz), 3.95 (2H, t, *J* = 6.45 Hz), 1.84-1.77 (4 H, m), 1.58-1.41 (4 H, m), 1.16-1.08 (2H, m), 1.03 (3H, t, *J* = 7.31 Hz), 0.73 (3 H, t, *J* = 7.38 Hz);¹³C NMR (100 MHz, CDCl₃): δ_C 159.1, 144.5, 137.4, 136.3, 133.8, 129.7(2 C), 128.5, 128.1 (2C), 127.9, 127.5, 72.3, 42.7, 32.0, 29.6, 20.4, 18.7, 13.8, 13.7. ESI-MS *m/z* 350.2114 [M+H]⁺.

3-Hydroxy-4-(3-methoxyphenyl)quinolin-2(1H)-one (58) The crude mixture was purified by flash chromatography using a gradient of Petroleum Ether/Ethyl Acetate (99:1). The purity of the compound was confirmed by NMR analysis corresponding to the reported data.²⁶⁴

3-Hydroxy-4-(3-methoxyphenyl)-1-methylquinolin-2(1H)-one (59) The crude mixture was purified by flash chromatography using a gradient of Petroleum Ether/Ethyl Acetate as eluent. ¹H NMR (400 MHz, CDCl₃): δ_H

7.49-7.40 (4H, m), 7.20 (1 H, t), 7.13(1 H, br s), 7.02-6.98 (2 H, m), 6.96(1H, br s), 3.90 (3 H, s), 3.85 (3 H, s). ^{13}C NMR (100 MHz, CDCl_3): δ_{C} 159.7, 140.8, 134.5, 134.3, 129.7 (2 C), 127.4, 126.3, 123.2, 123.1, 122.3, 122.1, 115.5, 114.2, 113.9, 55.3, 30.5. ESI-MS m/z 282.1124 $[\text{M}+\text{H}]^+$.

3-Hydroxy-4-(3-hydroxyphenyl) -1-methylquinolin-2(1H)-one (60) The crude mixture was purified by flash chromatography using a gradient of Petroleum Ether/Ethyl Acetate as eluent (90:10); ^1H NMR (400 MHz, CD_3SOCD_3): δ_{H} 9.56(1H, s), 9.12 (1H, s), 7.56 (1H, d, $J = 8.45$ Hz), 7.44-7.47 (1H, m), 7.30 (1H, t, $J = 7.84$ Hz), 7.16-7.18 (2H, m), 6.82 (1H, d, $J = 8.6$ Hz), 6.69-6.72 (2 H, m) 5.77 (3H, s). ^{13}C NMR (100 MHz, CDCl_3): δ_{C} 159.21, 157.08, 140.75, 134.5, 134.30, 129.08, 127.48, 126.58, 122.24, 121.39, 117.19, 115.66, 114.18, 29.75 (2 C), 29.72. ESI-MS m/z 268.0968 $[\text{M}+\text{H}]^+$.

4-(3-hydroxyphenyl)-3-methoxy-1-methylquinolin-2(1H)-one (61) The crude mixture was purified by flash chromatography using a gradient of Petroleum Ether/Ethyl Acetate as eluent (70:30); ^1H NMR (400 MHz, CDCl_3): δ_{H} 7.50 (1H, t $J = 8.2$ Hz), 7.32-7.40(3H, m), 7.15 (1H, t, $J = 7.7$ Hz), 6.99 (1H, d 7.7), 6.90 (1 H, br s), 6.83(2 H, d, $J = 7.5$ Hz), 3.82 (3H, s), 3.62 (3H, s); ^{13}C NMR (100 MHz, CDCl_3): δ_{C} 158.9, 156.9, 144.8, 137.7, 136.8, 134.2, 129.5, 129.03, 127.6, 122.6, 121.4, 121.0, 116.9, 115.6, 114.1, 60.2, 30.1. ESI-MS m/z 282.1124 $[\text{M}+\text{H}]^+$.

4-[3-(Benzyloxy)phenyl]-3-hydroxyquinolin-2(1H)-one (62) The crude mixture was purified by flash chromatography using a gradient of Petroleum Ether/Ethyl Acetate (70:30); ^1H NMR (400 MHz, CDCl_3): δ_{H} 10.7 (1H, s), 9.98 (1H, s), 7.46 (2H, t, $J = 8.19$ Hz), 7.39(3 H, t, $J = 7.46$), 7.33 (3H, t, $J = 7.17$), 7.15 (1 H, t, $J = 7.35$ Hz), 7.10 (dd, 1H, $J = 2.05, 8.13$),

7.07 (1 H, s), 7.05(1H, d, $J = 7.59$ Hz), 6.93 (1H, s), 5.10 (2 H, s). ^{13}C NMR (100 MHz, CDCl_3): δ_{C} 159.09, 159.07, 141.22, 136.95, 134.21, 132.29, 129.93, 128.76 (2 C), 128.17, 127.73(2 C), 127.54, 125.9, 123.55, 122.58, 121.77, 116.36, 115.81, 115.15, 70.23. ESI-MS m/z 344.12812 $[\text{M}+\text{H}]^+$.

4-[3-(Benzyloxy)phenyl]-3-hydroxy-1-methylquinolin-2(1H)-one (63)

The crude mixture was purified by flash chromatography using a gradient of Petroleum Ether/Ethyl Acetate as eluent (80:20); ^1H NMR (400 MHz, CDCl_3): δ_{H} 9.98 (1 H,s), 7.47-7.41 (4H, m), 7.40-7.37 (3H, t, $J = 7.44$), 7.33 (1 H, t, $J = 7.52$ Hz), 7.18 (1 H, t, $J = 7.92$ Hz), 7.12 (1 H, br s), 7.08 (1H, dd, $J = 2.18, 8.51$ Hz), 7.04 (1 H,s), 7.02 (d, 1 H, $J = 7.52$ Hz), 5.10(2 H ,s), 3.90 (3H, s); ^{13}C NMR (100 MHz, CDCl_3): δ_{C} 159.20, 159.06, 140.91, 136.98, 134.57, 134.42, 129.98, 128.75 (2 C), 128.14, 127.73 (2 C), 127.47, 126.42, 123.26, 123.24, 122.72, 122.18, 116.51, 115.03, 114.31, 70.20, 30.64. ESI-MS m/z 358.1437 $[\text{M}+\text{H}]^+$.

4-[3-(Benzyloxy) phenyl]-3-methoxy-1-methylquinolin-2(1H)-one (64)

The crude mixture was purified by flash chromatography using a gradient of Petroleum Ether/Ethyl Acetate as eluent (90:10); ^1H NMR (400 MHz, CDCl_3): δ_{H} 7.34 (1 H , t, $J = 7.71$ Hz), 7.29-7.27 (3H ,m), 7.21-7.24 (3H, m), 7.17(1H, t, $J = 7.23$ Hz), 7.10-7.09 (1H, m), 6.97 (1H, t, $J = 8.25$ Hz), 6.94 (1H, dd, $J = 2.58, 8.34$ Hz), 6.77 (1H , d, $J = 7.68$ Hz), 6.79 (1H, t, $J = 1.54$ Hz), 4.95 (2H, s), 3.67 (3H, s), 3.59 (3H, s); ^{13}C NMR (100 MHz, CDCl_3): δ_{C} 159.4, 158.33, 145.18, 137.23, 137.19, 136.89, 134.98, 129.69, 129.01, 128.71, 128.14(2 C), 127.67 (2 C), 127.50, 122.48, 122.23, 121.30, 116.04, 115.02, 114.06, 70.12, 60.34, 30.05. ESI-MS m/z 372.1594 $[\text{M}+\text{H}]^+$.

Pharmacology

Human leukocytes and A549 cells

Human neutrophils and monocytes were freshly isolated from leukocyte concentrates obtained from the Institute of Transfusion Medicine, University Hospital Jena. Donors were healthy adult volunteers and gave written consent, after they were informed about the aim of the study. Also, the ethical commission of the University Hospital in Jena approved the protocol for experiments, and all methods were performed in accordance with the relevant guidelines and regulations. Briefly, neutrophils were isolated [61] by dextran sedimentation, centrifugation on lymphocyte separation medium (LSM 1077, PAA, Coelbe, Germany) and hypotonic lysis of erythrocytes. Neutrophils were resuspended in PBS containing glucose (0.1%) to a final cell density of 5×10^6 cells/ml. Monocytes were separated from peripheral blood mononuclear cells (PBMC) by adherence to cell culture flasks (Greiner Bio-one, Nuertingen, Germany) for 1.5 h (37 °C, 5% CO₂) in RPMI 1640 containing L-glutamine (1 μM), heat-inactivated FCS (10%), penicillin (100 U/mL) and streptomycin (100 μg/mL), followed by cell-scraping and resuspension in PBS. Human lung carcinoma A549 cells were purchased from Cell Application Inc., Sigma-Aldrich, Merck (Darmstadt, Germany) and maintained in DMEM supplemented with 10% heat-inactivated fetal bovine serum (Invitrogen, Carlsbad, CA, USA), in a 5% CO₂ humid atmosphere. To ensure logarithmic growth, the cells were subcultured every 2 days. The cell line was tested for mycoplasma using PCR analysis.

Cell viability assay on A549 cell line

The viability of A549 cells after incubation with test compounds was determined by MTT conversion assay. Briefly, the cells (2×10^4) were

seeded in triplicate in 96 well/plates and incubated with compound **5** (10 μM) and or DMSO 0.1% (v/v) for 48 h in DMEM (37 °C, 5%). MTT (5 mg/mL) was added and after 1 h (37 °C, 5% CO₂) the medium was replaced with DMSO (100 μL per well). Finally, formazan formation was detected by measurement of absorbance at 570 nm.

Cell viability assay on monocytes

Acute cytotoxicity of compound **5** was analysed in isolated human monocytes. Cells (0.2×10^6 per well) were seeded in 100 mL buffer on 96-well plates and treated with the test (10 μM), triton (0.1%, positive control) or vehicle (0.5% DMSO) over 24 h (37 °C, 5% CO₂). MTT (5 mg/mL) was added and after 2 h (37 °C, 5% CO₂) cells were lysed by SDS treatment (10%, pH 4.5). After 17 h, formazan formation was detected by measurement of absorbance at 570 nm.

Determination of 5-LO products in intact cells

Freshly isolated neutrophils were resuspended in 1 mL PBS buffer containing 0.1% glucose and 1 mM CaCl₂ to a final cell density of 5×10^6 /mL. Cells were pre-incubated with test compounds or DMSO vehicle (0.1%) at 37 °C for 10 min. Then, 2.5 μM Ca²⁺-ionophore A23187 with or without supplementation of 20 μM AA was added as stimulus, and cells were left at 37 °C for 10 min. 5-LO product formation was stopped on ice, after the addition of 1 mL ice-cold methanol, and 530 μL acidified PBS and PGB1 as internal standard were added. Afterwards, cells were centrifuged (2000xg, 10 min, rt) and supernatants were submitted to solid phase extraction. 5-LO product formation (LTB₄ and its trans isomers and 5HETE) was quantified by RP-HPLC as described elsewhere.²⁶⁸

Cell-free mPGES-1 activity assay

The mPGES-1 was obtained from microsomes of A549 cells stimulated with IL-1b (1 ng/ml) for 48 h. Cells were sonicated and the homogenate was submitted to differential centrifugation at 10,000xg for 10 min and 174,000xg for 1 h at a temperature of 4 °C. The pellet (microsomal fraction) was resuspended in 1 ml homogenization buffer (0.1 M potassium phosphate buffer, pH 7.4, 1 μM phenylmethanesulphonyl fluoride, 60 μg/mL soybean trypsin inhibitor, 1 μg/mL leupeptin, 2.5 mM glutathione, and 250 mM sucrose), the total protein concentration was determined, and microsomes were diluted in potassium phosphate buffer (0.1 M, pH 7.4) containing glutathione (2.5 mM) and seeded in a 96-well plate. Test compounds or DMSO (1%) were added, and preincubated for 15 min on ice, and the reactions was started by adding 20 μM of PGH₂. After 1 min, 100 ml of a stop solution (40 mM FeCl₃, 80 mM citric acid, and 10 mM 11β-PGE₂) were added. PGE₂ and 11β-PGE₂ were extracted by solid-phase extraction, and RP-HPLC was used to quantify the product formation, as previously described.²⁶⁹

Cell-free 5-LO activity assay

Human recombinant 5-LO was expressed in *E. coli* BL21 transformed with pT3-5-LO plasmid at 30 °C overnight as described before [64]. The cells were lysed in a buffer containing triethanolamine (50 mM, pH 8.0), EDTA (5 mM), phenylmethanesulphonyl fluoride (1 mM), soybean trypsin inhibitor (60 μg /mL), dithiothreitol (2 mM) and lysozyme (1 μg/mL) by sonification (3 x 15 s). Then, a centrifugation step was performed (40,000 g, 20 min, 4 °C) and the supernatant was collected. The 5-LO enzyme was purified by affinity chromatography using an ATP-

agarose column and diluted with PBS buffer containing 1 mM EDTA. Afterwards, 0.5 mg purified 5-LO in 1 mL PBS plus 1 mM EDTA was pre-incubated with the test compounds or vehicle (0.1% DMSO) on ice for 10 min and then stimulated with 20 μ M AA and 2 mM CaCl₂ for 10 min at 37 °C. Ice-cold methanol (1 mL) was added to stop the reactions, and 530 μ l acidified PBS and PGB1 as internal standard were added, and solid phase extraction of 5-LO products (trans isomers of LTB₄ and 5HETE) was performed using C18 RP-columns (100 mg, UCT, Bristol, PA, USA). 5-LO products were analyzed by RP-HPLC as previously described.²⁶⁸

Cell-free COXs activity assay

Isolated ovine COX-1 and recombinant human COX-2, respectively, were used for the evaluation of the activity of compound 5 on cyclooxygenases. COXs were diluted in Tris buffer (100 mM, pH 8) supplemented with glutathione (5 mM), EDTA (100 μ M) and haemoglobin (5 μ gM) to a final concentration of 50 U/ mL for COX-1 and 20 U/ mL for COX-2, and pre-incubated with test compounds or vehicle (0.1% DMSO) for 5 min at room temperature. After 1 min at 37 °C, reactions were started adding arachidonic acid to a final concentration of 5 μ M for COX-1 and 2 μ M for COX-2. After 5 min at 37 °C, 1 mL of ice-cold methanol was added, and the reactions were stopped on ice. Internal PGB1 standard and 530 μ l acidified PBS were added, solid phase extraction was performed, and COX product formation was determined using RP-HPLC by analysis of 12-HHT formation.^{270,271}

Expression, purification and activity assay of human recombinant sEH

Human recombinant sEH was expressed and purified as reported before.⁸⁸ In brief, Sf9 cells were infected with a recombinant baculovirus, provided by Dr. B. Hammock, University of California, Davis, CA. After 72 h, cells were pelleted and sonicated (3 x 10 s at 4 °C) in lysis buffer containing NaHPO₄ (50 mM, pH 8), NaCl (300 mM), glycerol (10%), EDTA (1 mM), phenylmethanesulphonyl fluoride (1 mM), leupeptin (10 µg /mL), and soybean trypsin inhibitor (60 µg /mL). A centrifugation (100,000 g, 60 min, 4 °C) was applied, and supernatants were collected and applied to benzylthio-sepharose-affinity chromatography in order to purify sEH by elution with 4-fluorochalcone oxide in PBS containing DTT (1 mM) and EDTA (1 mM). Dialyzed and concentrated (Millipore Amicon-Ultra-15 centrifugal filter) enzyme solution was assayed for total protein with BioRad protein detection kit (BioRad Laboratories, Munich, Germany) and the activity of sEH was determined by using a fluorescence-based assay as described before.²⁷² Thus, sEH was diluted in Tris buffer (25 mM, pH 7) supplemented with BSA (0.1 mg/mL) to an appropriate enzyme concentration and pre-incubated with compound **5** (10 µM) or vehicle (0.1% DMSO) for 15 min at room temperature. The reaction was started by addition of 50 µg 3-phenyl-cyano(6-methoxy-2-naphthalenyl)methyl ester-2-oxiraneacetic acid (PHOME), a nonfluorescent compound that is enzymatically converted into fluorescent 6-methoxy-naphthaldehyde at rt. After 60 min, the reaction was stopped by ZnSO₄ (200 mM) and fluorescence was detected (λ_{em} 465 nm, λ_{ex} 330 nm).

Animals

Male CD-1 mice (10 and 14 weeks of age, 25 and 30 g of weight) were obtained from Charles River (Milan, Italy) and kept in an animal care facility under controlled temperature, humidity, and on a 12 h:12 h light:dark cycle, with ad libitum access to water and standard laboratory chow diet. All experimental procedures were carried out according to the international and national law and policies (EU Directive 2010/63/EU for animal experiments, ARRIVE guidelines, and the Basel declaration including the 3R concept).²⁷³ All procedures were carried out to minimize the number of animals (n = 6 per group) and their suffering.

Induction of peritonitis in mice

To examine the anti-inflammatory action of compound **5**, mice were randomly divided into different experimental groups: control group (Ctrl), model group (zymosan + vehicle compound **5**), zymosan + compound **5** (0.1, 1, and 10 mg/kg), and zymosan þ dexamethasone (3 mg/kg) group. Animals received the selected compound or dexamethasone intraperitoneally (i.p.) 30 min after i.p. injection of zymosan (500 mg/kg). Ctrl and model group received an equal volume of vehicle (PBS or DMSO/ saline 1:3, respectively) according to the same schedule. Peritonitis was induced in mice as previously described.^{274,275,276} In brief, 500 mg/kg of zymosan A were dissolved in PBS and then boiled before the i.p. injection (0.5 mL). Peritoneal exudates were collected at selected time points (4 and 24 h) by washing the cavity with 2 mL of PBS. Then cell number of lavage fluids was determined by TC10 automated cell counter (Bio-Rad, Milan, Italy) using disposable slides, TC10 trypan blue dye (0.4% trypan blue dye w/v in 0.81% sodium chloride and 0.06% potassium phosphate dibasic solution), and a CCD camera to count cells based on the analyses of captured images. The remaining lavage fluids

were centrifuged at 3000 rpm for 20 min at 4 °C, and supernatants were frozen at -80 °C for further ELISA analysis.²⁷⁵ Dexamethasone and zymosan A were purchased from Sigma-Aldrich (Milan, Italy). DMSO was purchased from Merck (Italy). Unless otherwise stated, all the other reagents were purchased from Carlo Erba (Milan, Italy).

Enzyme-linked immunosorbent assay (ELISA)

The levels of IL-1 β , IL-6, IL-10 and TNF- α in the peritoneal exudates at 4 and 24 h were measured using commercially available ELISA kits (eBioscience Co., San Diego, CA, USA) according to the manufacturer instructions. Briefly, 100 μ L of peritoneal exudates, diluted standards, quality controls, and dilution buffer (blank) were applied on a pre-coated plate with the monoclonal antibody for 2 h. After washing, 100 μ L of biotin-labeled antibody was added, and incubation continued for 1 h. The plate was washed and 100 μ L of the streptavidineHRP conjugate was added, and the plate was incubated for a further 30 min period in the dark. The addition of 100 μ L of the substrate and stop solution represented the last steps before the reading of absorbance (measured at 450 nm) on a microplate reader.^{277,278}

Statistical analysis

The data and statistical analysis in this study comply with the international recommendations on experimental design and analysis in pharmacology²⁷³ and data sharing and presentation in preclinical pharmacology.^{279,280} The results obtained were expressed as the mean \pm S.D. or as mean \pm S.E.M., as reported in the figure legends. IC₅₀ values were calculated by nonlinear regression using GraphPad Prism Version 6 software (San Diego, CA) one site binding competition. Statistical

evaluation of the data was performed by one-way ANOVA followed by a Bonferroni post hoc test for multiple comparison. GraphPad Prism 8.0 software (San Diego, CA, USA) was used for analysis. Differences between means were considered statistically significant when $P \leq 0.05$ was achieved. Sample size was chosen to ensure alpha 0.05 and power 0.8. Animal weight was used for randomization and group allocation to reduce unwanted sources of variations by data normalization. No animals and related ex vivo samples were excluded from the analysis. In vivo studies were carried out to generate groups of equal size ($n = 6$ of independent values), using randomization and blinded analysis.

Antibiotics and Strains

Vancomycin and oxacillin were purchased from Sigma-Aldrich (Milan, Italy). *Staphylococcus aureus* ATCC 43300 (a methicillin-resistant strain characterized by the presence of the mec operon), *S. aureus* ATCC 29213, *P. aeruginosa* ATCC 27853, and *K. pneumoniae* ATCC 13883 were obtained from the American Type Culture Collection (Rockville, MD).

Antimicrobial Susceptibility Testing

Minimal inhibitory concentrations (MIC) of all the compounds were determined in Mueller–Hinton medium (MH) by the broth microdilution assay, following the procedure already described.²⁸¹ The compounds were added to bacterial suspension in each well yielding a final cell concentration of 1×10^6 CFU/mL and a final compound concentration ranging from 1.56 to 100 μ M. Compounds **7** and **33** were further tested at the final compound concentration of 1, 2, 4, 8 μ M. Negative control wells were set to contain bacteria in Mueller–Hinton broth plus the amount of vehicle (DMSO) used to dilute each compound. Positive controls included vancomycin (2 μ g/mL) and oxacillin (2 and 10 μ g/mL). The MIC was

defined as the lowest concentration of drug that caused a total inhibition of microbial growth after 24 h incubation time at 37 °C. Medium turbidity was measured by a microtiter plate reader (Biorad mod 680, Milan, Italy) at 595 nm. Minimum bactericidal concentration (MBC) was defined as the lowest test concentration that kills the organism (exhibited no growth on agar plates) after 24 h of incubation at 37 °C.

Killing Rate

Bacterial suspension (10^5 CFU/mL) was added to microplates along with compound **33** at the MIC value. Plates were incubated at 37°C on an orbital shaker at 120 rpm. Viability assessments were performed at 0, 2, 4, 6, and 24 h by plating 0.01 mL undiluted and 10-fold serially diluted samples onto Mueller–Hinton plates in triplicate. After the overnight incubation at 37°C, bacterial colonies were counted and compared with counts from control cultures.²⁸¹

Checkerboard Method

The interaction between compound **33** and oxacillin against MRSA was evaluated by the checkerboard method in 96-well microtiter plates containing Mueller–Hinton broth. Briefly, compound **33** and oxacillin were serially diluted along the y and x axes, respectively. The final concentration ranged from 0.03 to 10 mg/mL for oxacillin and from 0.5 to 3.12 μ M (0.5, 0.78, 1, 1.56, 2, 3.12 μ M) for **33**. The checkerboard plates were inoculated with bacteria at an approximate concentration of $10^5 \times$ CFU/mL and incubated at 37°C for 24 h, following which bacterial growth was assessed visually and the turbidity measured by microplate reader at 595 nm. The FIC index for each combination was calculated as follows: FIC index = FIC of 12 + FIC of oxacillin, where FIC of **33** (or oxacillin) was defined as the ratio of MIC of **33** (or oxacillin) in combination and

MIC of **33** (or oxacillin) alone. The FIC index values were interpreted as follows: ≤ 0.5 , synergistic; >0.5 to ≤ 1.0 , additive; >1.0 to ≤ 2.0 , indifferent; and >2.0 , antagonistic effects.²⁸²

Molecular Analysis

RNA extraction was performed by using GenUp Total RNA kit (BiotechRabbit) according to the manufacturer's instructions. Five hundred nanograms of total cellular RNA were reverse-transcribed (RevertUP II Reverse Transcriptase, BiotechRabbit) into cDNA using random hexamer primers (Random hexamer, Roche Diagnostics, Germany) at 48 °C for 60 min according to the manufacturer's instructions. RT-PCR was carried out using 2 μ L of cDNA amplified in a reaction mixture containing 10 mM Tris-HCl (pH 8.3), 1.5 mM MgCl₂, 50 mM KCl, 10 μ M dNTP, 10 μ M forward and reverse primers (*mecA*, *mecI*, *mecR1*), or 1 μ M forward and reverse 16S rRNA primers, and 2.5 U of Taq DNA polymerase (BiotechRabbit) in a final volume of 25 μ L. The cycling conditions are reported in Table 6. The reaction was carried out in a DNA thermal cycler (MyCycler, Biorad, USA). The PCR products were analysed by electrophoresis on 1.8% agarose gel in TBE and analysed on a Gel Doc EZ System (BioRad). Quantification data were normalized to the reference gene for 16S rRNA gene and analyzed by Image Lab software 5.2.1 (BioRad).

Table 6. *Staphylococcal sense and antisense primers sequences and expected PCR products (bp: base pairs).*

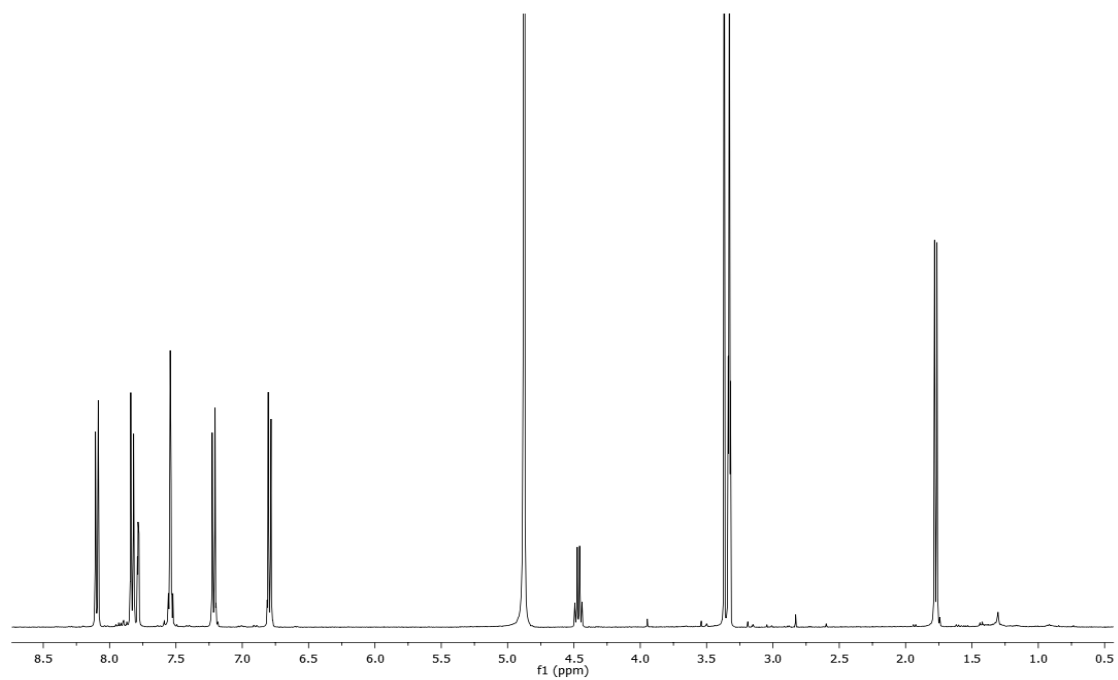
<i>Gene</i>	Sense and Antisense sequences	Conditions	bp
<i>mecA</i>	5'-TCCACCCTCAAACAGGTGAA- 3' 5'-TGGAACCTTGTTGAGCAGAGGT-3'	95°C for 5'	139
<i>mecI</i>	5'- TCATCTGCAGAATGGGAAGTT -3' 5'- TTGGACTCCAGTCCTTTTGC -3'	94°C for 30'', 55°C for 30'', 72°C for 30'' for 33 cycles	103
<i>mecRI</i>	5'- AGCACCGTTACTATCTGCACA -3' 5'- AGAATAAGCTTGCTCCCGTTCA -3'	72°C for 7'	142
rRNA 16S	5'- CGGTCCAGACTCCTACGGGAGGCAGCA -3' 5'-GCGTGGACTACCAGGGTATCTAATCC -3'		450

Bioscreens In Vitro for Cytotoxicity Studies

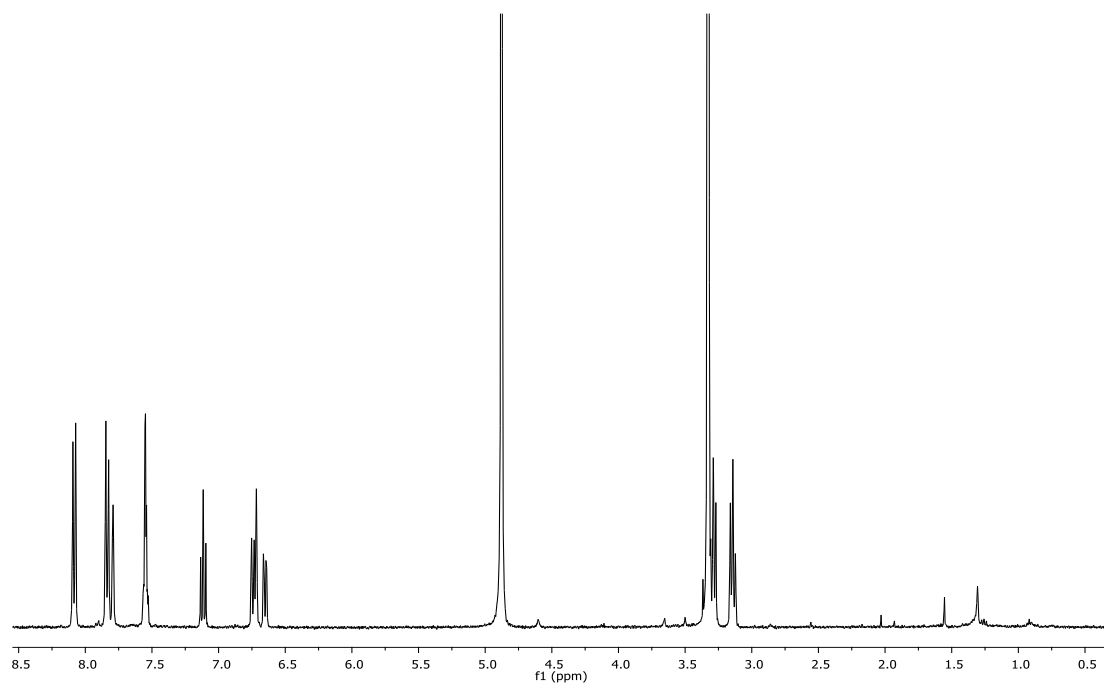
For cytotoxicity studies human HaCaT keratinocytes were grown in DMEM (Invitro-gen, Paisley, UK) supplemented with 10% fetal bovine serum (FBS, Cambrex, Verviers, Belgium), L-glutamine (2 mM, Sigma, Milan, Italy), penicillin (100 units/ml, Sigma) and streptomycin (100 µg/ml, Sigma), and cultured in a humidified 5% carbon dioxide atmosphere at 37 °C, according to ATCC recommendations. Cells were inoculated, and allowed to grow for 24 h, in 96-microwell culture plates at a density of 10⁴ cells/well. The medium was then replaced with fresh medium and cells were treated for further 48 h with a range of concentrations (1 → 400 µM) of **33**. Using the same experimental procedure, cell cultures were also incubated with vehicle DMSO as negative control. Cytotoxic activity of compound **33** was investigated through the estimation of a “cell survival index”, arising from the combination of cell viability evaluation with cell counting.²⁸³ Cell viability was evaluated using the MTT assay procedure, which measures the level of mitochondrial dehydrogenase activity using

the yellow 3-(4,5-dimethyl-2-thiazolyl)-2,5-diphenyl-2H-tetrazolium bromide (MTT, Sigma) as substrate. Briefly, after the treatments, the medium was removed, and the cells were incubated with 20 μ l/well of a MTT solution (5 mg/mL) for 1 h in a humidified 5% CO₂ incubator at 37 °C. The incubation was stopped by removing the MTT solution and by adding 100 μ l/well of DMSO to solubilize the obtained formazan. Finally, the absorbance was monitored at 550 nm using a microplate reader (iMark microplate reader, Bio-Rad, Milan, Italy). Cell number was determined by TC20 automated cell counter (Bio-Rad, Milan, Italy), providing an accurate and reproducible total count of cells and a live/dead ratio in one step by a specific dye (trypan blue) exclusion assay. Bio-Rad's TC20 automated cell counter uses disposable slides and TC20 trypan blue dye (0.4% trypan blue dye w/v in 0.81% sodium chloride and 0.06% potassium phosphate dibasic solution). Once the loaded slide is inserted into the slide port, the TC20 automatically focuses on the cells and detects the presence of trypan blue dye, providing the count. The calculation of the concentration required to inhibit the net increase in the cell number and viability by 50% (IC₅₀) is based on plots of data (n = 6 for each experiment) and repeated five times (total n = 30). IC₅₀ values were obtained by means of a concentration response curve by nonlinear regression using a curve fitting program, GraphPad Prism 8.0, and are expressed as mean values \pm SEM (n = 30) of five independent experiments.

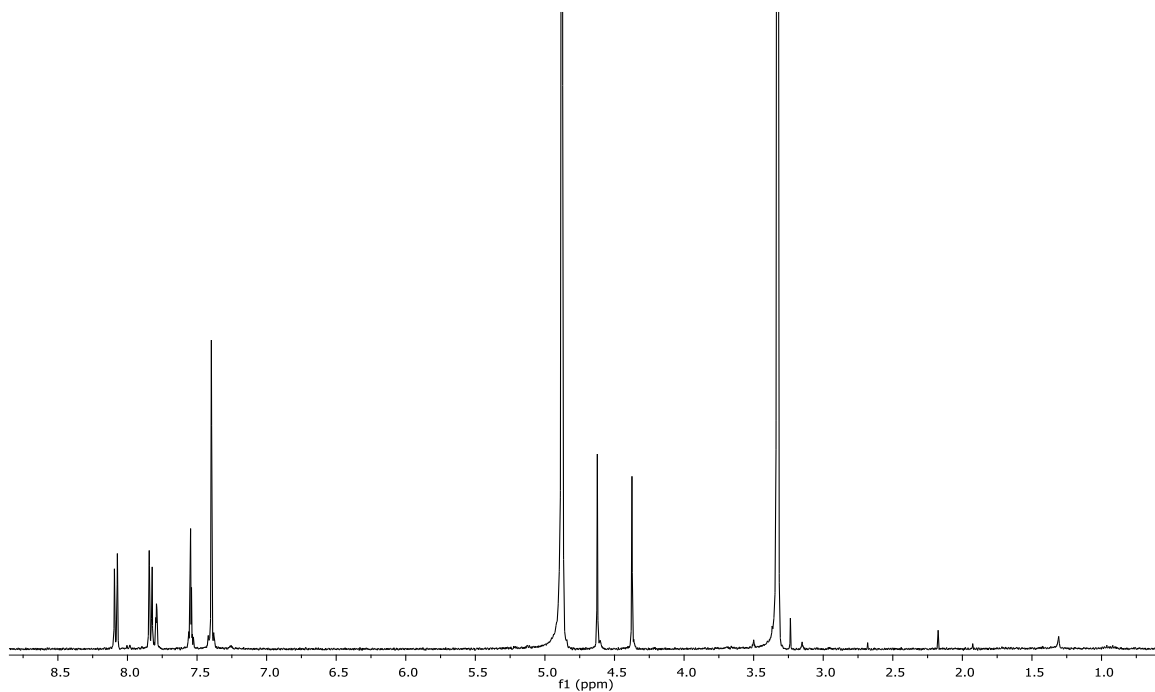
NMR SPECTRA



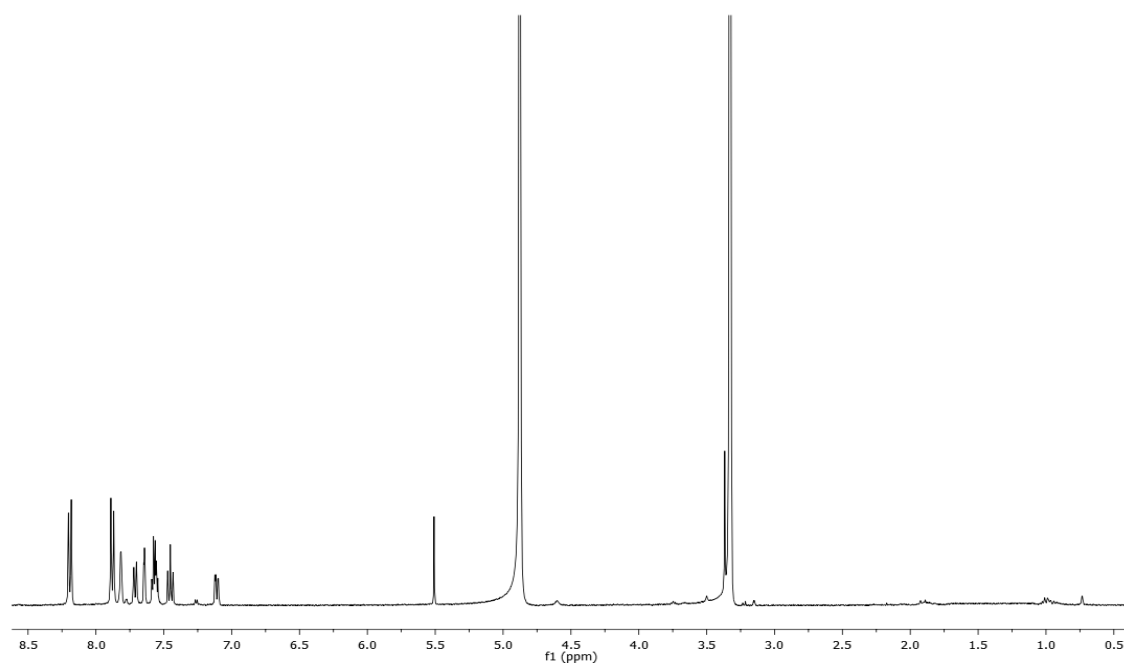
^1H NMR of compound **1** (CD_3OD , 400 MHz).



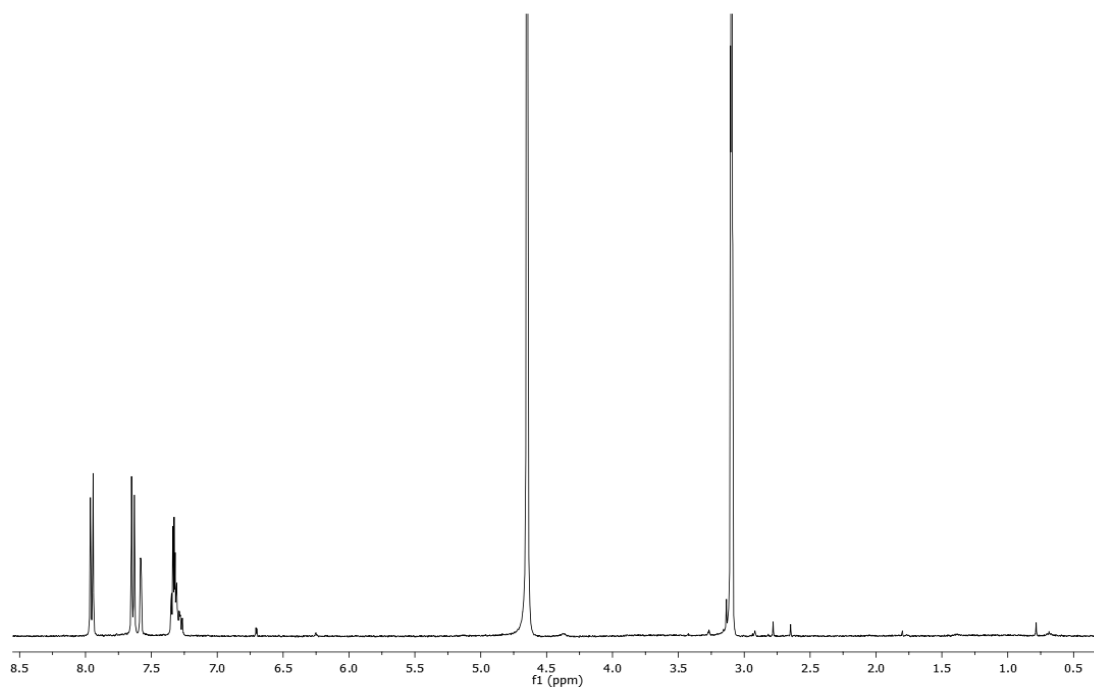
^1H NMR of compound **2** (CD_3OD , 400 MHz).



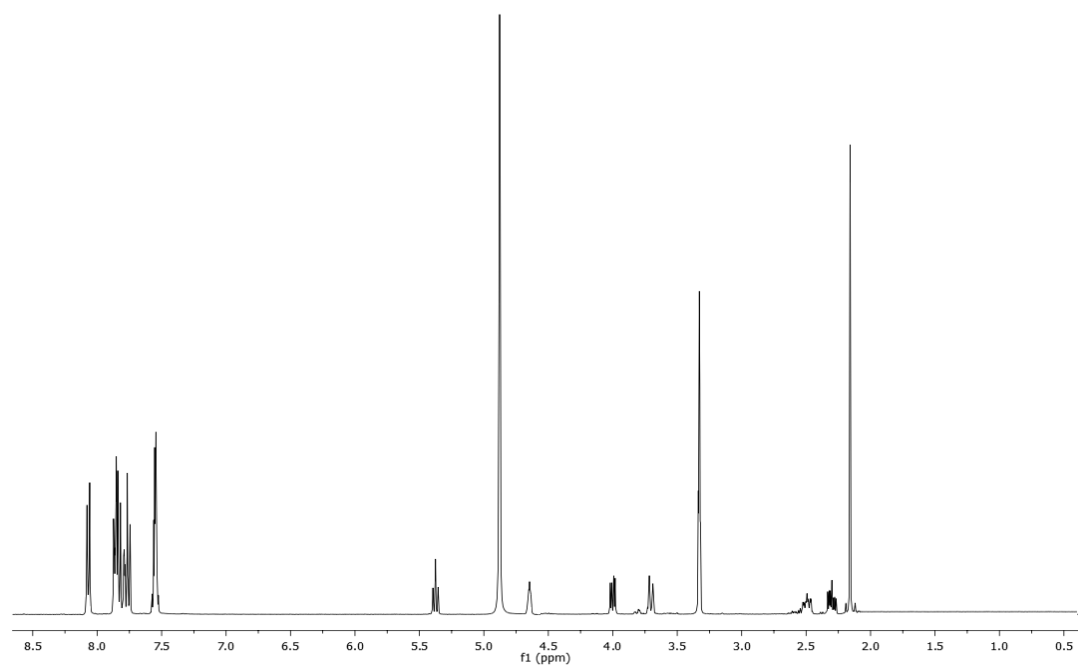
^1H NMR of compound **3** (CD_3OD , 400 MHz)



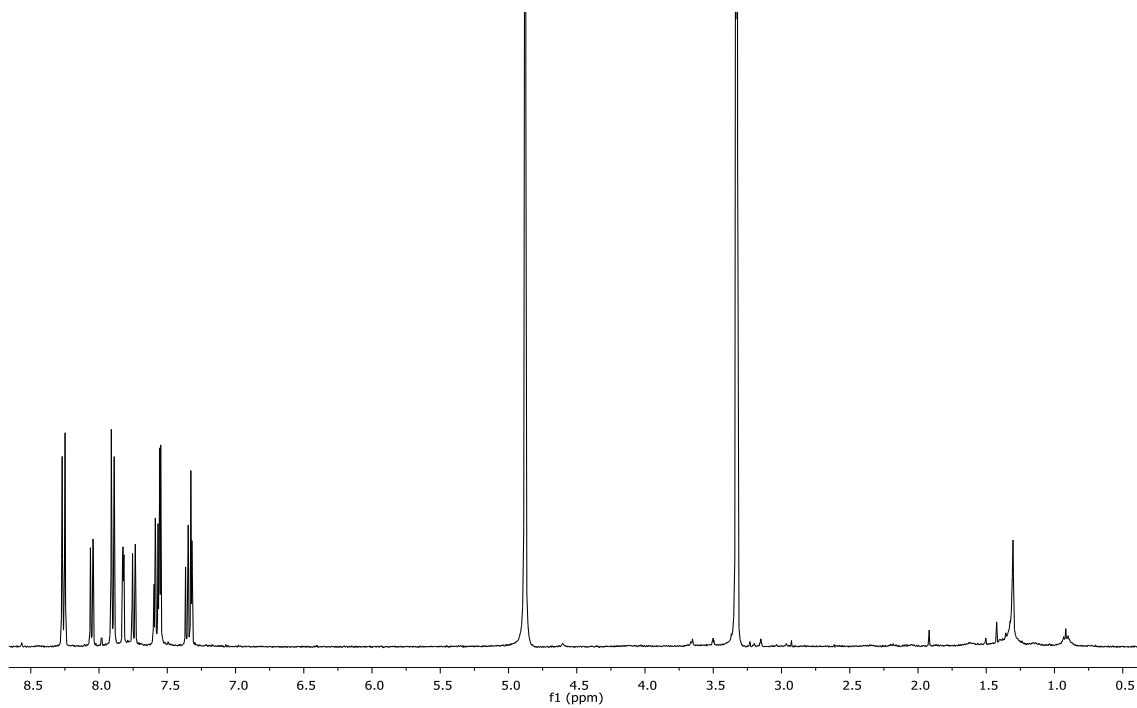
^1H NMR of compound **4** (CD_3OD , 400 MHz).



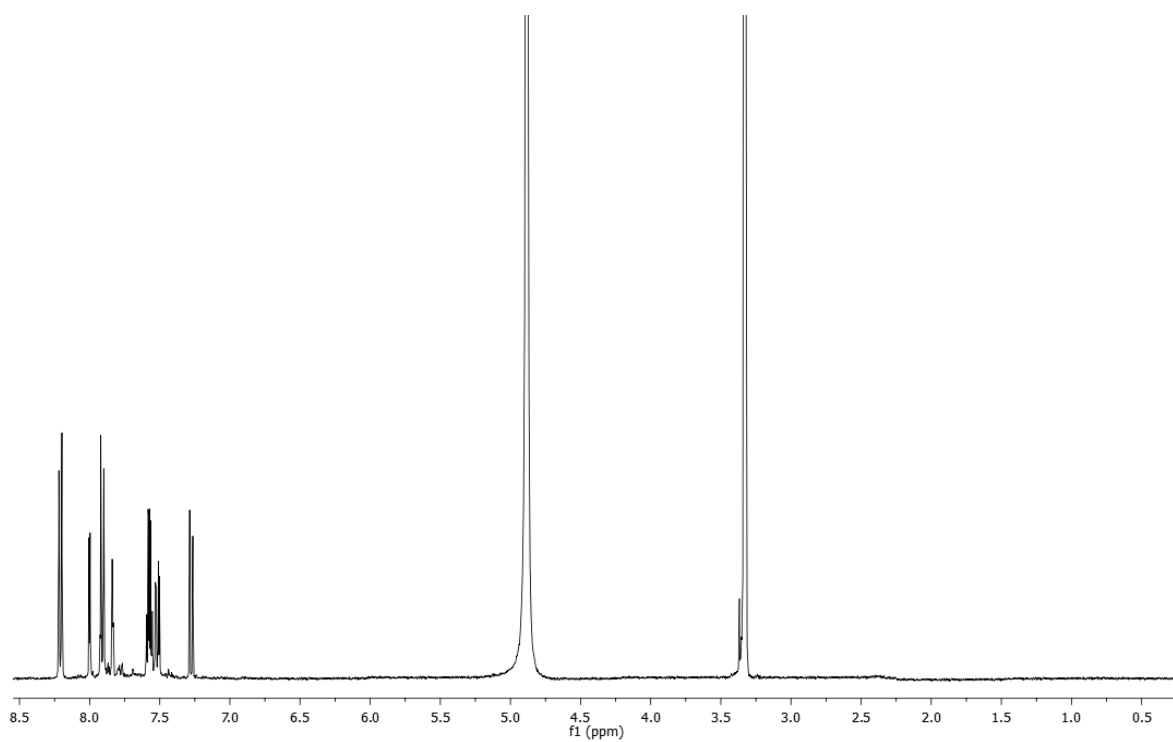
^1H NMR of compound **5** (CD_3OD , 400 MHz)



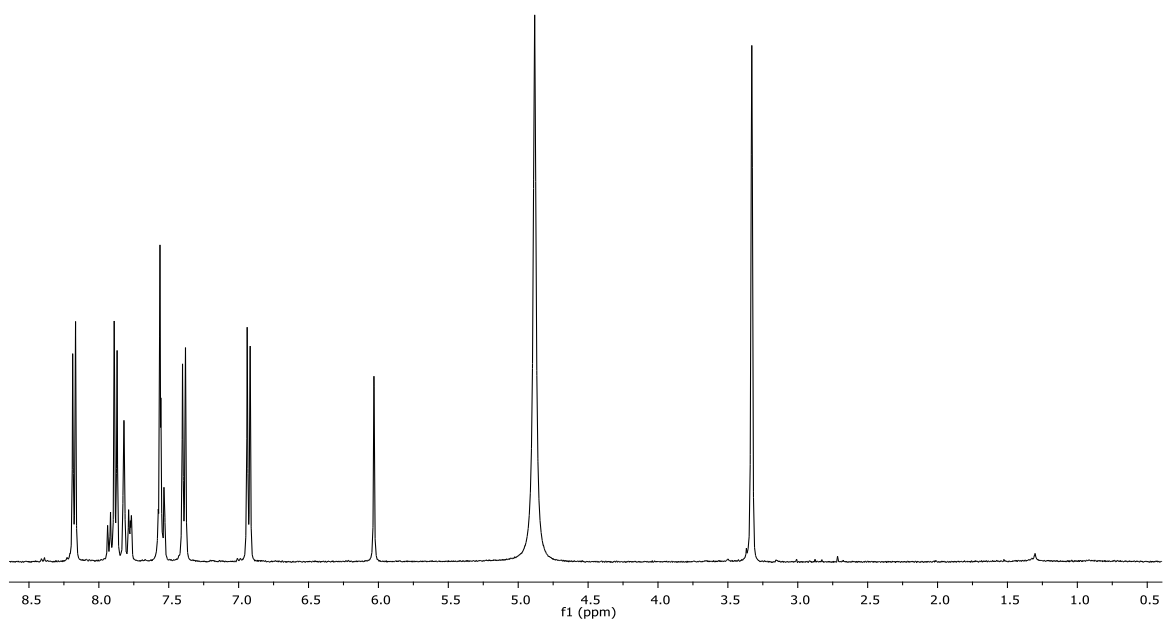
^1H NMR of compound **6** (CD_3OD , 400 MHz)



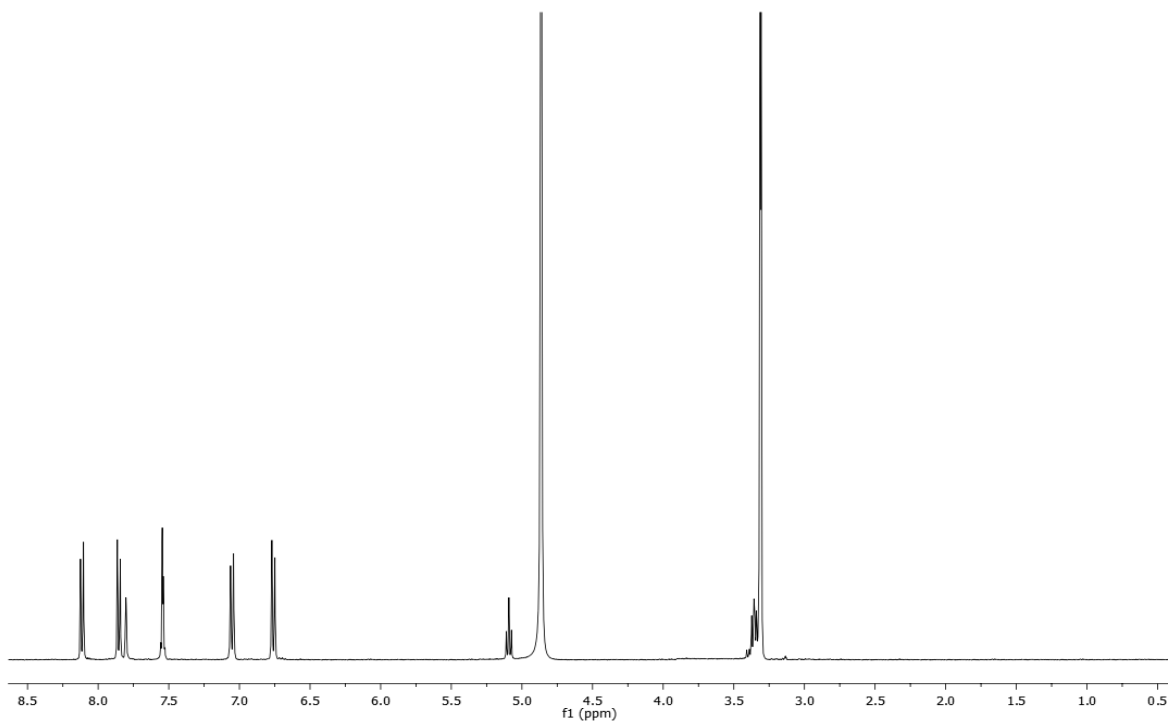
^1H NMR of compound **7** (CD_3OD , 400 MHz)



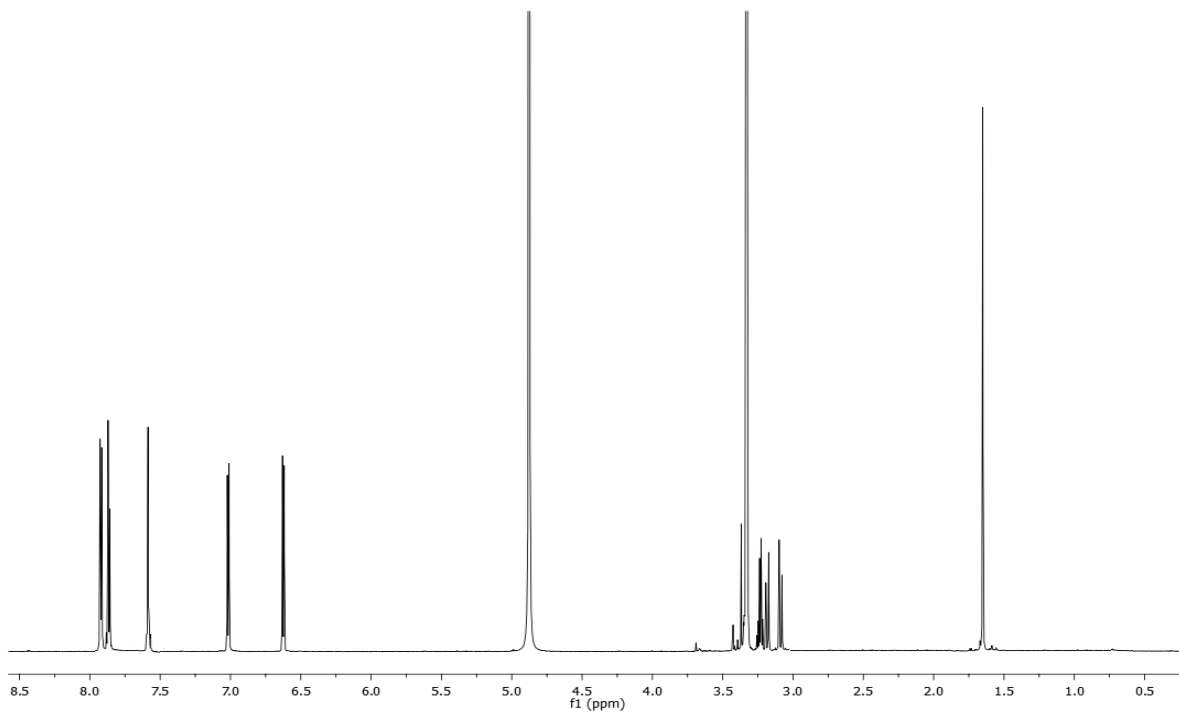
^1H NMR of compound **8** (CD_3OD , 400 MHz)



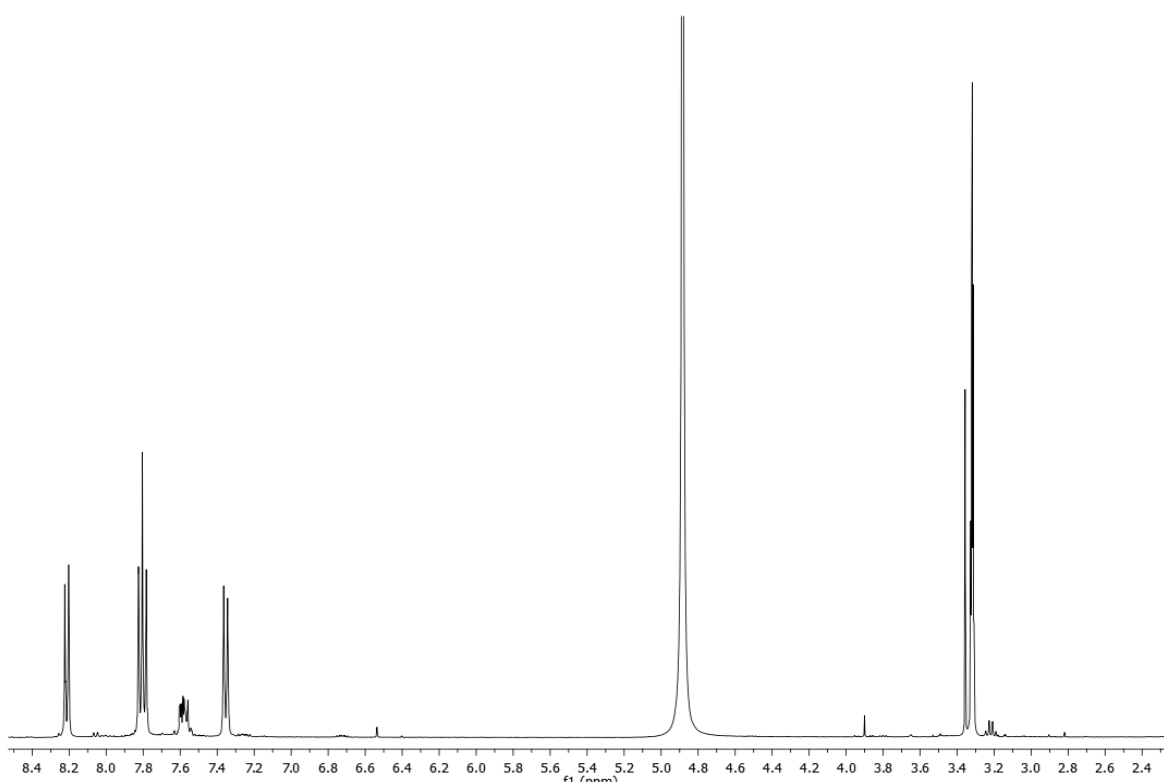
^1H NMR of compound **9** (CD_3OD , 400 MHz)



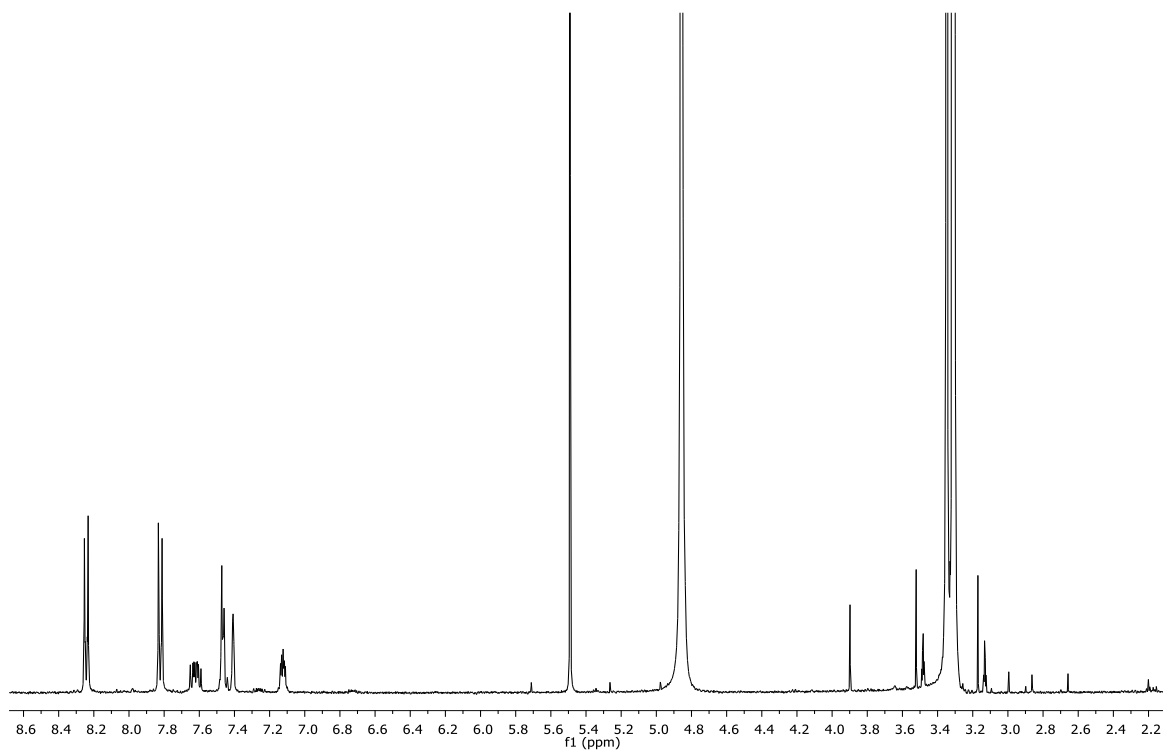
^1H NMR of compound **10** (CD_3OD , 400 MHz).



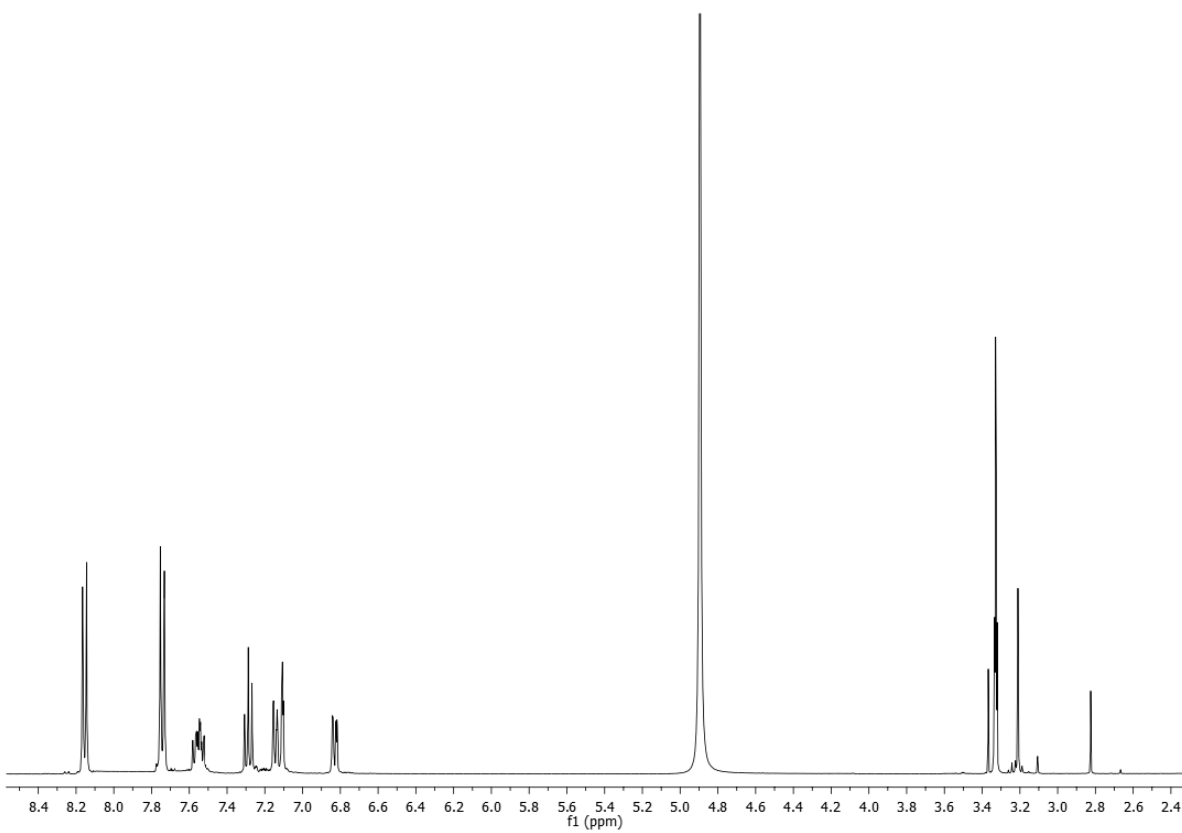
^1H NMR of compound **11** (CD_3OD , 400 MHz)



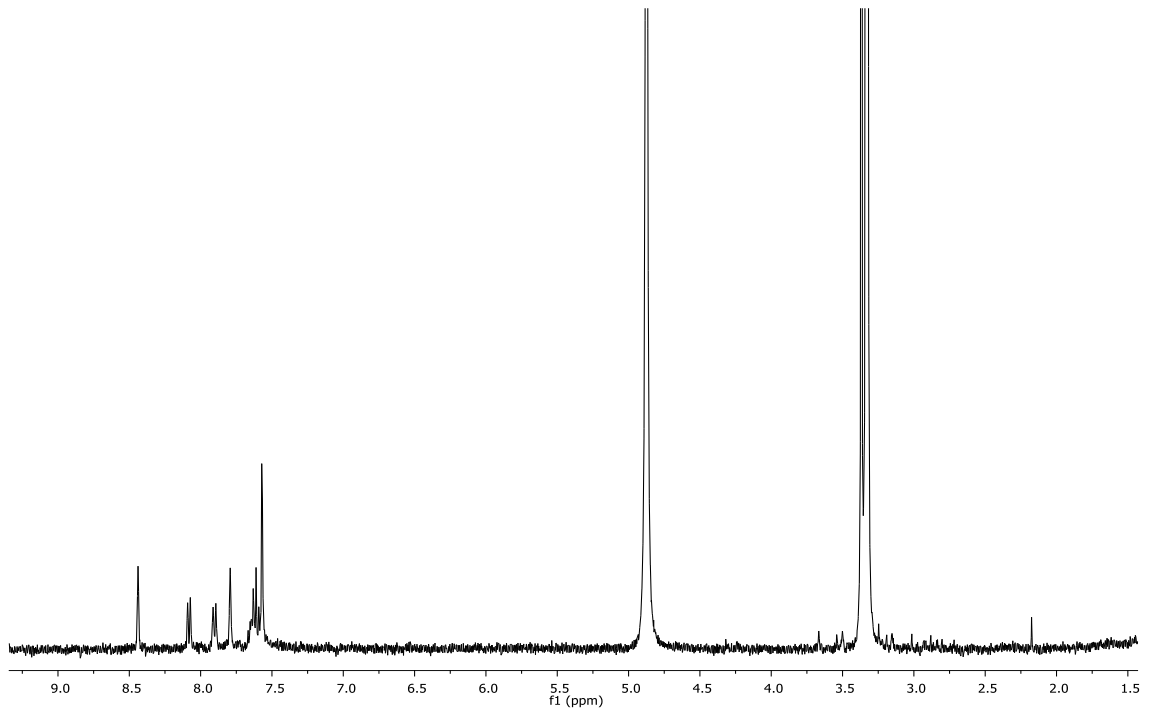
^1H NMR of compound **16** (700 MHz, CD_3OD)



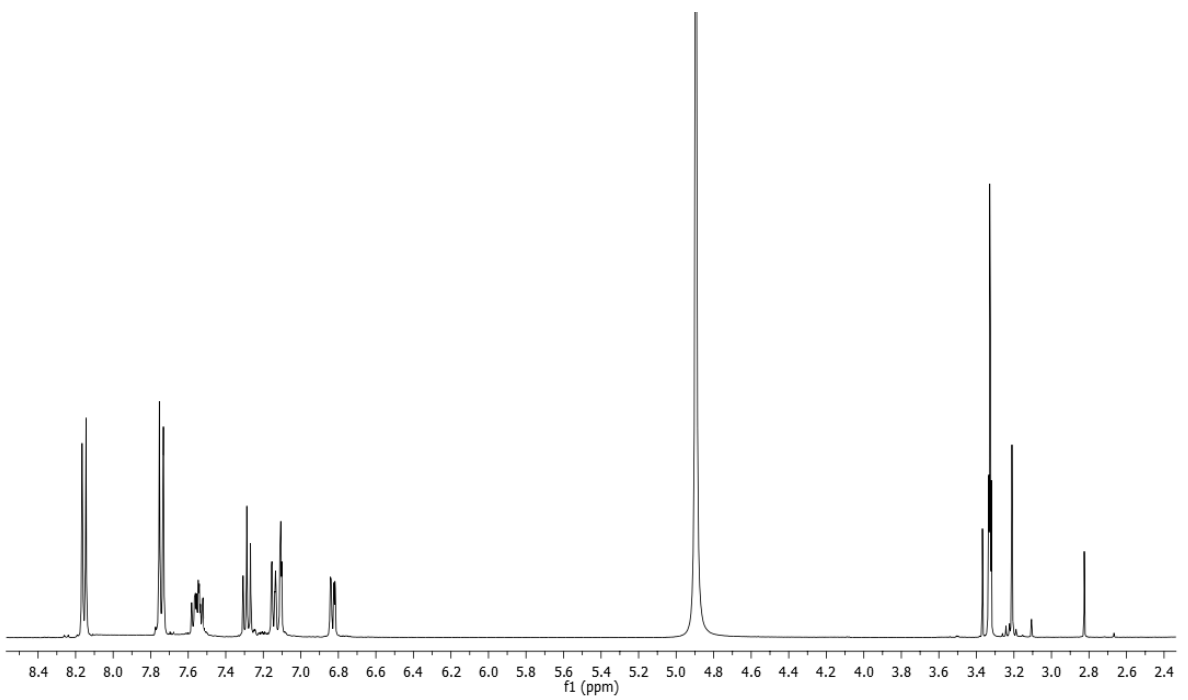
¹H NMR of compound **17** (400 MHz, CD₃OD)



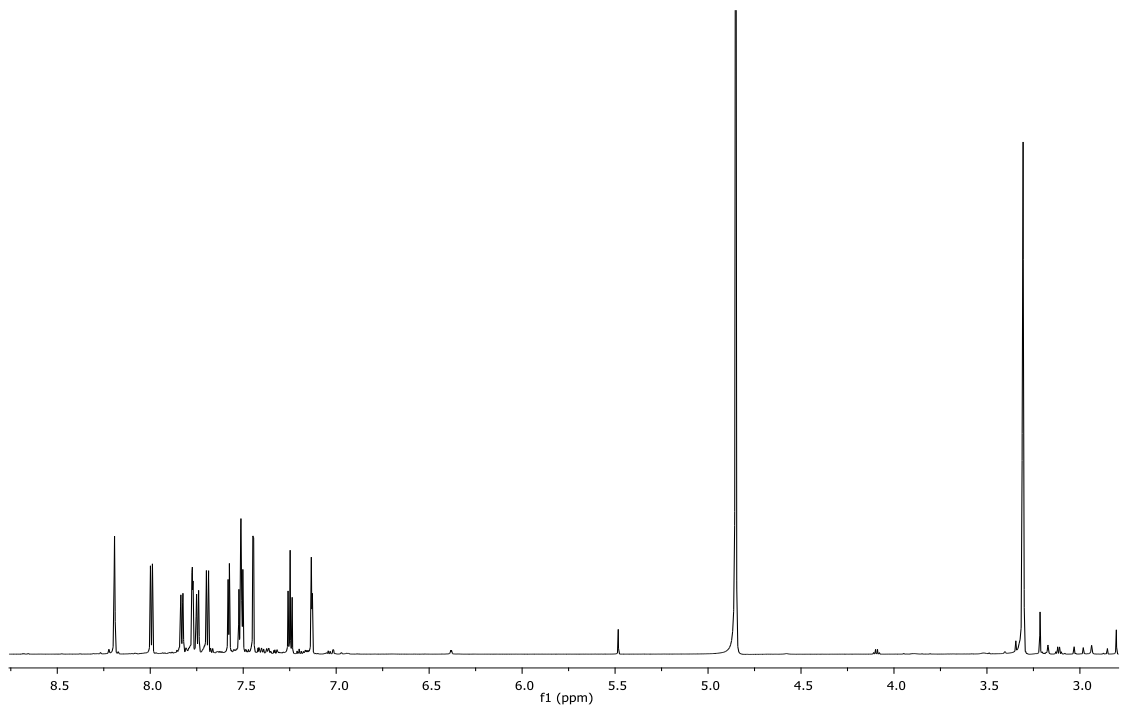
¹H NMR of compound **18** (400 MHz, CD₃OD)



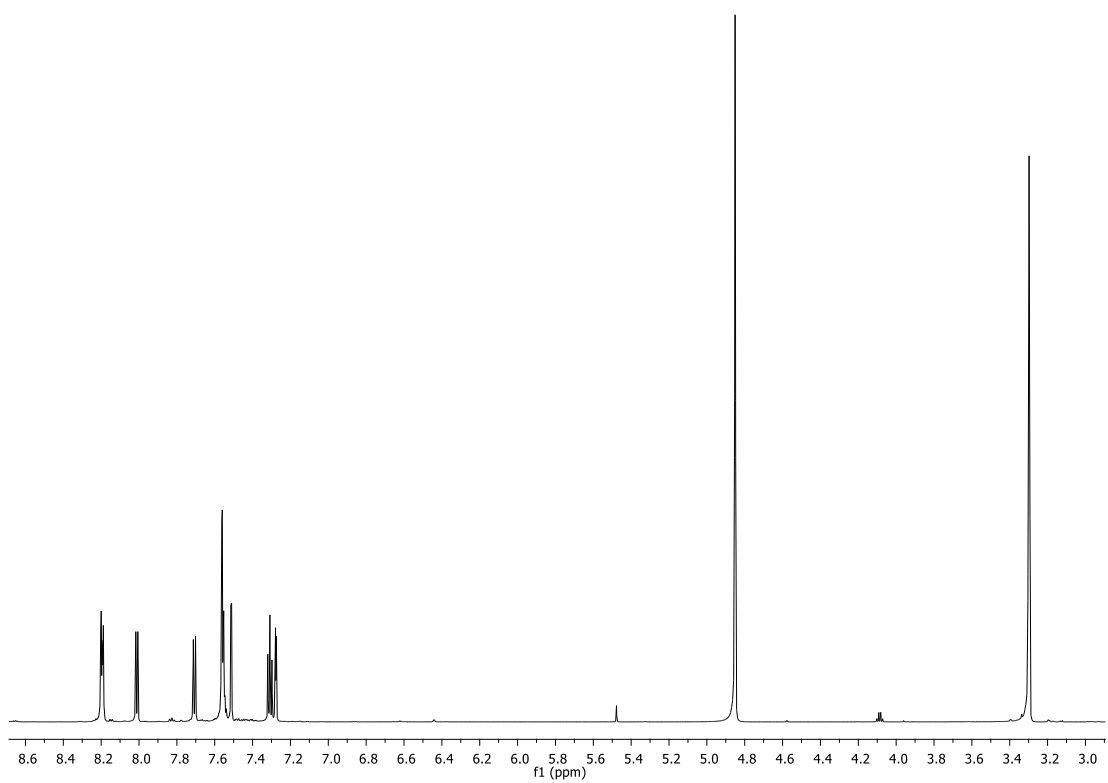
^1H NMR of compound **19** (400 MHz, CD_3OD)



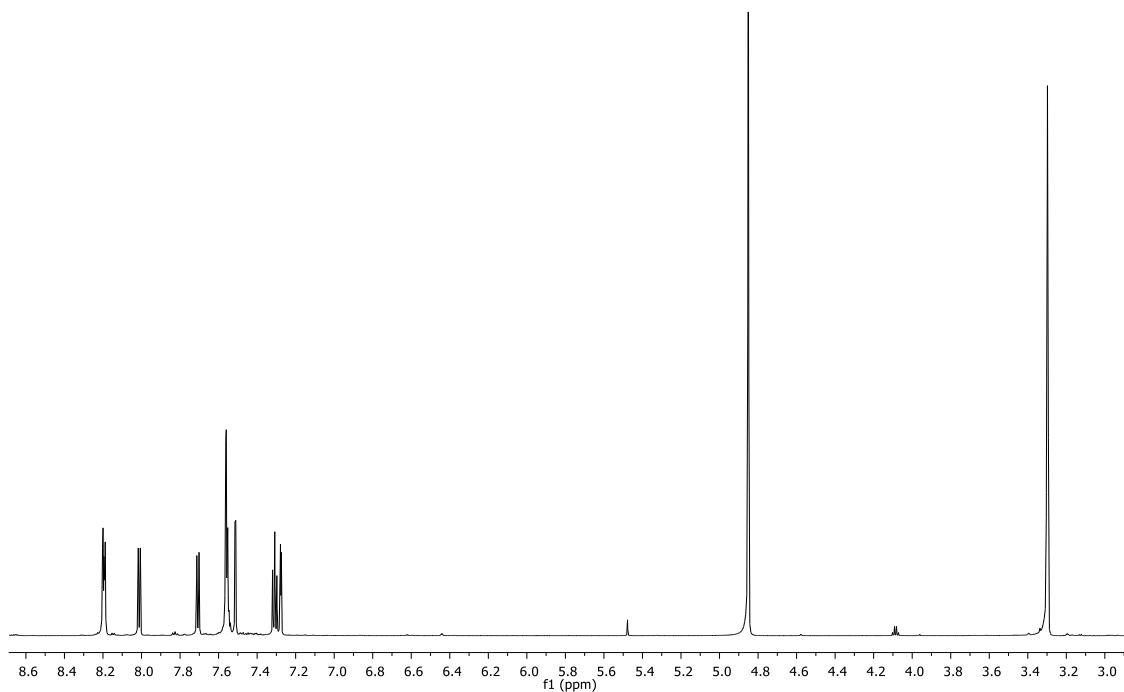
^1H NMR of compound **20** (400 MHz, CD_3OD)



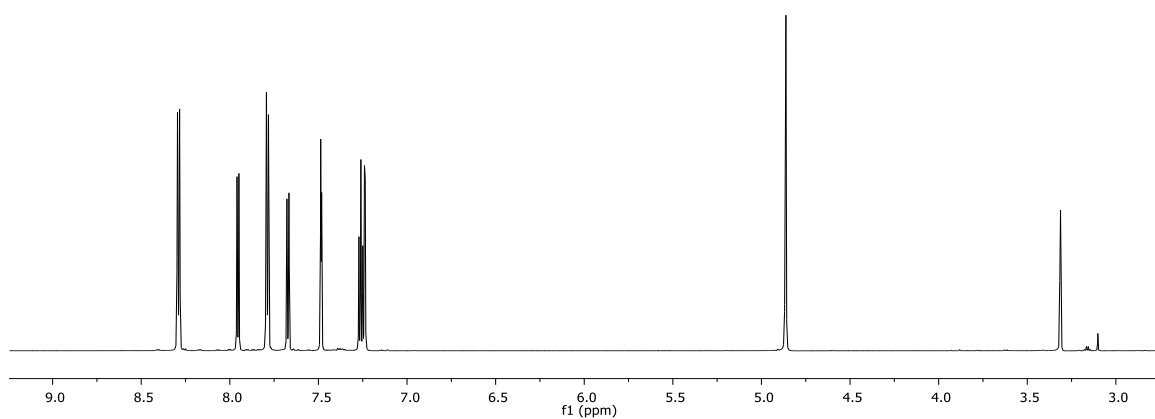
^1H NMR of compound **25** (700 MHz, CD_3OD)



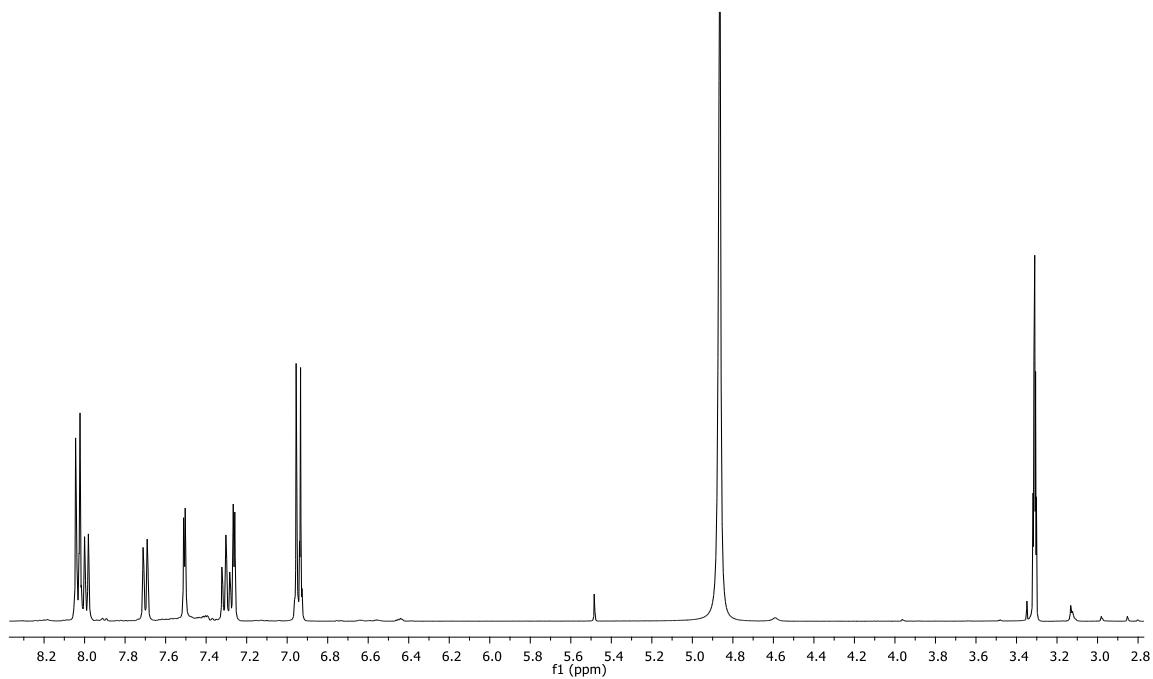
^1H NMR of compound **26** (700 MHz, CD_3OD)



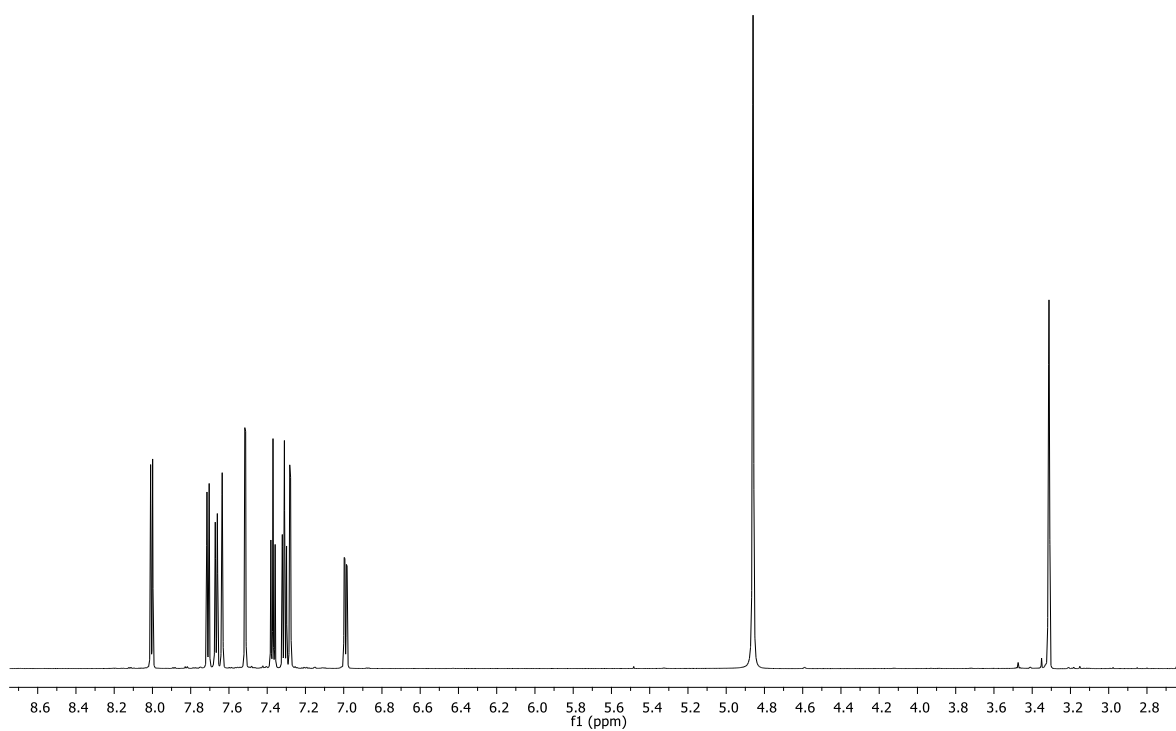
^1H NMR of compound **27** (700 MHz, CD_3OD)



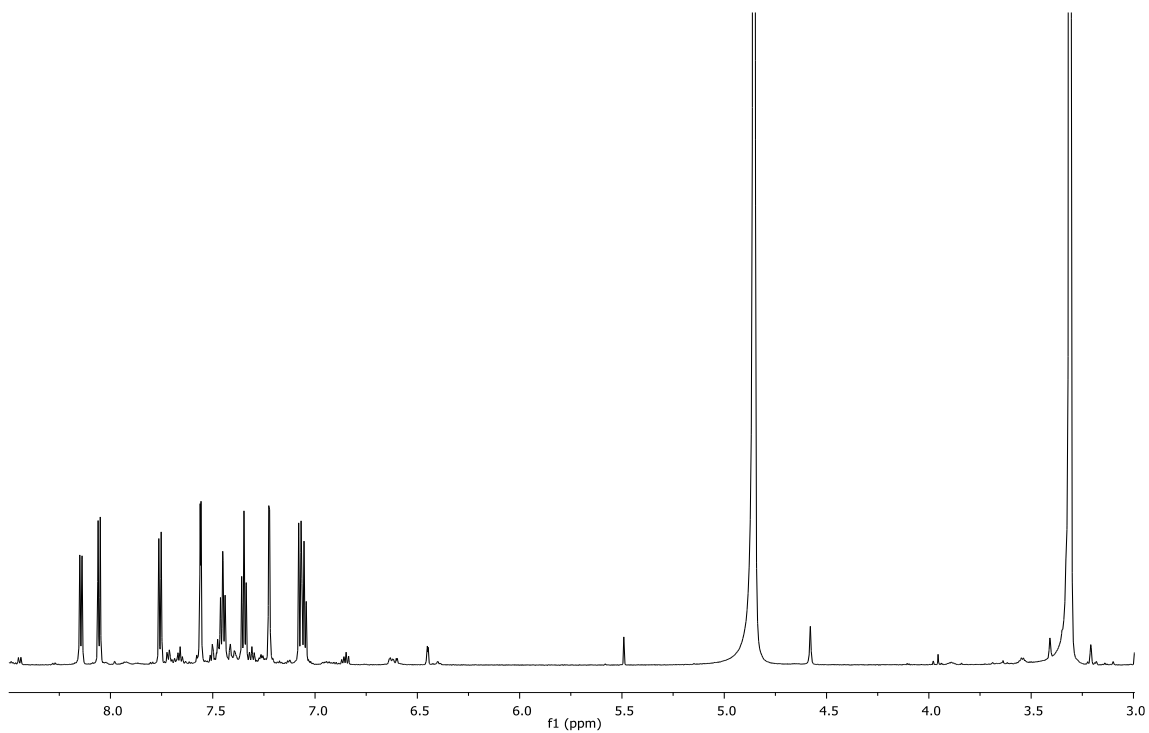
^1H NMR of compound **28** (700 MHz, CD_3OD)



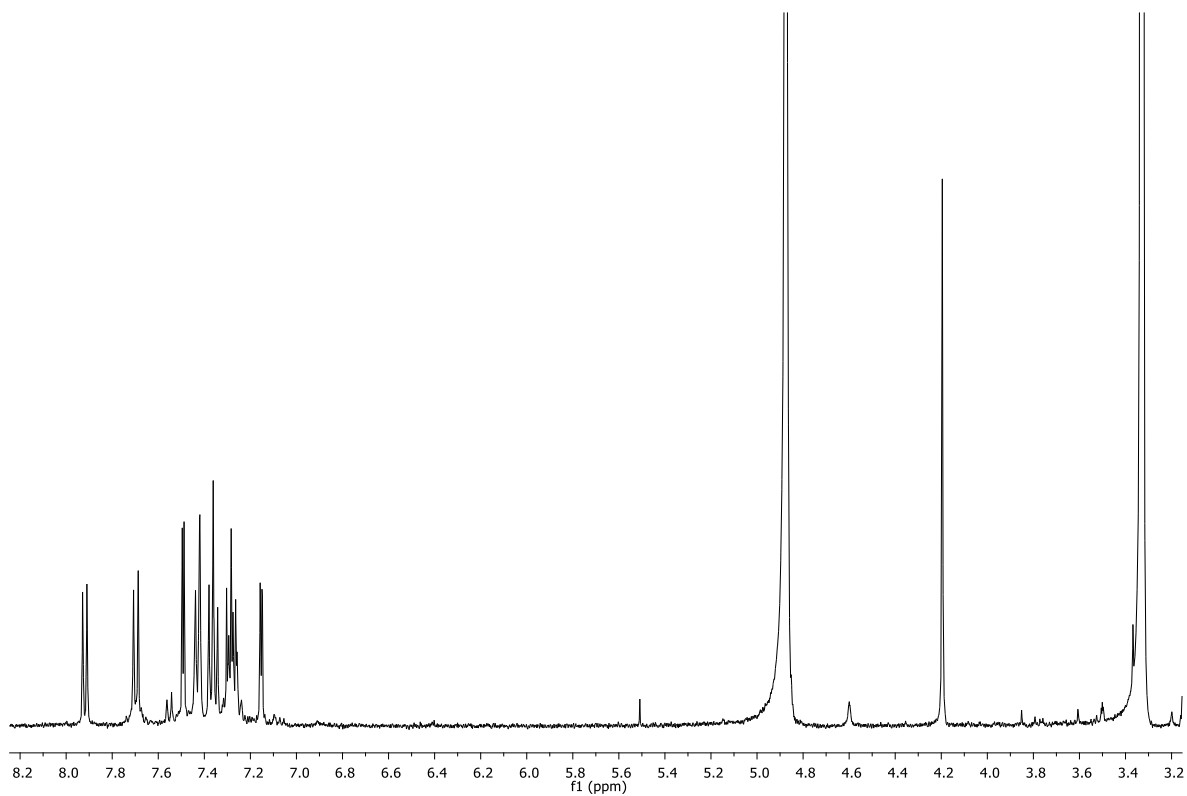
^1H NMR of compound **29** (400 MHz, CD_3OD)



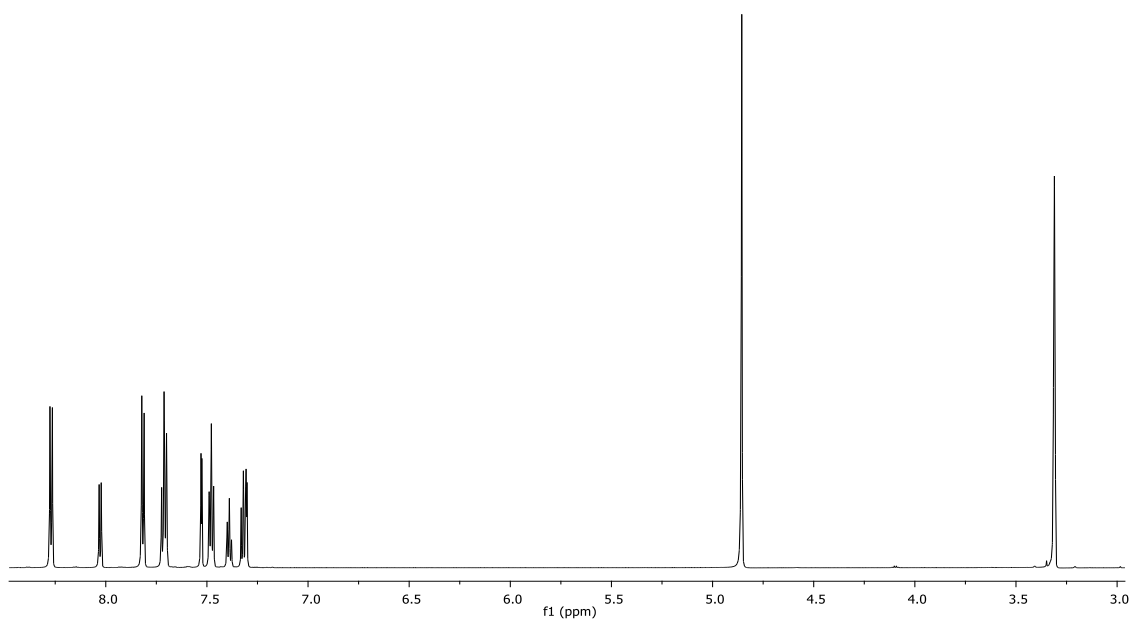
^1H NMR of compound **30** (400 MHz, CD_3OD)



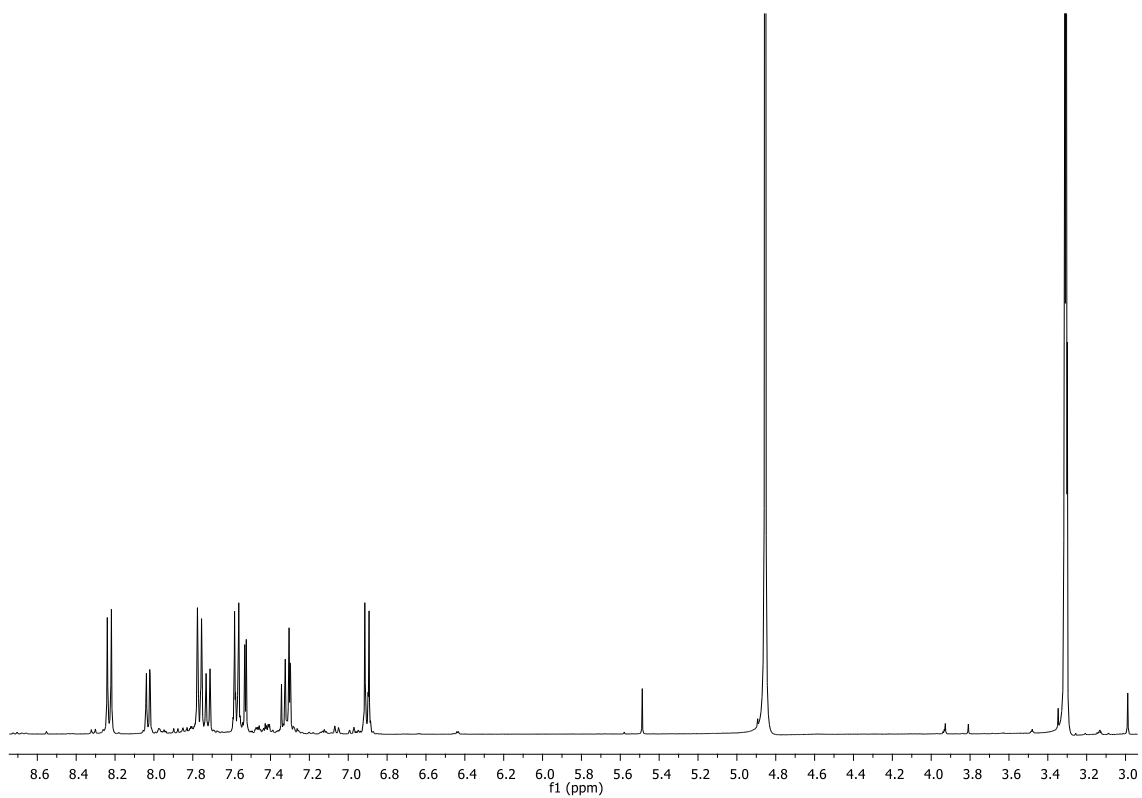
¹H NMR of compound **31** (400 MHz, CD₃OD)



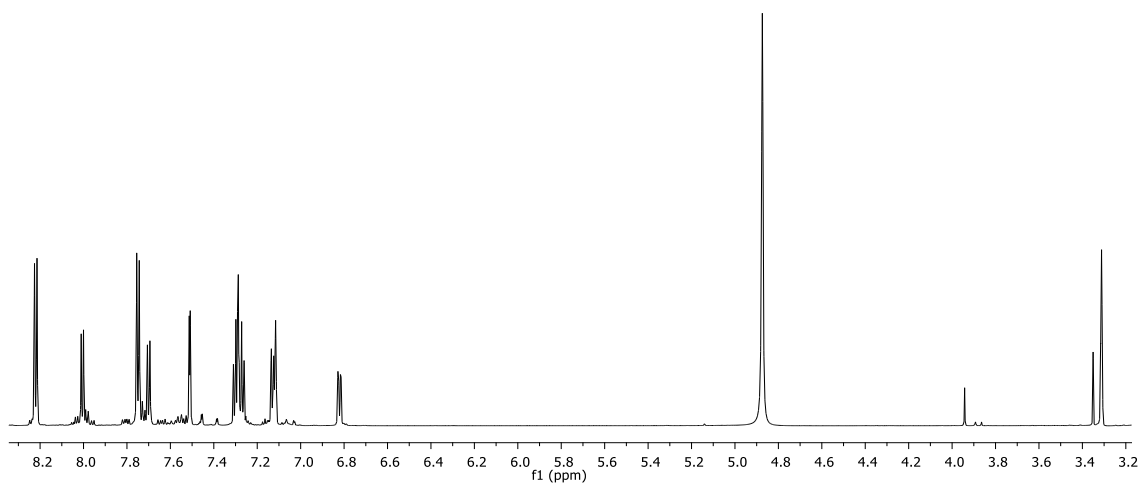
¹H NMR of compound **32** (400 MHz, CD₃OD)



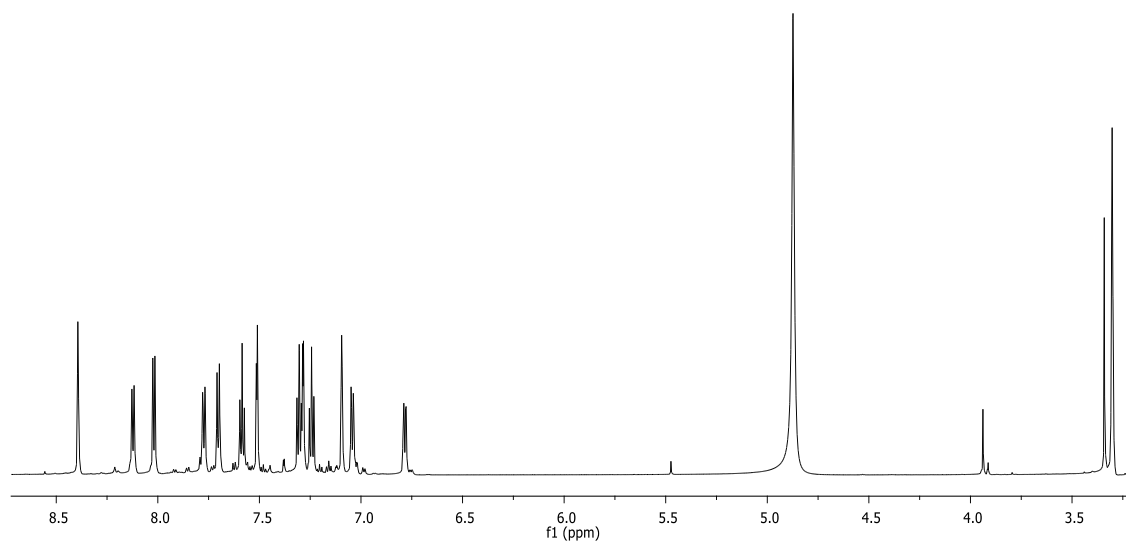
^1H NMR of compound **33** (700 MHz, CD_3OD)



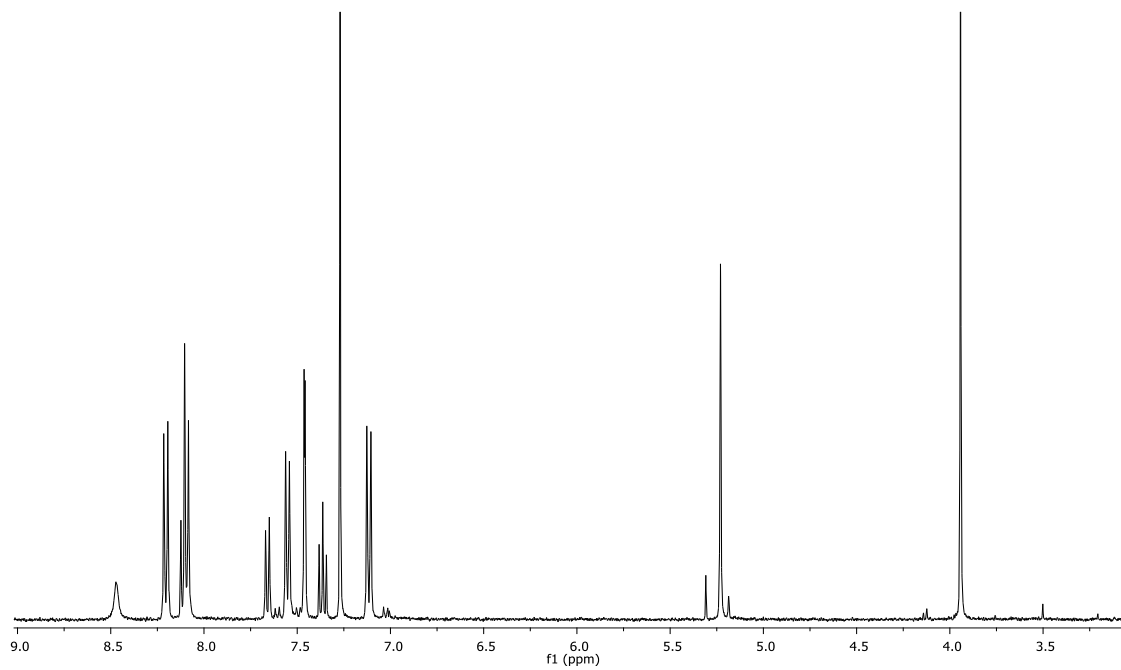
^1H NMR of compound **34** (400 MHz, CD_3OD)



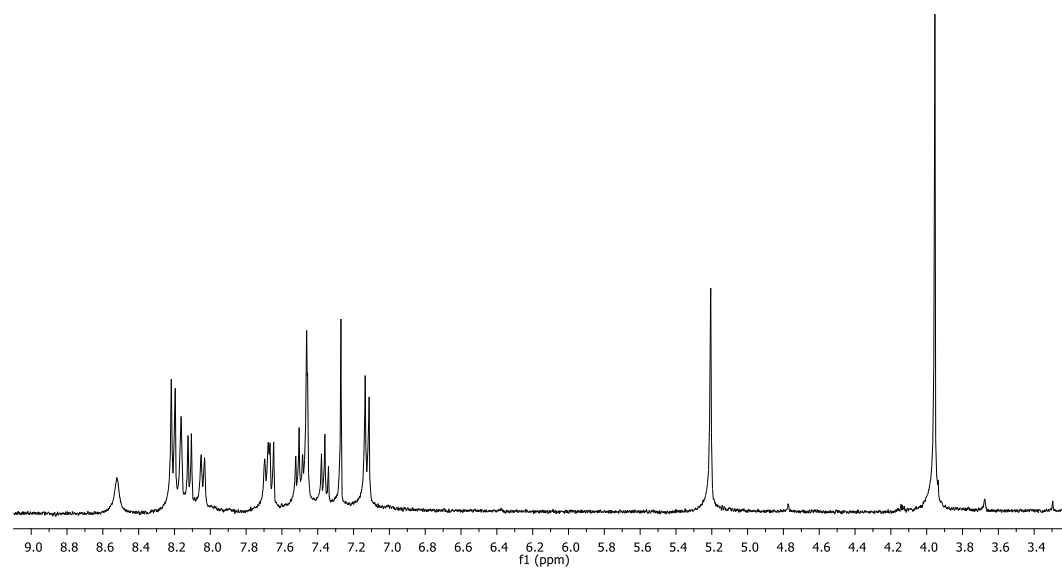
^1H NMR of compound **35** (700 MHz, CD_3OD)



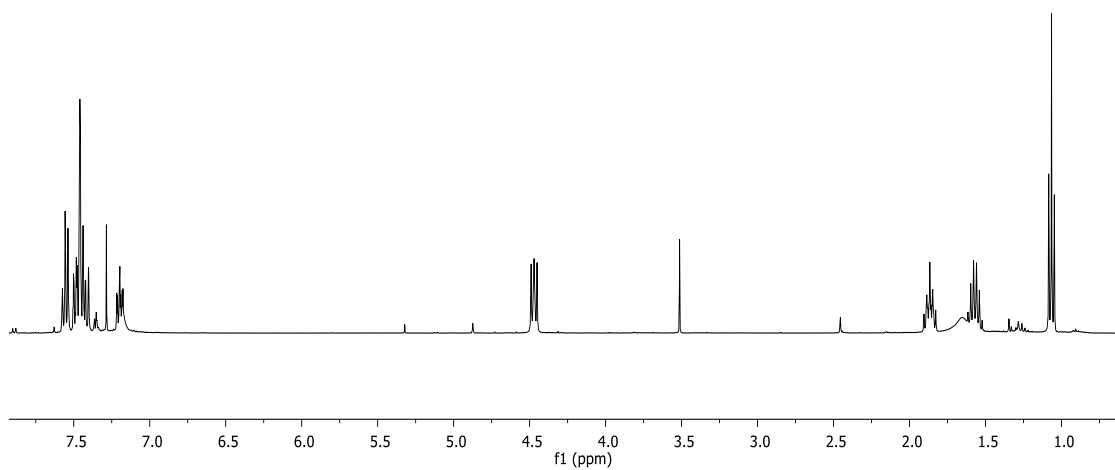
^1H NMR of compound **36** (700 MHz, CD_3OD)



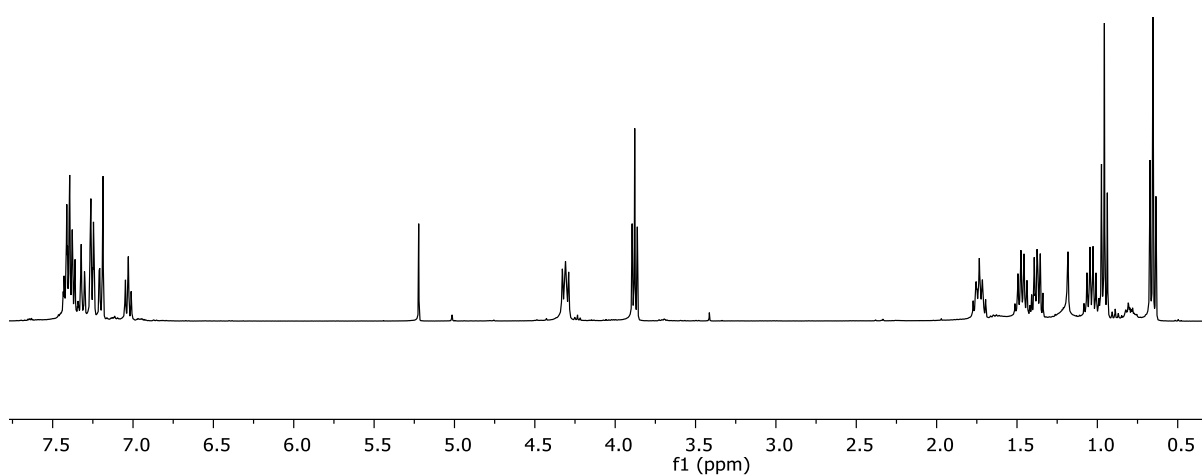
^1H NMR of compound **37** (400 MHz, CDCl_3)



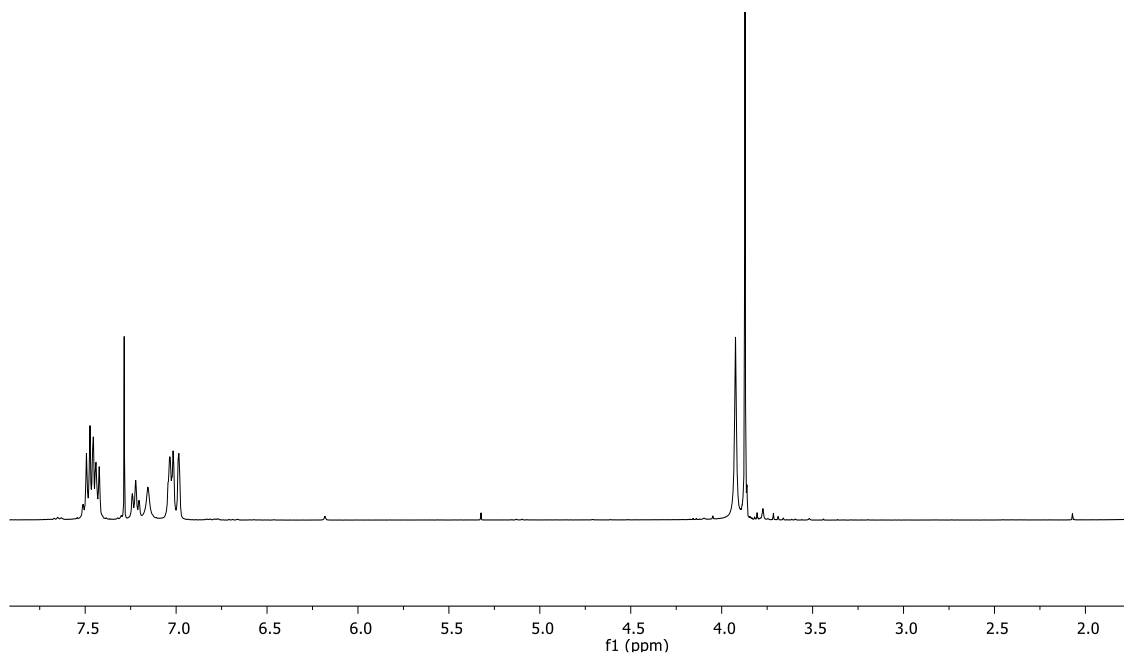
^1H NMR of compound **38** (400 MHz, CDCl_3)



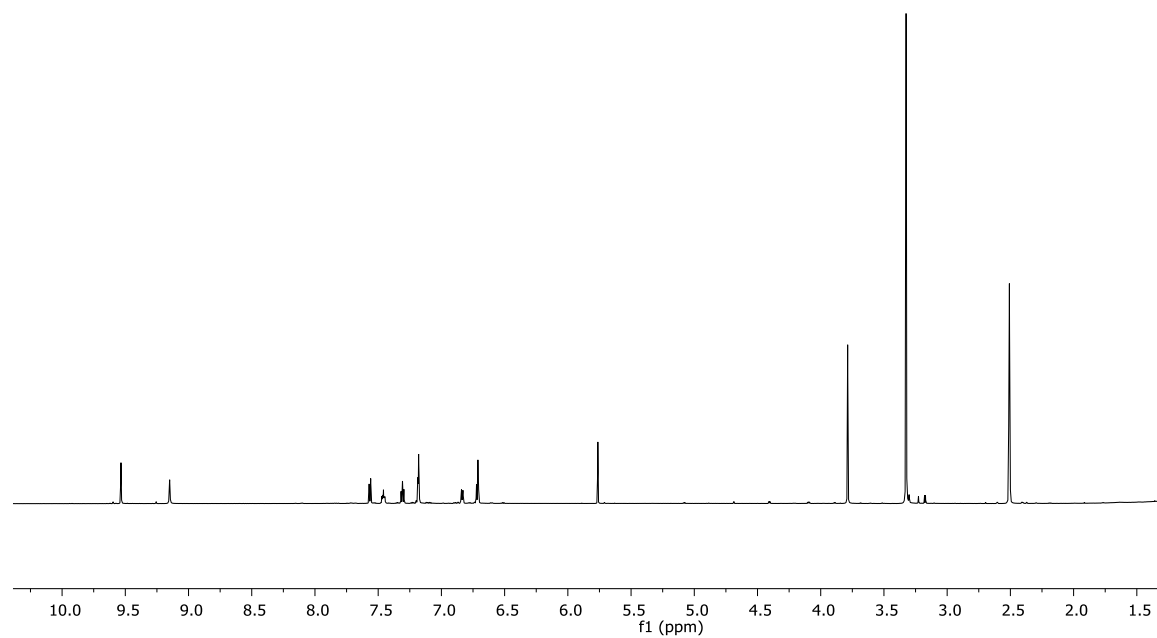
¹H-NMR of compound **56** (CDCl₃, 400 MHz)



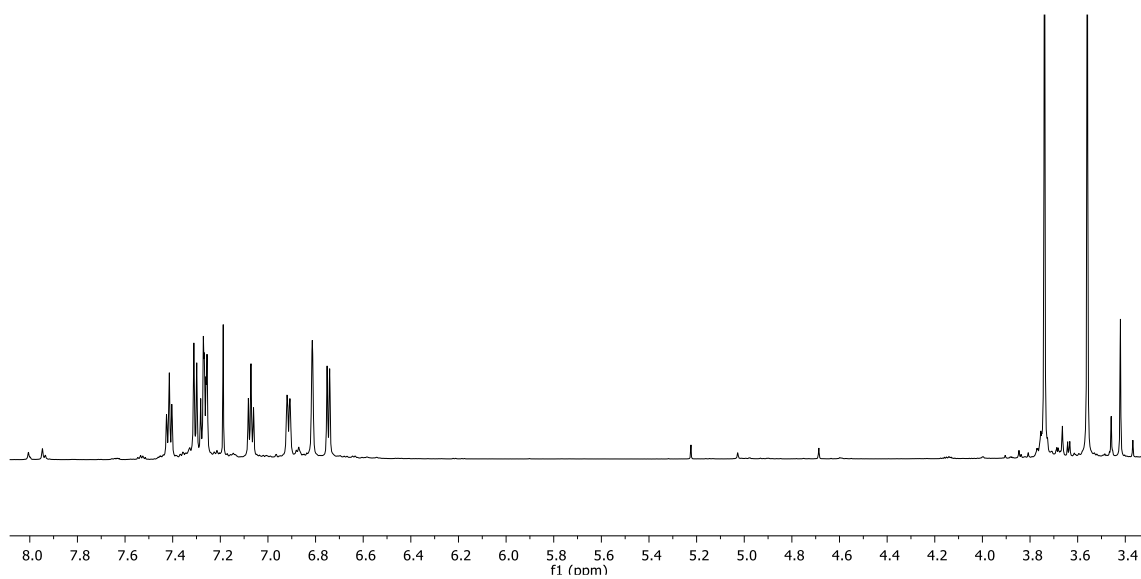
¹H-NMR of compound **57** (CDCl₃, 400 MHz)



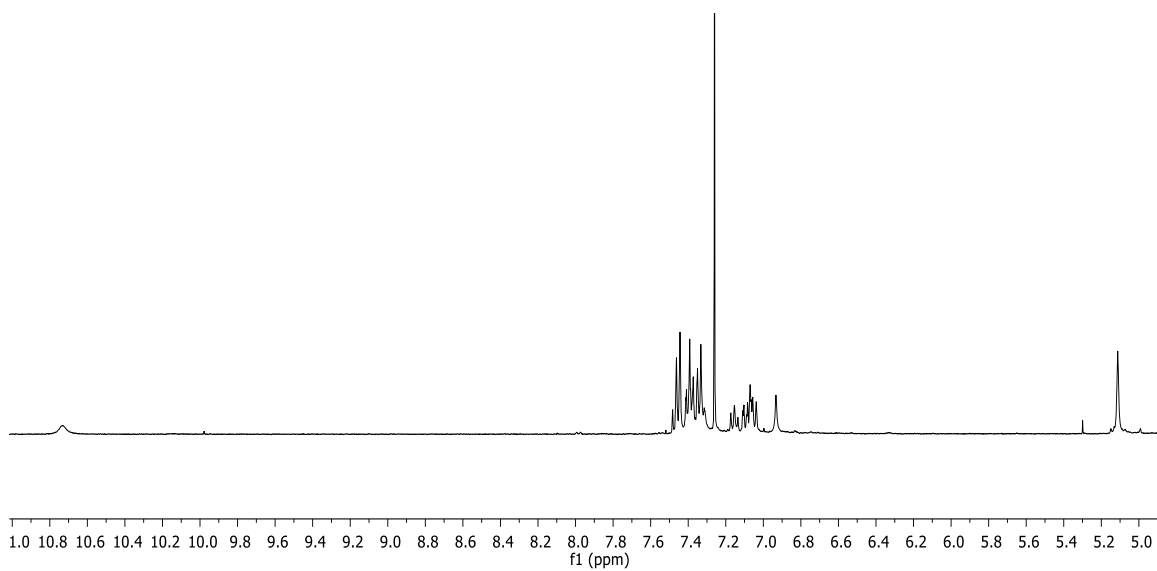
$^1\text{H-NMR}$ of compound **59** (CDCl_3 , 400 MHz)



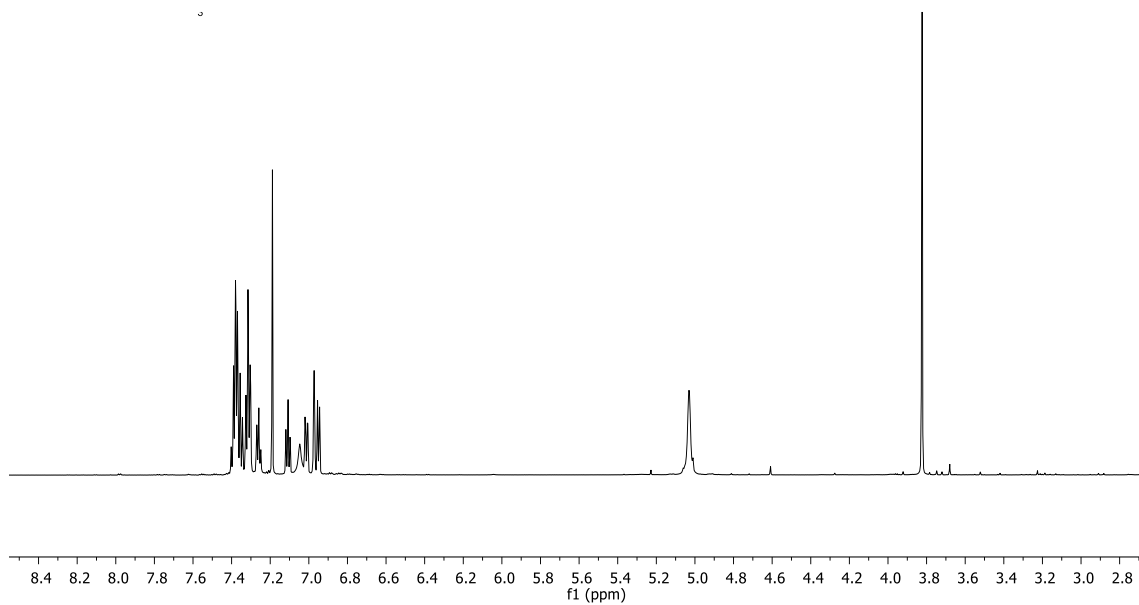
$^1\text{H-NMR}$ of compound **60** (CD_3SOCD_3 , 400 MHz)



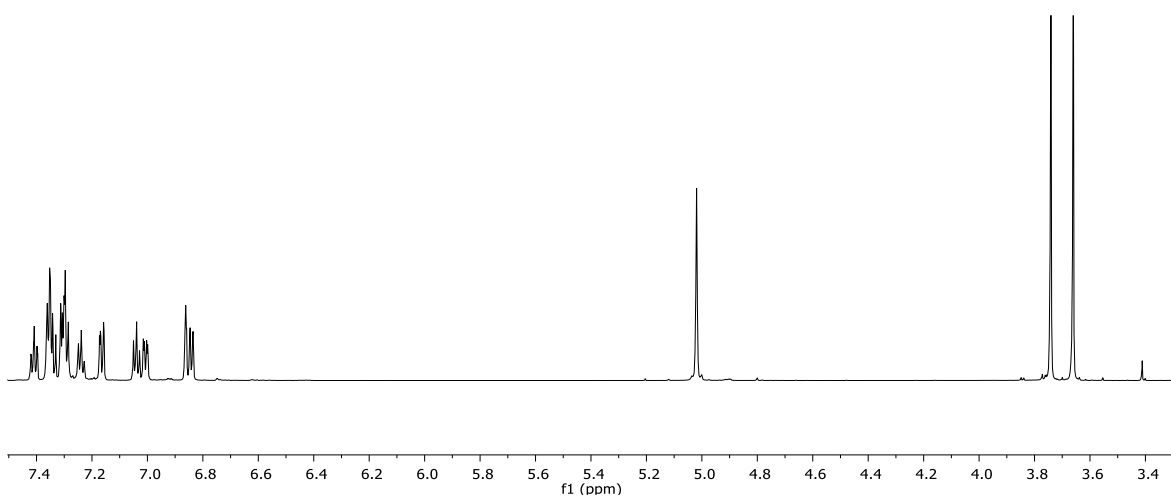
$^1\text{H-NMR}$ of compound **61** (CDCl_3 , 400 MHz)



$^{13}\text{C-NMR}$ of compound **62** (CDCl_3 , 100 MHz)



$^1\text{H-NMR}$ of compound **63** (CDCl_3 , 400 MHz)



$^1\text{H-NMR}$ of compound **64** (CDCl_3 , 400 MHz)

References

- (1) Dias, D. A., Urban, S., Roessner, U. A historical overview of natural products in drug discovery. *Metabolites*, **2012**, 2 (2), 303-336.
- (2) Mohs R.C., Greig N.H.; Drug discovery and development: Role of basic biological research, *Alzheimer's & Dementia: Translational Research & Clinical Interventions*, **2017**, 3, 651-657.
- (3) Hughes, J. P., Rees, S., Kalindjian, S. B., & Philpott, K. L., Principles of early drug-discovery, *Br. J. Pharmacol.* **2011**, 162, 1239 – 1249.
- (4) Burley, S. K.; Park, F. Meeting, The challenges of drug discovery: a multidisciplinary re-evaluation of current practices; *Genome Biol.* **2005**, 6, 330-330.
- (5) Leelananda, S. P., & Lindert, S. Computational methods in drug discovery, *Beilstein J. Org. Chem.* **2016**, 12 (1), 2694–2718.
- (6) Anderson, A. C. The process of structure-based drug design. *Chemistry & biology*, **2003**, 10(9), 787-797.
- (7) Pharmaceutical Research and Manufacturers Association (PREMA) *Introduction to drug development process*. 30th PREMA Anniversary.
- (8) Steinmetz, K. L., & Spack, E. G. The basics of preclinical drug development for neurodegenerative disease indications. *BMC Neurology*, **2009**, 9 (1), 1-13.
- (9) Muntha P., Drug Discovery & Development - A Review, *Res. Rev.: j. pharm. pharm. sci.*, **2016**, 5 (1), 135-142.
- (10) Nicolaou K.C., Advancing the Drug Discovery and Development Process, *Angew. Chem. Int. Ed.* **2014**, 126 (35), 9280-9292.
- (11) MacCoss, M., Baillie, T. A. Organic chemistry in drug discovery. *Science*, **2004**, 303, 1810-1813.

- (12) Schreiber, S. L. Organic synthesis toward small-molecule probes and drugs, *PNAS*, **2011**, *108*, 6699-6702.
- (13) Newman, D. J., Cragg, G. M., Natural Products as Sources of New Drugs over the 30 Years from 1981 to 2010, *J. Nat. Prod.*, **2012**, *75*(3), 311-335.
- (14) Liu, R., Li, X., & Lam, K. S. Combinatorial chemistry in drug discovery. *Current Opinion in. Chemical. Biology*, **2017**, *38*, 117-126.
- (15) Bleicher, K. H.; Bohm, H. J.; Muller, K.; Alanine, A. I. Hit and lead generation: beyond high-throughput screening, *Nature Reviews Drug Discovery.*, **2003**, *2* (5), 369-78.
- (16) Lionta, E., Spyrou, G., K Vassilatis, D., & Cournia, Z. Structure-based virtual screening for drug discovery: principles, applications and recent advances, *Curr. Top. Med. Chem.* **2014**. *14*(16), 1923-1938.
- (17) Vyas, V., Anurekha J., Avijeet J., Arun G., Virtual Screening: A fast tool for drug design. *Sci. Pharm.* **2008**, *76* (3), 333–360.
- (18) von Behren, M. M.; Rarey, M., Ligand-based virtual screening under partial shape constraints. *Journal of Computer-Aided Molecular Design*, **2017**, *31* (4), 335-347.
- (19) Prajapat P., Role of organic, medicinal & pharmaceutical chemistry in drug design: introduction, *Nanomed. Res. J.*, **2018**, *7* (2), 70–71.
- (20) Prakash N, Devangi P., Drug Discovery. *J. Antivir. Antiretr.*, **2010**, *2*, 063-068.
- (21) Zhao, H.; Dietrich, J., Privileged scaffolds in lead generation. *Expert Opin. Drug Disc.* **2015**, *10* (7), 781-790.
- (22) Welsch, M. E.; Snyder, S. A.; Stockwell, B. R., Privileged scaffolds for library design and drug discovery. *Current Opinion on Chemical Bioogy*, **2010**, *14* (3), 347-361.

- (23) Evans, B. E.; Rittle, K. E.; Bock, M. G.; DiPardo, R. M.; Freidinger, R. M.; Whitter, W. L.; Lundell, G. F.; Veber, D. F.; Anderson, P. S.; Chang, R. S. L., Methods for drug discovery: development of potent, selective, orally effective cholecystokinin antagonists. *J. Med. Chem.*, **1988**, *31* (12), 2235-2246.
- (24) DeSimone, R. W., Currie, K. S., Mitchell, S. A., Darrow, J. W., Pippin, D. A. Privileged structures: applications in drug discovery. *Comb. Chem. High Throughput Screen.* **2004**, *7*(5), 473-493.
- (25) L. Costantino, D. Barlocco, Privileged Structures as Leads in Medicinal Chemistry, *Curr. Med. Chem.*, **2006**, *13* (1), 65-85.
- (26) Mugnaini, C.; Pasquini, S.; Corelli, F., The 4-quinolone-3-carboxylic acid motif as a multivalent scaffold in medicinal chemistry. *Current Medicinal Chemistry*, **2009**, *16*, 1746-1767.
- (27) Subramaniam S., Mehrotra M., Gupta D. Virtual high throughput screening (vHTS): a perspective. *Bioinformation*, **2008**, *3* (1), 14–17.
- (28) Chen, J.; Houk, K. N., Molecular Modelling: Principles and Applications By Andrew R. Leach. Addison Wesley Longman Limited: Essex, England, 1996. 595. *J. Chem. Inf. Comput. Sci.* **1998**, *38* (5), 939-939.
- (29) Jorgensen, W. L., Efficient Drug Lead Discovery and Optimization. *Accounts of Chemical Research.* **2009**, *42* (6), 724-733.
- (30) Abi Hussein, H.; Geneix, C.; Petitjean, M.; Borrel, A.; Flatters, D.; Camproux, A. C., Global vision of druggability issues: applications and perspectives. *Drug Discov Today*, **2017**, *22* (2), 404-415.
- (31) Zhang, M. Q.; Wilkinson, B. Drug discovery beyond the 'rule-of-five'. *Current Opinion on Biotechnology*, **2007**, *18* (6), 478-88.

- (32) Lopez-Vallejo, F.; Caulfield, T.; Martinez-Mayorga, K.; Giulianotti, M. A.; Nefzi, A.; Houghten, R. A.; Medina-Franco, J. L. Integrating virtual screening and combinatorial chemistry for accelerated drug discovery. *Comb. Chem. High Throughput Screen.*, **2011**, *14* (6), 475-87.
- (33) Kappe, C. O.; Dallinger, D. The impact of microwave synthesis on drug discovery. *Nature Reviews Drug Discovery*, **2006**, *5* (1), 51-63.
- (34) Wirth, T. Flow Chemistry: Enabling Technology in Drug Discovery and Process Research. *ChemSusChem* **2012**, *5*(2), 215-216.
- (35) Li P, Terrett J.A, Zbieg J. R. Visible-Light Photocatalysis as an Enabling Technology for Drug Discovery: A Paradigm Shift for Chemical Reactivity. *ACS Med. Chem. Lett.* **2020**, *11*(11), 2120-2130.
- (36) Skinner, A. L.; Laurence, J. S. High-field Solution NMR Spectroscopy as a Tool for Assessing Protein Interactions with Small Molecule Ligands. *J. Pharm. Sci.* **2008**, *97*, 4670-4695.
- (37) Kassel, D. B. The expanding role of HPLC in drug discovery. *HPLC for Pharmaceutical Sciences*, **2007**, 533-575.
- (38) N. W Hird, Automated synthesis: new tools for the organic chemist, *Drug Discovery Today*, **1999**, *4* (6), 265-274.
- (39) Lombardino, J. G.; Lowe, J. A., The role of the medicinal chemist in drug discovery: then and now. *Nature Reviews Drug Discovery*, **2004**, *3* (10), 853-62.
- (40) Potoski, J. Timely synthetic support for medicinal chemists. *Drug Discovery Today*, **2005**, *10* (2), 115-20.
- (41) Pace, A.; Pierro, P. The new era of 1,2,4-oxadiazoles. *Organic & Biomolecular Chemistry*, **2009**, *7* (21), 4337-4348.
- (42) Khan I., Ibrar A., Abbas N., Oxadiazoles as privileged motifs for promising anticancer leads: recent advances and future prospects. *Archive*

der Pharmazie (Weinheim), **2014**, 347 (1), 1-20. doi: 10.1002/ardp.201300231.

(43) Anuj, S., Gupta M., 1, 3, 4-oxadiazoles and their pharmacological properties: a review, *World J. Pharm. Sci.* **2020**, 9 (8), 886-904.

(44) Saha R., Tanwar O., Marella A., Alam M.M., Akhter M. Recent updates on biological activities of oxadiazoles. *Mini Rev. Med. Chem.* **2013** 13 (7), 1027-46.

(45) Pitasse-Santos, P., Sueth-Santiago, V., Lima, M. E. 1,2,4- and 1,3,4-Oxadiazoles as Scaffolds in the Development of Antiparasitic Agents, *J. Braz. Chem. Soc.*, **2018**, 29 (3), 435-456,

(46) Moussebois, C., Oth, J. F. M., Etude spectroscopique d'oxadiazoles-1, 2, 4 en relation avec leur degré d'aromaticité, *Helv. Chim. Acta* **1964**, 47 (4), 942-946.

(47) Tiemann, F.; Krüger, P. Ueber amidoxime und azoxime. *Berichte der deutschen chemischen Gesellschaft*, **1884**, 17 (2), 1685-1698.

(48) Pace, A.; Buscemi, S.; Piccionello, A. P.; Pibiri, I. Recent advances in the chemistry of 1, 2, 4-oxadiazoles. *Adv. Heterocycl. Chem.*, **2015**, 116, 85-136.

(49) Ajay Kumar K., Lokeshwari D.M., Pavithra G., Vasanth Kumar G. 1,2,4-Oxadiazoles: A potential pharmacological agents-An overview, *Research Journal of Pharmacy and Technology*, **2012**, 5 (12), 1490-1496.

(50) Silvestrini, B. Un antitosse-antinfiammatorio, l'Oxolamina (Perebron). *Minerva Medica*, **1960**, 51, 4091-4094.

(51) Ardiçlı, D.; Haliloğlu, G.; Alikasıfoğlu, M.; Topaloğlu, H. Diagnostic pathway to nonsense mutation dystrophinopathy: a tertiary-center, retrospective experience. *Neuropediatrics* **2019**, 50 (01), 041-045.

- (52) Chawla, G. 1, 2, 4-Oxadiazole as a privileged scaffold for anti-inflammatory and analgesic activities: A review. *Mini reviews in medicinal chemistry* **2018**, 18 (18), 1536-1547.
- (53) Durgashivaprasad, E.; Mathew, G.; Sebastian, S.; Reddy, S. M.; Mudgal, J.; Nampurath, G. K. Novel 2, 5-disubstituted-1, 3, 4-oxadiazoles as anti-inflammatory drugs. *Indian journal of pharmacology* **2014**, 46 (5), 521.
- (54) Dogné, J. M.; Hanson, J.; Supuran, C.; Pratico, D. Coxibs and cardiovascular side-effects: from light to shadow. *Curr Pharm Des* **2006**, 12 (8), 971-975. DOI: 10.2174/138161206776055949.
- (55) Davies, N. M.; Smith, G. D.; Windmeijer, F.; Martin, R. M. COX-2 selective nonsteroidal anti-inflammatory drugs and risk of gastrointestinal tract complications and myocardial infarction: an instrumental variable analysis. *Epidemiology* **2013**, 24 (3), 352-362. DOI: 10.1097/EDE.0b013e318289e024.
- (56) Zarghi, A.; Arfaei, S. Selective COX-2 inhibitors: a review of their structure-activity relationships. *Iranian journal of pharmaceutical research: IJPR* **2011**, 10 (4), 655.
- (57) Medzhitov, R. Origin and physiological roles of inflammation. *Nature* **2008**, 454 (7203), 428-435. DOI: 10.1038/nature07201.
- (58) Kumar V., Cotran R.S., Robbins S.L. , *Robbins Basic Pathology*, 7th edition, **2003**.
- (59) Barton, G. M. A calculated response: control of inflammation by the innate immune system. *J. Clin. Investig.* **2008**, 118 (2), 413-420.
- (60) Serhan, C. N.; Savill, J. Resolution of inflammation: the beginning programs the end. *Nature Immunology* **2005**, 6 (12), 1191-1197.

- (61) Nathan, C. Points of control in inflammation. *Nature* **2002**, 420 (6917), 846-852.
- (62) Rock, K. L.; Kono, H. The inflammatory response to cell death. *Annu. Rev. Pathol. Mech. Dis.* **2008**, 3, 99-126.
- (63) Stables, M. J.; Gilroy, D. W. Old and new generation lipid mediators in acute inflammation and resolution. *Prog. Lipid Res.* **2011**, 50 (1), 35-51.
- (64) Greenhough, A.; Smartt, H. J.; Moore, A. E.; Roberts, H. R.; Williams, A. C.; Paraskeva, C.; Kaidi, A. The COX-2/PGE2 pathway: key roles in the hallmarks of cancer and adaptation to the tumour microenvironment. *Carcinogenesis* **2009**, 30 (3), 377-386. DOI: 10.1093/carcin/bgp014.
- (65) Martínez-Colón, G. J.; Moore, B. B. Prostaglandin E. *Pharmacol Ther* **2018**, 185, 135-146. DOI: 10.1016/j.pharmthera.2017.12.008.
- (66) Akasaka, H.; So, S.-P.; Ruan, K.-H. Relationship of the topological distances and activities between mPGES-1 and COX-2 versus COX-1: Implications of the different post-translational endoplasmic reticulum organizations of COX-1 and COX-2. *Biochemistry* **2015**, 54 (23), 3707-3715.
- (67) Ricciotti, E.; FitzGerald, G. A. Prostaglandins and inflammation. *Arteriosclerosis, thrombosis, and vascular biology* **2011**, 31 (5), 986-1000.
- (68) Murakami, M. Naraba H, Tanioka T, Semmyo N, Nakatani Y, Kojima F, Ikeda T, Fueki M, Ueno A, Oh S, and Kudo I. Regulation of prostaglandin E₂ biosynthesis by inducible membrane-associated prostaglandin E₂ synthase that acts in concert with cyclooxygenase-2. *J Biol Chem* **2000**, 275 (32), 783-732,792.

- (69) Koeberle, A.; Werz, O. Perspective of microsomal prostaglandin E2 synthase-1 as drug target in inflammation-related disorders. *Biochemical pharmacology* **2015**, *98* (1), 1-15.
- (70) Larsson, K.; Jakobsson, P.-J. Inhibition of microsomal prostaglandin E synthase-1 as targeted therapy in cancer treatment. *Prostaglandins Other Lipid Mediat.* **2015**, *120*, 161-165.
- (71) Sampey, A. V.; Monrad, S.; Crofford, L. J. Microsomal prostaglandin E synthase-1: the inducible synthase for prostaglandin E 2. *Arthritis Res. & Ther.* **2005**, *7* (3), 1-4.
- (72) Jakobsson, P.-J.; Morgenstern, R.; Mancini, J.; Ford-Hutchinson, A.; Persson, B. Common structural features of MAPEG—a widespread superfamily of membrane associated proteins with highly divergent functions in eicosanoid and glutathione metabolism. *Protein Sci.* **1999**, *8* (3), 689-692.
- (73) Bergqvist, F.; Morgenstern, R.; Jakobsson, P.-J. A review on mPGES-1 inhibitors: From preclinical studies to clinical applications. *Prostaglandins Other Lipid Mediat.* **2020**, *147*, 106383.
- (74) Sjögren, T.; Nord, J.; Ek, M.; Johansson, P.; Liu, G.; Geschwindner, S. Crystal structure of microsomal prostaglandin E2 synthase provides insight into diversity in the MAPEG superfamily. *Proceedings of the National Academy of Sciences* **2013**, *110* (10), 3806-3811.
- (75) Koeberle, A.; Laufer, S. A.; Werz, O. Design and development of microsomal prostaglandin E2 synthase-1 inhibitors: challenges and future directions. *J. Med. Chem.* **2016**, *59* (13), 5970-5986.
- (76) Raouf, J.; Rafique, N.; Goodman, M. C.; Idborg, H.; Bergqvist, F.; Armstrong, R. N.; Jakobsson, P.-J.; Morgenstern, R.; Spahiu, L. Arg126 and Asp49 are essential for the catalytic function of microsomal

prostaglandin E2 synthase 1 and Ser127 is not. *PloS one* **2016**, *11* (9), e0163600.

(77) Gatti, D.; Adami, S. Coxibs: a significant therapeutic opportunity. *Acta Biomed.* **2010**, *81* (3), 217-224.

(78) Chini, M. G.; Giordano, A.; Potenza, M.; Terracciano, S.; Fischer, K.; Vaccaro, M. C.; Colarusso, E.; Bruno, I.; Riccio, R.; Koeberle, A. Targeting mPGES-1 by a combinatorial approach: identification of the aminobenzothiazole scaffold to suppress PGE2 levels. *ACS Med. Chem. Lett.* **2020**, *11* (5), 783-789.

(79) Di Micco, S.; Terracciano, S.; Cantone, V.; Fischer, K.; Koeberle, A.; Foglia, A.; Riccio, R.; Werz, O.; Bruno, I.; Bifulco, G. Discovery of new potent molecular entities able to inhibit mPGES-1. *Eur. J. Med. Chem.* **2018**, *143*, 1419-1427.

(80) Chini, M. G.; Ferroni, C.; Cantone, V.; Dambruoso, P.; Varchi, G.; Pepe, A.; Fischer, K.; Pergola, C.; Werz, O.; Bruno, I. Elucidating new structural features of the triazole scaffold for the development of mPGES-1 inhibitors. *MedChemComm* **2015**, *6* (1), 75-79.

(81) Korotkova, M.; Jakobsson, P. J. Characterization of microsomal prostaglandin E synthase 1 inhibitors. *Basic & clinical pharmacology & toxicology* **2014**, *114* (1), 64-69.

(82) Psarra, A.; Nikolaou, A.; Kokotou, M. G.; Linnios, D.; Kokotos, G. Microsomal prostaglandin E2 synthase-1 inhibitors: a patent review. *Expert Opin. Ther.Pat.* **2017**, *27* (9), 1047-1059.

(83) Riendeau, D.; Aspiotis, R.; Ethier, D.; Gareau, Y.; Grimm, E. L.; Guay, J.; Guiral, S.; Juteau, H.; Mancini, J. A.; Méthot, N. Inhibitors of the inducible microsomal prostaglandin E2 synthase (mPGES-1) derived from MK-886. *Bioorganic Med. Chem. Lett.* **2005**, *15* (14), 3352-3355.

- (84) Gür, Z. T.; Çalışkan, B.; Garscha, U.; Olgaç, A.; Schubert, U. S.; Gerstmeier, J.; Werz, O.; Banoglu, E. Identification of multi-target inhibitors of leukotriene and prostaglandin E2 biosynthesis by structural tuning of the FLAP inhibitor BRP-7. *Eur. J. Med. Chem.* **2018**, *150*, 876-899.
- (85) Chang, H.-H.; Meuillet, E. J. Identification and development of mPGES-1 inhibitors: where we are at? *Future Med. Chem.* **2011**, *3* (15), 1909-1934.
- (86) Lauro, G.; Cantone, V.; Potenza, M.; Fischer, K.; Koeberle, A.; Werz, O.; Riccio, R.; Bifulco, G. Discovery of 3-hydroxy-3-pyrrolin-2-one-based mPGES-1 inhibitors using a multi-step virtual screening protocol. *MedChemComm* **2018**, *9* (12), 2028-2036.
- (87) Iranshahi, M.; Chini, M. G.; Masullo, M.; Sahebkar, A.; Javidnia, A.; Chitsazian Yazdi, M.; Pergola, C.; Koeberle, A.; Werz, O.; Pizza, C. Can small chemical modifications of natural pan-inhibitors modulate the biological selectivity? The case of curcumin prenylated derivatives acting as HDAC or mPGES-1 inhibitors. *J. Nat. Prod.* **2015**, *78* (12), 2867-2879.
- (88) Wixtrom, R. N.; Silva, M. H.; Hammock, B. D. Affinity purification of cytosolic epoxide hydrolase using derivatized epoxy-activated Sepharose gels. *Anal.* **1988**, *169* (1), 71-80.
- (89) CombiGlide, L.L.C. Schrodinger, New York, NY (**2017**).
- (90) Schrodinger LigPrep, LLC, New York, NY (**2017**).
- (91) Schrodinger QikProp, LLC, New York, NY (**2017**).
- (92) Lipinski, C. A. Lead-and drug-like compounds: the rule-of-five revolution. *Drug discovery today: Technologies* **2004**, *1* (4), 337-341.
- (93) Schrodinger QikProp, LLC, New York, NY (**2017**)
- (94) Schrodinger LigFilter, LLC, New York, NY (**2017**).

- (95) Partridge, K. M.; Antonysamy, S.; Bhattachar, S. N.; Chandrasekhar, S.; Fisher, M. J.; Fretland, A.; Gooding, K.; Harvey, A.; Hughes, N. E.; Kuklish, S. L. Discovery and characterization of [(cyclopentyl) ethyl] benzoic acid inhibitors of microsomal prostaglandin E synthase-1. *Bioorganic Med. Chem. Lett.* **2017**, *27* (6), 1478-1483.
- (96) Schrodinger Glide, LLC, New York, NY (**2017**)
- (97) Daina, A.; Michielin, O.; Zoete, V. SwissADME: a free web tool to evaluate pharmacokinetics, drug-likeness and medicinal chemistry friendliness of small molecules. *Scientific reports* **2017**, *7* (1), 1-13.
- (98) Gerstmeier, J.; Weinigel, C.; Rummler, S.; Rådmark, O.; Werz, O.; Garscha, U. Time-resolved in situ assembly of the leukotriene-synthetic 5-lipoxygenase/5-lipoxygenase-activating protein complex in blood leukocytes. *The FASEB Journal* **2016**, *30* (1), 276-285.
- (99) Pannunzio, A.; Coluccia, M. Cyclooxygenase-1 (COX-1) and COX-1 inhibitors in cancer: a review of oncology and medicinal chemistry literature. *Pharmaceuticals* **2018**, *11* (4), 101.
- (100) Meanwell, N. A. Fluorine and fluorinated motifs in the design and application of bioisosteres for drug design. *J. Med. Chem.* **2018**, *61* (14), 5822-5880.
- (101) Cuzzocrea, S.; Filippelli, A.; Zingarelli, B.; Falciani, M.; Caputi, A. P.; Rossi, F. Role of nitric oxide in a nonseptic shock model induced by zymosan in the rat. *Shock (Augusta, Ga.)* **1997**, *7* (5), 351-357.
- (102) d'Acquisto, F.; Maione, F.; Pederzoli-Ribeil, M. From IL-15 to IL-33: the never-ending list of new players in inflammation. Is it time to forget the humble aspirin and move ahead? *Biochem.* **2010**, *79* (4), 525-534.

- (103) Liu, S.; Zhang, J.; Pang, Q.; Song, S.; Miao, R.; Chen, W.; Zhou, Y.; Liu, C. The protective role of curcumin in zymosan-induced multiple organ dysfunction syndrome in mice. *Shock (Augusta, Ga.)* **2016**, *45* (2), 209.
- (104) Moore, K. W.; de Waal Malefyt, R.; Coffman, R. L.; O'Garra, A. Interleukin-10 and the interleukin-10 receptor. *Annual review of immunology* **2001**, *19* (1), 683-765.
- (105) Schwab, J. M.; Chiang, N.; Arita, M.; Serhan, C. N. Resolvin E1 and protectin D1 activate inflammation-resolution programmes. *Nature* **2007**, *447* (7146), 869-874.
- (106) Cash, J. L.; White, G. E.; Greaves, D. R. Zymosan-induced peritonitis as a simple experimental system for the study of inflammation. *Meth. Enzymol.* **2009**, *461*, 379-396.
- (107) Hanke, T.; Dehm, F.; Liening, S.; Popella, S. D.; Maczewsky, J.; Pillong, M.; Kunze, J.; Weinigel, C.; Barz, D.; Kaiser, A.; et al. Aminothiazole-featured pirinixic acid derivatives as dual 5-lipoxygenase and microsomal prostaglandin E2 synthase-1 inhibitors with improved potency and efficiency in vivo. *J. Med. Chem.* **2013**, *56* (22), 9031-9044. DOI: 10.1021/jm401557w.
- (108) Nambiar, P. R.; Girnun, G.; Lillo, N. A.; Guda, K.; Whiteley, H. E.; Rosenberg, D. W. Preliminary analysis of azoxymethane induced colon tumors in inbred mice commonly used as transgenic/knockout progenitors. *Int. J. Oncol.* **2003**, *22* (1), 145-150.
- (109) Lorke, D. A new approach to practical acute toxicity testing. *Arch. Toxicol.* **1983**, *54* (4), 275-287.
- (110) Walton, J. R. Antibiotic resistance: an overview. *Vet Rec* **1988**, *122* (11), 249-251. DOI: 10.1136/vr.122.11.249.

- (111) Stapleton, P. D.; Taylor, P. W. Methicillin resistance in *Staphylococcus aureus*: mechanisms and modulation. *Sci. Prog.* **2002**, *85* (Pt 1), 57-72. DOI: 10.3184/003685002783238870.
- (112) Turner, N. A.; Sharma-Kuinkel, B. K.; Maskarinec, S. A.; Eichenberger, E. M.; Shah, P. P.; Carugati, M.; Holland, T. L.; Fowler, V. G. Methicillin-resistant *Staphylococcus aureus*: an overview of basic and clinical research. *Nat. Rev. Microbiol.* **2019**, *17* (4), 203-218. DOI: 10.1038/s41579-018-0147-4.
- (113) Raygada, J. L.; Levine, D. P. Methicillin-Resistant *Staphylococcus aureus*: A Growing Risk in the Hospital and in the Community. *Am Health Drug Benefits* **2009**, *2* (2), 86-95.
- (114) Wu, S.-C.; Liu, F.; Zhu, K.; Shen, J.-Z. Natural products that target virulence factors in antibiotic-resistant *Staphylococcus aureus*. *J. Agric. Food Chem.* **2019**, *67* (48), 13195-13211.
- (115) Chambers, H. F.; DeLeo, F. R. Waves of resistance: *Staphylococcus aureus* in the antibiotic era. *Nat. Rev. Microbiol.* **2009**, *7* (9), 629-641.
- (116) Laupland, K. B.; Lyytikäinen, O.; Sgaard, M.; Kennedy, K.; Knudsen, J. D.; Ostergaard, C.; Galbraith, J.; Valiquette, L.; Jacobsson, G.; Collignon, P. The changing epidemiology of *Staphylococcus aureus* bloodstream infection: a multinational population-based surveillance study. *Clin. Microbiol. Infect.* **2013**, *19* (5), 465-471.
- (117) van den Broek, P. J.; Buys, L. F.; Mattie, H.; van Furth, R. Effect of penicillin G on *Staphylococcus aureus* phagocytosed by human monocytes. *J Infect Dis* **1986**, *153* (3), 586-592. DOI: 10.1093/infdis/153.3.586.
- (118) Kimberlin, C.; Khalid, F.; Hariri, A. Resistance of staphylococci to penicillin-G and cloxacillin. *Pahlavi Med. J.* **1978**, *9* (2), 182-192.

- (119) Worthington, R. J.; Melander, C. Overcoming resistance to β -lactam antibiotics. *J Org Chem* **2013**, *78* (9), 4207-4213. DOI: 10.1021/jo400236f.
- (120) Fishovitz, J.; Hermoso, J. A.; Chang, M.; Mobashery, S. Penicillin-binding protein 2a of methicillin-resistant *Staphylococcus aureus*. *IUBMB Life* **2014**, *66* (8), 572-577. DOI: 10.1002/iub.1289.
- (121) Kennedy, A. D.; Otto, M.; Braughton, K. R.; Whitney, A. R.; Chen, L.; Mathema, B.; Mediavilla, J. R.; Byrne, K. A.; Parkins, L. D.; Tenover, F. C. Epidemic community-associated methicillin-resistant *Staphylococcus aureus*: recent clonal expansion and diversification. *PNAS* **2008**, *105* (4), 1327-1332.
- (122) McAdam, P. R.; Templeton, K. E.; Edwards, G. F.; Holden, M. T.; Feil, E. J.; Aanensen, D. M.; Bargawi, H. J.; Spratt, B. G.; Bentley, S. D.; Parkhill, J. Molecular tracing of the emergence, adaptation, and transmission of hospital-associated methicillin-resistant *Staphylococcus aureus*. *PNAS* **2012**, *109* (23), 9107-9112.
- (123) David, M. Z.; Daum, R. S.; Bayer, A. S.; Chambers, H. F.; Fowler Jr, V. G.; Miller, L. G.; Ostrowsky, B.; Baesa, A.; Boyle-Vavra, S.; Eells, S. J. *Staphylococcus aureus* bacteremia at 5 US academic medical centers, 2008–2011: significant geographic variation in community-onset infections. *Clin.* **2014**, *59* (6), 798-807.
- (124) Casey, J. A.; Curriero, F. C.; Cosgrove, S. E.; Nachman, K. E.; Schwartz, B. S. High-density livestock operations, crop field application of manure, and risk of community-associated methicillin-resistant *Staphylococcus aureus* infection in Pennsylvania. *JAMA internal medicine* **2013**, *173* (21), 1980-1990.

- (125) Guo, Y.; Song, G.; Sun, M.; Wang, J.; Wang, Y. Prevalence and Therapies of Antibiotic-Resistance in. *Front Cell Infect Microbiol* **2020**, *10*, 107. DOI: 10.3389/fcimb.2020.00107.
- (126) Dhameliya, T. M.; Chudasma, S. J.; Patel, T. M.; Dave, B. P. A review on synthetic account of 1,2,4-oxadiazoles as anti-infective agents. *Mol Divers* **2022**. DOI: 10.1007/s11030-021-10375-4.
- (127) O'Daniel, P. I.; Peng, Z.; Pi, H.; Testero, S. A.; Ding, D.; Spink, E.; Leemans, E.; Boudreau, M. A.; Yamaguchi, T.; Schroeder, V. A. Discovery of a new class of non- β -lactam inhibitors of penicillin-binding proteins with gram-positive antibacterial activity. *J. Am. Chem. Soc.* **2014**, *136* (9), 3664-3672.
- (128) Irwin, J. J.; Shoichet, B. K. ZINC– a free database of commercially available compounds for virtual screening. *J. Chem. Inf. Model.* **2005**, *45* (1), 177-182.
- (129) Lim, D.; Strynadka, N. C. Structural basis for the β lactam resistance of PBP2a from methicillin-resistant *Staphylococcus aureus*. *Nat. Struct.* **2002**, *9* (11), 870-876.
- (130) Boucher, H. W.; Talbot, G. H.; Bradley, J. S.; Edwards, J. E.; Gilbert, D.; Rice, L. B.; Scheld, M.; Spellberg, B.; Bartlett, J. Bad bugs, no drugs: no ESCAPE! An update from the Infectious Diseases Society of America. *Clin.* **2009**, *48* (1), 1-12.
- (131) Spink, E.; Ding, D.; Peng, Z.; Boudreau, M. A.; Leemans, E.; Lastochkin, E.; Song, W.; Lichtenwalter, K.; O'Daniel, P. I.; Testero, S. A. Structure–activity relationship for the oxadiazole class of antibiotics. *J. Med. Chem.* **2015**, *58* (3), 1380-1389.
- (132) Potenza, M.; Sciarretta, M.; Chini, M. G.; Saviano, A.; Maione, F.; D'Auria, M. V.; De Marino, S.; Giordano, A.; Hofstetter, R. K.; Festa, C.

Structure-based screening for the discovery of 1, 2, 4-oxadiazoles as promising hits for the development of new anti-inflammatory agents interfering with eicosanoid biosynthesis pathways. *Eur. J. Med. Chem* **2021**, *224*, 113693.

(133) Sharma, K. K.; Maurya, I. K.; Khan, S. I.; Jacob, M. R.; Kumar, V.; Tikoo, K.; Jain, R. Discovery of a membrane-active, ring-modified histidine containing ultrashort amphiphilic peptide that exhibits potent inhibition of *Cryptococcus neoformans*. *J. Med. Chem.* **2017**, *60* (15), 6607-6621.

(134) Rudkin, J. K.; Laabei, M.; Edwards, A. M.; Joo, H.-S.; Otto, M.; Lennon, K. L.; O'Gara, J. P.; Waterfield, N. R.; Massey, R. C. Oxacillin alters the toxin expression profile of community-associated methicillin-resistant *Staphylococcus aureus*. *Antimicrob.* **2014**, *58* (2), 1100-1107.

(135) Peacock, S. J.; Paterson, G. K. Mechanisms of Methicillin Resistance in *Staphylococcus aureus*. *Annu. Rev. Biochem.* **2015**, *84* (1), 577-601. DOI: 10.1146/annurev-biochem-060614-034516.

(136) Bellavita, R.; Vollaro, A.; Catania, M. R.; Merlino, F.; De Martino, L.; Nocera, F. P.; Della Greca, M.; Lembo, F.; Grieco, P.; Buommino, E. Novel Antimicrobial Peptide from Temporin L in The Treatment of *Staphylococcus pseudintermedius* and *Malassezia pachydermatis* in Polymicrobial Inter-Kingdom Infection, *Antibiotics* **2020**, *9* (9), 530.

(224) Lahlou, M. The success of natural products in drug discovery, *Pharmacol. Pharm.* **2013**, *4*, 17-31.

(225) Davison, E. K.; Brimble, M. A. Natural product derived privileged scaffolds in drug discovery. *Curr Opin Chem Biol* **2019**, *52*, 1-8. DOI: 10.1016/j.cbpa.2018.12.007.

- (226) Atanasov, A. G.; Zotchev, S. B.; Dirsch, V. M.; Supuran, C. T. Natural products in drug discovery: Advances and opportunities. *Nat. Rev. Drug Discov.* **2021**, *20* (3), 200-216.
- (227) Thomas C Sparks T.C., Hahn D.R. , Garizi N.V., Natural products, their derivatives, mimics and synthetic equivalents: role in agrochemical discovery, *Pest Manag Sci*, **2017**, *73* (4), 700–71
- (228) Sharma, S.; Kelly, T. K.; Jones, P. A. Epigenetics in cancer. *Carcinogenesis* **2010**, *31* (1), 27-36. DOI: 10.1093/carcin/bgp220.
- (229) Waddington, C. H. The epigenotype. *Int. J. Epidemiol.* **2012**, *41* (1), 10-13.
- (230) Wang, G. G.; Allis, C. D.; Chi, P. Chromatin remodeling and cancer, Part II: ATP-dependent chromatin remodeling. *Trends Mol. Med.* **2007**, *13* (9), 373-380.
- (231) Jenuwein, T.; Allis, C. D. Translating the histone code. *Science* **2001**, *293* (5532), 1074-1080.
- (232) Ntranos, A.; Casaccia, P. Bromodomains: Translating the words of lysine acetylation into myelin injury and repair. *Neurosci.* **2016**, *625*, 4-10.
- (233) Musselman, C. A.; Lalonde, M.-E.; Côté, J.; Kutateladze, T. G. Perceiving the epigenetic landscape through histone readers. *Nat. Struct.* **2012**, *19* (12), 1218-1227.
- (234) Sanchez, R.; Meslamani, J.; Zhou, M.-M. The bromodomain: from epigenome reader to druggable target. *Biochimica et Biophysica Acta (BBA)-Gene Regulatory Mechanisms* **2014**, *1839* (8), 676-685.
- (235) Tamkun, J. W.; Deuring, R.; Scott, M. P.; Kissinger, M.; Pattatucci, A. M.; Kaufman, T. C.; Kennison, J. A. brahma: A regulator of Drosophila

homeotic genes structurally related to the yeast transcriptional activator SNF2SWI2. *Cell* **1992**, *68* (3), 561-572.

(236) Filippakopoulos, P.; Picaud, S.; Mangos, M.; Keates, T.; Lambert, J.-P.; Barsyte-Lovejoy, D.; Felletar, I.; Volkmer, R.; Müller, S.; Pawson, T. Histone recognition and large-scale structural analysis of the human bromodomain family. *Cell* **2012**, *149* (1), 214-231.

(237) Vidler, L. R.; Brown, N.; Knapp, S.; Hoelder, S. Druggability analysis and structural classification of bromodomain acetyl-lysine binding sites. *J. Med. Chem.* **2012**, *55* (17), 7346-7359.

(238) Knapp, S. Targeting bromodomains: epigenetic readers of lysine acetylation [J]. *Nature Reviews Drug Discovery* **2014**, *13* (5), 337-356.

(239) Florence, B.; Faller, D. V. You bet-cha: a novel family of transcriptional regulators. *Front. Biosci* **2001**, *6* (1), D1008-1018.

(240) Kadoch, C.; Hargreaves, D. C.; Hodges, C.; Elias, L.; Ho, L.; Ranish, J.; Crabtree, G. R. Proteomic and bioinformatic analysis of mammalian SWI/SNF complexes identifies extensive roles in human malignancy. *Nature genetics* **2013**, *45* (6), 592-601.

(241) Mohrmann, L.; Verrijzer, C. P. Composition and functional specificity of SWI2/SNF2 class chromatin remodeling complexes. *Biochimica et Biophysica Acta (BBA)-Gene Structure and Expression* **2005**, *1681* (2-3), 59-73.

(242) Ghiboub, M.; Elfiky, A. M.; de Winther, M. P.; Harker, N. R.; Tough, D. F.; de Jonge, W. J. Selective Targeting of Epigenetic Readers and Histone Deacetylases in Autoimmune and Inflammatory Diseases: Recent Advances and Future Perspectives. *J. Pers. Med.* **2021**, *11* (5), 336.

(243) Michel, B. C.; D'Avino, A. R.; Cassel, S. H.; Mashtalir, N.; McKenzie, Z. M.; McBride, M. J.; Valencia, A. M.; Zhou, Q.; Bocker, M.;

Soares, L. M. A non-canonical SWI/SNF complex is a synthetic lethal target in cancers driven by BAF complex perturbation. *Nat. Cell Biol.* **2018**, *20* (12), 1410-1420.

(244) Wang, X.; Wang, S.; Troisi, E. C.; Howard, T. P.; Haswell, J. R.; Wolf, B. K.; Hawk, W. H.; Ramos, P.; Oberlick, E. M.; Tzvetkov, E. P. BRD9 defines a SWI/SNF sub-complex and constitutes a specific vulnerability in malignant rhabdoid tumors. *Nat. Comm.* **2019**, *10* (1), 1-11.

(245) Kang, J. U.; Koo, S. H.; Kwon, K. C.; Park, J. W.; Kim, J. M. Gain at chromosomal region 5p15. 33, containing TERT, is the most frequent genetic event in early stages of non-small cell lung cancer. *CANCER GENET CYTOGEN Journal* **2008**, *182* (1), 1-11.

(246) Scotto, L.; Narayan, G.; Nandula, S. V.; Subramaniam, S.; Kaufmann, A. M.; Wright, J. D.; Pothuri, B.; Mansukhani, M.; Schneider, A.; Arias-Pulido, H. Integrative genomics analysis of chromosome 5p gain in cervical cancer reveals target over-expressed genes, including Drosha. *Mol. Cancer* **2008**, *7* (1), 1-10.

(247) Picaud, S.; Leonards, K.; Lambert, J.-P.; Dovey, O.; Wells, C.; Fedorov, O.; Monteiro, O.; Fujisawa, T.; Wang, C.-Y.; Lingard, H. Promiscuous targeting of bromodomains by bromosporine identifies BET proteins as master regulators of primary transcription response in leukemia. *Sci. Adv.* **2016**, *2* (10), e1600760.

(248) Mirguet, O.; Gosmini, R.; Toum, J.; Clement, C. A.; Barnathan, M.; Brusq, J.-M.; Mordaunt, J. E.; Grimes, R. M.; Crowe, M.; Pineau, O. Discovery of epigenetic regulator I-BET762: lead optimization to afford a clinical candidate inhibitor of the BET bromodomains. *J. Med. Chem.* **2013**, *56* (19), 7501-7515.

- (249) Filippakopoulos, P.; Qi, J.; Picaud, S.; Shen, Y.; Smith, W. B.; Fedorov, O.; Morse, E. M.; Keates, T.; Hickman, T. T.; Felletar, I. Selective inhibition of BET bromodomains. *Nature* **2010**, *468* (7327), 1067-1073.
- (250) Dawson, M. A.; Prinjha, R. K.; Dittmann, A.; Giotopoulos, G.; Bantscheff, M.; Chan, W.-I.; Robson, S. C.; Chung, C.-w.; Hopf, C.; Savitski, M. M. Inhibition of BET recruitment to chromatin as an effective treatment for MLL-fusion leukaemia. *Nature* **2011**, *478* (7370), 529-533.
- (251) Gosmini, R.; Nguyen, V. L.; Toum, J.; Simon, C.; Brusq, J.-M. G.; Krysa, G.; Mirguet, O.; Riou-Eymard, A. M.; Boursier, E. V.; Trottet, L. The discovery of I-BET726 (GSK1324726A), a potent tetrahydroquinoline ApoA1 up-regulator and selective BET bromodomain inhibitor. *Journal of Medicinal Chemistry* **2014**, *57* (19), 8111-8131.
- (252) Fish, P. V.; Filippakopoulos, P.; Bish, G.; Brennan, P. E.; Bunnage, M. E.; Cook, A. S.; Federov, O.; Gerstenberger, B. S.; Jones, H.; Knapp, S. Identification of a chemical probe for bromo and extra C-terminal bromodomain inhibition through optimization of a fragment-derived hit. *J. Med. Chem.* **2012**, *55* (22), 9831-9837.
- (253) Flynn, E. M.; Huang, O. W.; Poy, F.; Oppikofer, M.; Bellon, S. F.; Tang, Y.; Cochran, A. G. A subset of human bromodomains recognizes butyryllysine and crotonyllysine histone peptide modifications. *Structure* **2015**, *23* (10), 1801-1814.
- (254) Dymock, B. W. The rise of epigenetic drug discovery. *Future Science*: 2016; Vol. 8, pp 1523-1524.
- (255) Theodoulou, N. H.; Bamborough, P.; Bannister, A. J.; Becher, I.; Bit, R. A.; Che, K. H.; Chung, C.-w.; Dittmann, A.; Drewes, G.; Drewry, D. H. Discovery of I-BRD9, a selective cell active chemical probe for

bromodomain containing protein 9 inhibition. *J. Med. Chem.* **2016**, *59* (4), 1425-1439.

(256) Burrows, A. E.; Smogorzewska, A.; Elledge, S. J. Polybromo-associated BRG1-associated factor components BRD7 and BAF180 are critical regulators of p53 required for induction of replicative senescence. *PNAS*, **2010**, *107* (32), 14280-14285.

(257) Wu, W. J.; Hu, K. S.; Chen, D. L.; Zeng, Z. L.; Luo, H. Y.; Wang, F.; Wang, D. S.; Wang, Z. Q.; He, F.; Xu, R. H. Prognostic relevance of BRD 7 expression in colorectal carcinoma. *Eur. J. Clin. Invest.* **2013**, *43* (2), 131-140.

(258) Clark, P. G.; Vieira, L. C.; Tallant, C.; Fedorov, O.; Singleton, D. C.; Rogers, C. M.; Monteiro, O. P.; Bennett, J. M.; Baronio, R.; Müller, S. LP99: discovery and synthesis of the first selective BRD7/9 bromodomain inhibitor. *Ang. Chem.* **2015**, *127* (21), 6315-6319.

(259) Picaud, S.; Strocchia, M.; Terracciano, S.; Lauro, G.; Mendez, J.; Daniels, D. L.; Riccio, R.; Bifulco, G.; Bruno, I.; Filippakopoulos, P. 9H-purine scaffold reveals induced-fit pocket plasticity of the BRD9 bromodomain. *J. Med. Chem.* **2015**, *58* (6), 2718-2736. DOI: 10.1021/jm501893k.

(260) Martin, L. J.; Koegl, M.; Bader, G.; Cockcroft, X.-L.; Fedorov, O.; Fiegen, D.; Gerstberger, T.; Hofmann, M. H.; Hohmann, A. F.; Kessler, D. Structure-based design of an in vivo active selective BRD9 inhibitor. *J. Med. Chem.* **2016**, *59* (10), 4462-4475.

(261) Karim, R. M.; Chan, A.; Zhu, J.-Y.; Schönbrunn, E. Structural basis of inhibitor selectivity in the BRD7/9 subfamily of bromodomains. *J. Med. Chem.* **2020**, *63* (6), 3227-3237.

- (262) Liang, P.; Zhang, Y. Y.; Yang, P.; Grond, S.; Zhang, Y.; Qian, Z.-J. Viridicatol and viridicatin isolated from a shark-gill-derived fungus *Penicillium polonicum* AP2T1 as MMP-2 and MMP-9 inhibitors in HT1080 cells by MAPKs signaling pathway and docking studies. *Med. Chem. Res.* **2019**, *28* (7), 1039-1048.
- (263) Clegg, M. A. et al. Application of Atypical Acetyl-lysine Methyl Mimetics in the Development of Selective Inhibitors of the Bromodomain-Containing Protein 7 (BRD7)/Bromodomain-Containing Protein 9 (BRD9) Bromodomains. *J. Med. Chem.* **2020**, *63*, 5816–5840.
- (264) Tangella, Y.; Manasa, K. L.; Krishna, N. H.; Sridhar, B.; Kamal, A.; Nagendra Babu, B. Regioselective ring expansion of isatins with in situ generated α -aryldiazomethanes: direct access to viridicatin alkaloids. *Org. Lett.* **2018**, *20* (12), 3639-3642.
- (265) Lashgari, N.; Ziarani, G. M. Synthesis of heterocyclic compounds based on isatin through 1, 3-dipolar cycloaddition reactions. *ARKIVOC: Online Journal of Organic Chemistry* **2012**.
- (266) Schrodinger Glide, LLC, New York, NY (**2017**)
- (267) Azizian, J.; Fallah-Bagher-Shaidaei, H.; Kefayati, H. A facile one-pot method for the preparation of N-alkyl isatins under microwave irradiation. *Synthetic communications* **2003**, *33* (5), 789-793.
- (268) Fischer, L.; Hornig, M.; Pergola, C.; Meindl, N.; Franke, L.; Tanrikulu, Y.; Dodt, G.; Schneider, G.; Steinhilber, D.; Werz, O. The molecular mechanism of the inhibition by licofelone of the biosynthesis of 5-lipoxygenase products. *Br J Pharmacol* **2007**, *152* (4), 471-480. DOI: 10.1038/sj.bjp.0707416.

- (269) Koeberle, A.; Siemoneit, U.; Bühring, U.; Northoff, H.; Laufer, S.; Albrecht, W.; Werz, O. Licofelone suppresses prostaglandin E2 formation by interference with the inducible microsomal prostaglandin E2 synthase-1. *J. Pharmacol. Exp. Ther.* **2008**, *326* (3), 975-982. DOI: 10.1124/jpet.108.139444.
- (27) Albert, D.; Zündorf, I.; Dingermann, T.; Müller, W. E.; Steinhilber, D.; Werz, O. Hyperforin is a dual inhibitor of cyclooxygenase-1 and 5-lipoxygenase. *Biochem.* **2002**, *64* (12), 1767-1775.
- (271) Garscha, U.; Romp, E.; Pace, S.; Rossi, A.; Temml, V.; Schuster, D.; König, S.; Gerstmeier, J.; Liening, S.; Werner, M. Pharmacological profile and efficiency in vivo of diflapolin, the first dual inhibitor of 5-lipoxygenase-activating protein and soluble epoxide hydrolase. *Sci. Rep.* **2017**, *7* (1), 1-14.
- (272) Waltenberger, B.; Garscha, U.; Temml, V.; Liers, J.; Werz, O.; Schuster, D.; Stuppner, H. Discovery of potent soluble epoxide hydrolase (sEH) inhibitors by pharmacophore-based virtual screening, *J. Chem. Inf. Model* **2016**, *56* (4), 747-762.
- (273) Curtis, M. J.; Bond, R. A.; Spina, D.; Ahluwalia, A.; Alexander, S. P.; Giembycz, M. A.; Gilchrist, A.; Hoyer, D.; Insel, P. A.; Izzo, A. A. Experimental design and analysis and their reporting: new guidance for publication in BJP. Wiley Online Library: 2015; Vol. 172, pp 3461-3471.
- (274) Bellavita, R.; Raucci, F.; Merlino, F.; Piccolo, M.; Ferraro, M. G.; Irace, C.; Santamaria, R.; Iqbal, A. J.; Novellino, E.; Grieco, P. Temporin L-derived peptide as a regulator of the acute inflammatory response in zymosan-induced peritonitis. *Biomedicine & Pharmacotherapy* **2020**, *123*, 109788.

- (275) Chatterjee, B. E.; Yona, S.; Rosignoli, G.; Young, R. E.; Nourshargh, S.; Flower, R. J.; Perretti, M. Annexin 1-deficient neutrophils exhibit enhanced transmigration in vivo and increased responsiveness in vitro. *J. Leukoc. Biol.* **2005**, 78 (3), 639-646.
- (276) Raucci, F.; Saviano, A.; Casillo, G. M.; Guerra-Rodriguez, M.; Mansour, A. A.; Piccolo, M.; Ferraro, M. G.; Panza, E.; Vellecco, V.; Irace, C. IL-17-induced inflammation modulates the mPGES-1/PPAR- γ pathway in monocytes/macrophages. *Br. J. Pharmacol.* **2021**.
- (277) Maione, F.; Iqbal, A. J.; Raucci, F.; Letek, M.; Bauer, M.; D'Acquisto, F. Repetitive exposure of IL-17 into the murine air pouch favors the recruitment of inflammatory monocytes and the release of IL-16 and TREM-1 in the inflammatory fluids. *Front. Immunol.* **2018**, 9, 2752.
- (278) Baradaran Rahimi, V.; Rakhshandeh, H.; Raucci, F.; Buono, B.; Shirazinia, R.; Samzadeh Kermani, A.; Maione, F.; Mascolo, N.; Askari, V. R. Anti-inflammatory and anti-oxidant activity of *Portulaca oleracea* extract on LPS-induced rat lung injury. *Molecules* **2019**, 24 (1), 139.
- (279) Alexander, S. P.; Roberts, R. E.; Broughton, B. R.; Sobey, C. G.; George, C. H.; Stanford, S. C.; Cirino, G.; Docherty, J. R.; Giembycz, M. A.; Hoyer, D. Goals and practicalities of immunoblotting and immunohistochemistry: A guide for submission to the British Journal of Pharmacology. *Wiley Online Library*, **2018**; 175, 407-411.
- (280) George, C. H.; Stanford, S. C.; Alexander, S.; Cirino, G.; Docherty, J. R.; Giembycz, M. A.; Hoyer, D.; Insel, P. A.; Izzo, A. A.; Ji, Y. Updating the guidelines for data transparency in the British Journal of Pharmacology—data sharing and the use of scatter plots instead of bar charts. *Wiley Online Library*, **2017**, 174, 2801-2804.

(281) Bellavita, R.; Falanga, A.; Buommino, E.; Merlino, F.; Casciaro, B.; Cappiello, F.; Mangoni, M. L.; Novellino, E.; Catania, M. R.; Paolillo, R.; et al. Novel temporin L antimicrobial peptides: promoting self-assembling by lipidic tags to tackle superbugs. *J. Enzyme Inhib. Med. Chem.* **2020**, *35* (1), 1751-1764. DOI: 10.1080/14756366.2020.1819258.

(282) Olajuyigbe, O. O.; Afolayan, A. J. In vitro antibacterial and time-kill evaluation of the *Erythrina caffra* Thunb. extract against bacteria associated with diarrhoea. *Sci. World J.* **2012**, *2012*.

(283) Irace, C.; Misso, G.; Capuozzo, A.; Piccolo, M.; Riccardi, C.; Luchini, A.; Caraglia, M.; Paduano, L.; Montesarchio, D.; Santamaria, R. Antiproliferative effects of ruthenium-based nucleolipidic nanoaggregates in human models of breast cancer in vitro: insights into their mode of action. *Scientific Rep.*, **2017**, *7* (1), 1-13.